UNIVERSITY OF SOUTHAMPTON

SYNTHESIS, CHARACTERISATION AND CHEMISTRY OF SILICA SUPPORTED ACIDS

CHEE PENG SHIP

A Thesis submitted for the degree of Doctor of Philosophy at the University of Southampton

Department of Chemistry

January 2002

UNIVERSITY OF SOUTHAMPTON

ABSTRACT

FACULTY OF SCIENCE

CHEMISTRY

Doctor of Philosophy

SYNTHESIS, CHARACTERISATION AND CHEMISTRY OF SILICA SUPPORTED ACIDS

By Chee Peng Ship

A series of silica based supports modified with 12-phosphotungstic acid (HPW), methane- and trifluoromethane-sulphonic acids have been synthesised. As a support, an amorphous silica and a liquid crystal templated mesoporous silica H_1SiO_2 were utilised. The effect of the acids on the structure and surface properties of the silica supports and further on the immobilisation of transition metals (metal carbonyl, zirconocene) on the support surface were investigated.

The supported acids were prepared by adsorption technique with an anhydrous organic solvent and followed by vacuum evaporation or filtration to obtain the dry modified silica with acids. EDX-SEM analysis for the tungsten content of the silica modified with HPW was found to be 15-18% for low loaded samples and 35-40% for high loaded samples. No crystal phase due to HPW was observed from the powder X-ray diffraction (PXRD) patterns even for high loaded samples. The supported HPW on both types of silica exhibited narrow pore size distributions with no large reduction in the pore diameter measurements. A Pyridine adsorption study on the supported HPW showed that HPW supported on Aerosil 200 displayed intense absorption peaks due to Brønsted acidity as compared to HPW on mesoporous silica, H_1SiO_2. Under comparable conditions, the loading was 0.24 molecules/nm^2 for HPW (18wt%)/Aerosil 200 but only 0.06 molecules/nm^2 for HPW (15wt%)/H_1SiO_2. ^{31}P solid state NMR results showed unambiguously that the Keggin structure was retained upon loading HPW on silica. TEM images of high loaded HPW on mesoporous silica showed strong contrast dark lines indicative of the regular crystal lattice of H_1SiO_2. After amorphisation with the electron beam, similar structure were observed which could be due to the presence of the HPW species in the pores.

Base titration of supported sulphonic acids showed the number of acid molecules loaded on the support was ~4 molecules/nm^2 and ~2 molecules/nm^2 for amorphous and H_1SiO_2 silica which were pretreated at 470°C. Pyridine adsorption studies showed protonation to pyridinium ion, indicating essentially saturation of the surface with the acid sites. ^{31}P NMR analysis of adsorbed triethylphosphine oxide showed chemical shifts of 85-90 ppm suggesting the presence of highly acidic sites. These supported sulphonic acids also possessed high thermal stability by temperature programmed desorption study where supported CH_3SO_3H decomposed at 680K and CF_3SO_3H at slight lower temperature, around 650K.

Finally, $[Fe(CO)_3(COT)]$ (COT=cyclooctatetraene) and $[ZrCp_2Me_2]$ were reacted with the modified silica with acids and the possible species present on the silica surface was investigated with infra red and solid state NMR spectroscopy.

Contents

Chapter 3 – Synthesis and Characterisation of the Silica Supports

Chapter 6 – Characterisation of Supported Zirconocene on Silica Modified with Acids

To my parents

Acknowledgements

Firstly, I would like to thank my supervisor, Prof. John Evans for all his guidance, patience and useful discussions. I also wish to thank my PhD advisor, Dr. Paul Wyeth who I can turn to for advice and discussions during absence of my supervisor.

Many thanks to my research group members, Mark, Steve, Pete, Sandra, Tom, Daryl, Graham, Rohana and everyone in the second floor who have helped out and been good company during the course of my PhD.

Acknowledgement is due to Barbara at the Oceonography Centre for help with TEM and SEM, the Weller group for assistance with PXRD instrument and Ed. Blayden for being such a wonderful friend.

I would like to acknowledge the following people who have been good friends of mine whilst at Southampton : Sarah, Rehana, Naruo, Siew, Au Seong, Teresa, Sunkar, Fai, Ronnie and Priscilla and also my fellow flatmates in Montefiore House.

I would also like to thank my two best friends in Malaysia, Pui Yee and Sau Leng for constant support, care and encouragements through good and bad times.

To my parents and family, for having faith in me and lots of support and care during my PhD study in Southampton. To Mark Saeys for being such a wonderful distraction and the amount of time "well spent" on discussions over the phone!

Lastly, I must also acknowledge the financial support given by University of Southampton through a research studentship and the British ORS scheme which covers my tuition fees.

Chapter 1

Introduction

1.1 Introduction

This thesis describes the synthesis, characterisation and chemistry of silica based solid acid materials. The acids used in this work were two liquid acids, methanesulfonic and trifluoromethanesulfonic acids, which were supported on two types of oxide support. An amorphous silica, Aerosil 200 and a liquid crystal templated mesoporous silica were chosen as the support. The synthesis method for producing the mesoporous material followed that of Attard *et al* [1], which produces mesoporous material (H_1SiO_2) providing a pore range from 20Å to 50Å and a particle size that is in the range of mm (cf typical mesoporous materials [2], i.e. MCM 41 are typically is in the range of μm). The strongest acid among the Keggin heteropolyacids, 12-phosphotungstic acid (HPW) was also prepared and supported on these oxide surfaces. Heteropolyacids (HPAs) have special properties which are of great value for catalysis, such as strong Brønsted acidity [3], ability to catalyse reversible redox reactions under mild conditions [4], high solubility in water and oxygenated organic solvents and fairly high stability in the solid state, a "pseudoliquid phase" [5] etc. These properties render HPAs potentially promising acid, redox and bifunctional catalysts in homogeneous as well as in heterogeneous systems.

The ultimate goal of this work is to study the effect of the modifiers (acids) on the structure and the surface properties of the silica supports and further on the adsorption of transition metals (metal carbonyl, zirconocene) on the modified supports. The purpose of these studies is to produce active heterogeneous catalysts with the modified silica as support for zirconocene complex for ethylene polymerisation. This chapter provide an overview on mesoporous silica and its modifications, heteropolyacids, liquid superacids and metallocene compounds of zirconium with particular attention on cationic metallocene complexes.

1.2 Catalysis

A catalyst increases the rate at which a chemical reaction reaches equilibrium, by lowering its activation energy, without itself being consumed in the process. If several reaction pathways are possible, the catalyst may selectively lower the activation energy for just one of them, producing a greater proportion of the desired product. Catalysis may occur in two ways: heterogeneously, which is usually with the catalyst in a solid phase and reactants and products in a solution or gas phase, or homogeneously, in which the catalysts, reactants and products all in the same phase. The best catalysts are both effective in producing high product yields rapidly and selective in producing mainly the desired product. It has been estimated that approximately 70% of all industrial chemicals produced have required the use of a catalyst at some time during their manufacture [6]. Heterogeneous catalysts, due to the ease of separation of products from reactants in large scale industrial processes, represent the dominant share of the market.

Homogeneous catalysts are generally much easier to study than heterogeneous catalysts and are often highly selective but it is frequently difficult to separate catalyst from products, which can make the catalytic process expensive. Homogenous catalysts usually consist of a sequence of linked chemical reactions involving different intermediate metal species derived from a well characterised starting complex. The species involved in the reaction cycle are often discrete soluble transition metal complexes that can be easily characterised by standard spectroscopic techniques. Homogeneous catalysts generally provide a single active site, which leads often to high selectivity. By altering homogeneous catalysts (e.g. nature of the ligands), certain catalytic properties can also be refined to suit the purpose of the catalyst. Heterogeneous catalysts such as metals or metal complexes deposited on amorphous inorganic solids, on the other hand, are generally difficult to study due to the inhomogeneity of the catalyst. It is also usually very difficult to achieve optimum selectivity due to the amorphous nature of the support and the variety of surface reaction sites present in a catalyst but it is much easier to separate the products from the catalyst since they are in different phases. Therefore, by supporting a transition metal or transition metal complex on a well defined, easily characterisable support such as mesoporous silica (e.g. MCM-41), it is

possible to combine the advantages of heterogeneous catalysis with the advantages of homogenous catalysis i.e. this hybrid catalyst should enable reactions of a homogenous nature to occur in a heterogeneous environment.

1.3 Overview of Mesoporous Materials

Mesoporous materials have several great advantages over conventional inorganic supports for surface species. Amorphous supports such as silica, alumina and titania have small surface areas ($<200 m^2g^{-1}$) compared with mesoporous materials which have defined chemical architectures and as a consequence have much greater surface areas (typically > $1000 m^2g^{-1}$). This means that all the atoms can participate directly or can be implicated indirectly in the catalytic act rather than just the surface atoms as in conventional amorphous supports. This means that for mesoporous materials, characterisation of the surface species should lead to an improved understanding of the mechanism by which the catalysts function and hence lead to the development of newer and more selective catalysts. This is important as the more selective a catalyst can become, the smaller the amount of waste produced which is both good for the economics of production but also for environmental consequences. Therefore, the design, modification and use of various mesoporous materials has become very important.

In 1992, a new family of silicate/aluminosilicate mesoporous molecular sieves designated as M41S was discovered by Beck et al [2]. MCM-41, one member of the family, exhibits a hexagonal arrangement of uniform mesopores whose dimensions may be engineered in the range of ~15Å to greater than 100Å. Other members of the family, including a material exhibiting cubic symmetry, have been synthesised. At first, these materials were only limited to silicas [7] and modified layered materials [8] and were usually amorphous or paracrystalline (particles which are less than 30Å in size), with pores that were irregularly spaced and broadly distributed in size. However, recently, a new class of mesoporous materials with regular, repeating arrays of uniform channels, the dimensions of which can be tailored through the use of various surfactant molecules, auxiliary chemicals and reaction conditions has been discovered [9]. These materials are obvious candidates in the synthesis

of fine chemicals and catalysis chemistry. Due to the extended size of the pores, mesoporous materials can be used for many of the uses that zeolitic materials are used for at the present time as well as expanding the range of work covered by these materials.

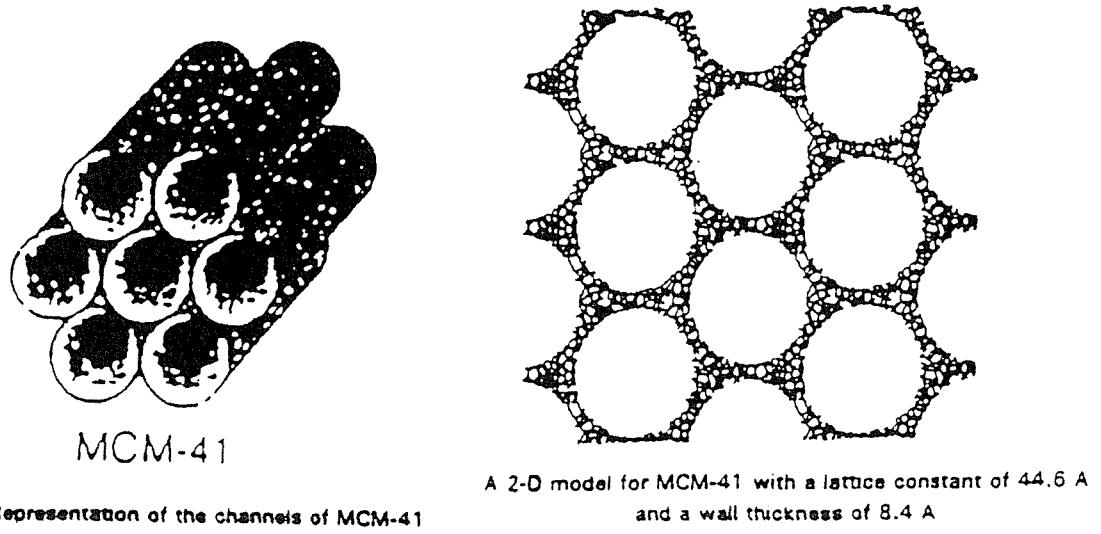

Figure 1.1 :- Diagram showing representations of the MCM-41 structure.

1.3.1 Synthesis of Mesoporous Materials

There are five main synthesis pathways currently known to produce mesoporous materials. The first four complementary synthesis pathways suggested by Huo *et al* [10] are all based on an electrostatic approach.

The first pathway involves the direct co-condensation of a cationic surfactant (S^+) with anionic inorganic species (I^-) to produce assembled ion pairs (S^+I^-). The original Beck synthesis [2] is a prime example of this pathway. In the second pathway, known as the charge-reversed situation pathway, an anionic template (S^-) was used to direct the self-assembly of cationic inorganic species (I^+) through S^-I^+ ion pairs. Pathways three and four involved counterion mediated assemblies of surfactants and inorganic species of similar charge. These counterion mediated pathways produced assembled solution species of the type $S^+X^-I^+$ (where $X^- = Cl^-$ or Br^-) or $S^-M^+I^-$ (where $M^+ = Na^+$ or K^+), respectively. The viability of pathway three was demonstrated by the synthesis of a hexagonal MCM-41 silica

with quaternary ammonium cations under strongly acidic conditions (5 to 10M HCl or HBr) to generate and assemble positively charged framework precursors [10]. The four synthetic pathways are all based on charge matching between ionic surfactants and ionic inorganic reagents with the template being strongly bonded to the charged framework, thereby making it very difficult to recover. In the original Beck approach, the template could not be recovered and so was burnt off by calcination at elevated temperatures. Recently, it has been found that ionic template recovery is possible providing that the exchange ions or ion pairs are present in the extraction process.

The fifth reported synthesis pathway is a neutral templating route to mesoporous materials and is based upon hydrogen bonding and self assembly between neutral primary amine micelles (S°) and neutral inorganic precursors (I°). This neutral templating route [11] produced mesostructures with larger wall thickness, small scattering domain sizes and complementary textural mesoporosities relative to those materials produced by pathways one to four. The neutral template pathway also allows for the easy recovery of the template by simple solvent extraction due to the fact that the bonding between the micelle and the inorganic precursor is hydrogen bonding. This synthesis has been used to prepare ordered mesoporous materials using C_8 to C_{18} primary amines in water with ethanol as a cosolvent. The cosolvent helps to improve the stability of the template.

In 1995, Attard *et al* reported the templating of purely siliceous mesoporous materials from ordered liquid-crystalline mesophases [1]. The resulting silica phase, with pores of approximately 30Å, is a cast of the organic mesophase. In the synthesis, a liquid-crystalline phase of non-ionic surfactants octaethylene glycol monododecyl ether ($C_{12}EO_8$) and octaethylene glycol monohexadecyl ether ($C_{16}EO_8$) were used to template the synthesis of mesoporous silica. It was found that as well as a hexagonal phase, other phases such as cubic or lamellar mesophases could be easily formed. The synthesis method was found to have several major advantages over conventional synthesis methods. The first advantage is that due to the nature of the synthesis, the particle size is much greater than the material produced by conventional methods and monoliths of different size and shapes could be synthesised. There is still research being carried out at present attempting to remove the

surfactant from these monoliths, either by calcination, solvent extraction or a combination of both. The other major advantage that this particular method has over other methods is that it is not only limited to silicas and silica type materials. As recent examples, this particular methodology has been utilised in the synthesis of mesoporous platinum [12] and, via an electrochemical method, the synthesis of mesoporous tin films [13].

1.3.2 Modification of Mesoporous Materials

The discovery of mesoporous materials has raised the general expectations that the catalytic efficiency of microporous zeolites can be expanded to mesoporous dimensions [2]. It is necessary to introduce functionality into the mesoporous structures, so surface modification techniques are enjoying a renewed interest, and it is clear that the pore walls of mesoporous materials are easily modified with either purely inorganic or with hybrid, semi-organic functional groups [14]. Feng *et al* [14] reported recently a route for the modification of the silica surface. Functional groups, thiol groups in their case, can be introduced onto the pore surface of mesoporous silica as terminal groups of an organic monolayer. This material, called functionalised monolayers on mesoporous supports can efficiently remove mercury or other heavy metals from contaminated solutions.

To increase the usefulness of mesoporous materials, other atoms apart from silicon and aluminium can be introduced into the mesoporous structure. There are generally two main methods of introducing catalytic sites into mesoporous materials. The first method involves the pre-modification of the material by addition of a metal during the synthesis procedure. This produces a mesoporous material, which can be used in catalysis in a variety of different chemical reactions. The second method involves the post modification of the mesoporous material by grafting metal species onto the surface of the material. By grafting bulky transition metal complexes or organometallic species onto the external surface, pore entrances or the internal surface of the material, the selectivity of the material can be altered. A good example of the use of organometallic complexes to modify the properties of a mesoporous material was shown by Maschmeyer *et al* [15]. By direct grafting of a titanocene-derived catalyst precursor to the pore walls of MCM-41, a shape selective

catalyst with a large concentration of accessible, well-spaced and structurally well defined sites was generated. This modified material was found to be a very promising catalyst for the epoxidation of cyclohexene and more bulky cyclic alkenes.

1.4 Overview of Heteropoly Compounds

Heteropolyacids (HPAs) are complex proton acids that incorporate polyoxometalate anions (heteropolyanions) having metal-oxygen octahedra as the basic structural units [16,17]. The first characterised and the best known of these is the Keggin heteropolyanion typically represented by the formula $XM_{12}O_{40}^{x-8}$ where X is the central atom (Si^{4+}, P^{5+}, etc), x is its oxidation state and M is the metal ion (Mo^{6+} or W^{6+}). The M^{6+} ions can be substituted by many other metal ions e.g. V^{5+}, Co^{2+}, Zn^{2+}, etc. The Keggin anion is composed of a central tetrahedron XO_4 surrounded by 12 edge and corner sharing metal-oxygen octahedra MO_6 (Figure 1.2) [18]. The octahedra are arranged in four M_3O_{13} groups. Each group is formed by three octahedra sharing edges and having a common oxygen atom which is also shared with the central tetrahedron XO_4. Among a wide variety of HPAs, the Keggins are the most stable and more easily available, these are most important for catalysis.

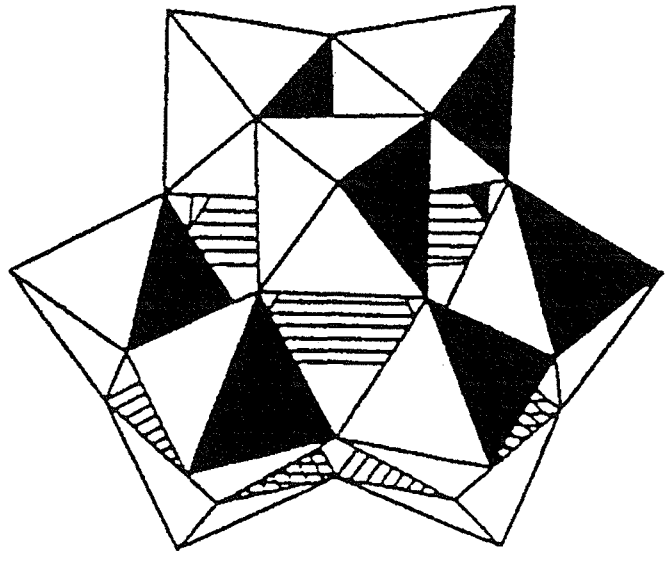

Figure 1.2 :- The structure of the heteropolyanion $XM_{12}O_{40}^{X-8}$.

HPAs in the solid state are ionic crystals (sometimes amorphous) consisting of large polyanions (primary structure), cations, water of crystalisation and other molecules. This

three-dimensional arrangement is the "secondary structure". Recently, it was realised that, in addition to these two structures, the tertiary structure is very influential on the catalytic function of solid HPAs [19]. The tertiary structure is the structure of solid HPAs as assembled. The size of the particles, pore structure, distribution of protons in the particle, etc., are the elements of the tertiary structure. Thus, HPAs in the solid bulk have hierarchic structure. As a reference to the differences, 12-phosphotungstic acid is shown in figure 1.3.

Heteropolyacids are synthesised under acidic conditions by apparently simple inorganic reactions of the type:

$$[PO_4]^{3-} + 12[MoO_4]^{2-} + 24H^+ \longrightarrow [PMo_{12}O_{40}]^{3-} + 12H_2O \qquad \textbf{1.1}$$

$$[SiO_4]^{4-} + 12[WO_4]^{2-} + 24H^+ \longrightarrow [SiW_{12}0_{40}]^{4-} + 12H_2O \qquad \textbf{1.2}$$

Unwanted side reactions and the presence of complex equilibria are possible, so caution must be taken during preparation in order to avoid hydrolytic decomposition of polyanions and nonhomogeneity of the metal cation to polyanion ratio in the solid. For instance, failure to recognise the hydrolytic instability of 12-molybdophosphoric acid and the formation of heteropoly species containing atomic ratios lower than 12 to 1 has led to the development of incorrect preparative procedures and misleading physicochemical results. Good results were obtained by either extraction of acidified solutions of sodium molybdate and sodium phosphate [20] or by a non-ether route by boiling molybdenum trioxide and phosphoric acid [21].

(a) Primary structure (Keggin structure, $PW_{12}O_{40}^{3-}$)

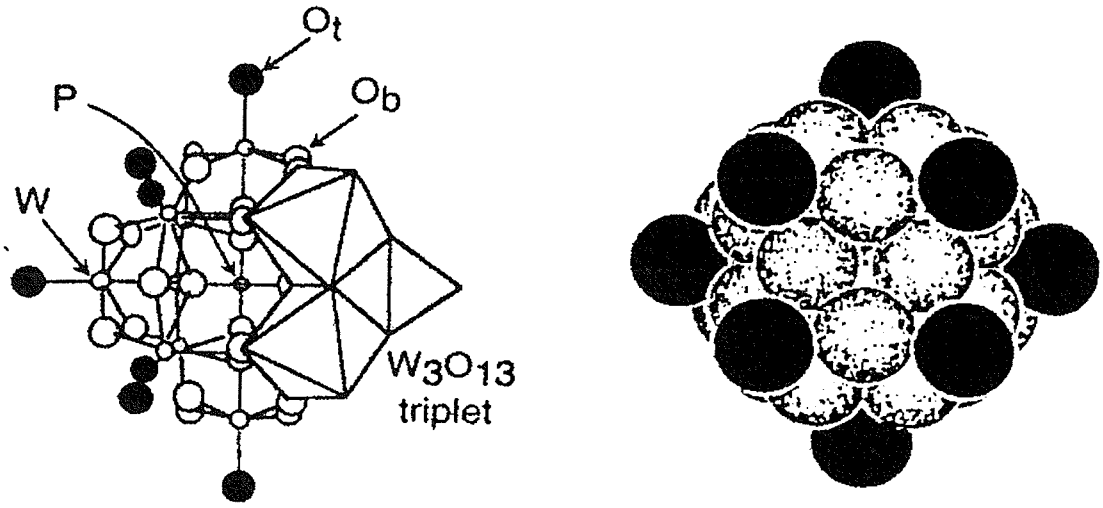

(b) Secondary structure ($H_3PW_{12}O_{40}\cdot 6H_2O$)

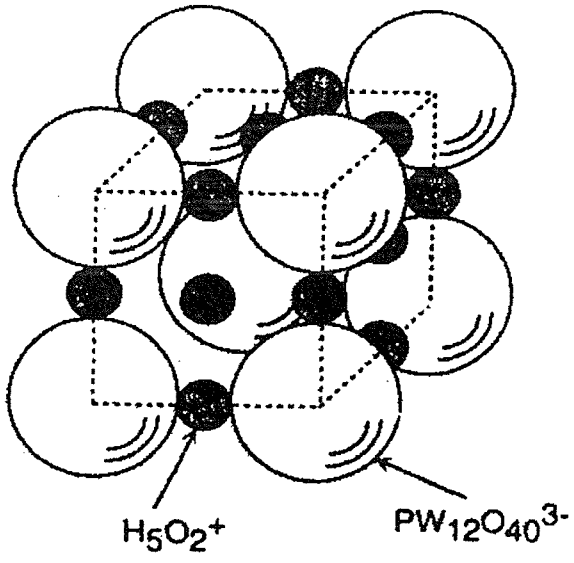

(c) Tertiary structure

Particle size, surface area,
pore, uniformity of composition

Figure 1.3 :- Primary, secondary and tertiary structures of HPAs : (a) primary structure (Keggin structure,$PW_{12}O_{40}$), (b) secondary structure ($H_3PW_{12}O_{40}.6H_2O$) and (c) tertiary structure.

HPAs in solution are stronger than the usual mineral acids such as H_2SO_4, HCl, HNO_3, etc. The strength of the Keggin HPAs depends weakly on their composition. Yet the tungsten acids are markedly stronger than molybdenum ones. The strongest and most stable acid in the Keggin series is $H_3PW_{12}O_{40}$ [3]. Solid HPAs possess purely Brønsted acidity and are stronger than such conventional solid acids as SiO_2-Al_2O_3, H_3PO_4/SiO_2, HX and HY zeolites [22]. The acid strength of crystalline HPAs decreases in the series :

$H_3PW_{12}O_{40} > H_4SiW_{12}O_{40} > H_3PMo_{12}O_{40} > H_4SiMo_{12}O_{40}$

which is identical with that in solutions [3,5]. Usually, relative catalytic activities of HPAs are consistent with this order both in homogeneous and in heterogeneous systems [3,5].

There are various kind of stabilities, for example, thermal stability and hydrolytic stability in solution and those stabilities change very much depending on the kind of HPAs [5,19]. The thermal stability of hydrogen forms of HPAs changes with heteroatom, polyatom and polyanion structure as follows. $H_3PW_{12}O_{40} > H_3PMo_{12}O_{40} > H_4SiMo_{12}O_{40}$.

Misono et al [5,19] demonstrated that crystalline HPAs in many aspects behave like solutions. This is due to the fact that these solids have discrete and and mobile ionic structures. Solid HPAs absorb a large amount of polar molecules, e.g. alcohol, ethers, amines, etc., in the catalyst bulk, forming HPA solvates [23]. Moreover, solid HPAs possess an extremely high proton mobility. By virtue of the easy absorption, polar molecules undergo catalytic reactions not only on the surface, but also in the bulk of the crystalline HPA. Thus, towards polar substances, solid HPAs behave like highly concentrated solutions, i.e., nearly all the HPA protons, not only the surface proton sites, participate in the catalytic reaction. This phenomenon, unusual for heterogeneous acid catalysis, is designated by the term "pseudoliquid phase" [5]. Unlike polar molecules, nonpolar reactants (e.g., hydrocarbons) are incapable of being absorbed in the HPA bulk [24]. They interact only with the surface of the catalyst. The pseudoliquid behaviour apparently brings about high catalytic activities for reactions of polar molecules at relatively low temperatures i.e., when

the sorption of the substrate in the catalyst bulk is rather high. Besides the activities, unique selectivities have been reported [5].

1.4.1 Nature of Acid Sites

HPAs are strong Brønsted acids [24]. Structural characterisation of the HPA proton sites is an important step toward understanding the catalytic activity [3,5]. Keggin anions have three types of outer oxygen atoms as potential protonation centers: terminal oxygens M=O and two types of bridging oxygens M-O-M, edge sharing and corner sharing cf. figure 1.4. Bond length-bond strength correlations [25] as well as ^{17}O nuclear magnetic resonance data [26] indicate that in the free polyanions in solution, the bridging oxygen atoms, having higher electron density than the terminal oxygen atoms, are protonated. In the free Keggin anion, edge bridging M-O-M oxygens are assumed to be the predominant protonation sites (figure 1.5a). In solid HPAs, the protons take part in the formation of the HPA crystal structure, linking the neigbouring heteropolyanions. In this case, the more accessible terminal oxygens can be protonated. Thus, from single crystal X-ray and neutron diffraction data [27], the proton sites in the crystalline $H_3PW_{12}O_{40}$ hexahydrate are represented as diaquahydrogen ions, $H_5O_2^+$, each of which links four neighbouring heteropolyanions by forming hydrogen bonds with the terminal W=O oxygens (figure 1.5b). The structure of proton sites in the dehydrated $H_3PW_{12}O_{40}$ is shown in figure 1.5c. This structure is assumed to be directly formed from the proton structure of the $H_3PW_{12}O_{40}$ hydrate upon dehydration. Stoichiometrically, each proton is shared by four equivalent terminal oxygens, belonging to four different heteropolyanions, like in $H_3PW_{12}O_{40}$ hexahydrate. It is suggested that the proton migrates between four equivalent positions, W=O...H^+...O=W, and thus links four heteropolyanions together, as does the $H_5O_2^+$ ion in $H_3PW_{12}O_{40}$ hexahydrate (figure 1.5 c).

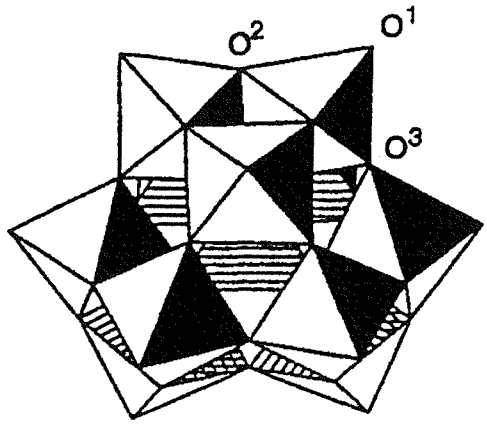

Figure 1.4 :- The Keggin structure of the $XM_{12}O_{40}^{X-8}$ anion: terminal (O^1), edge bridging (O^2) and corner bridging (O^3) oxygen atoms.

(a)

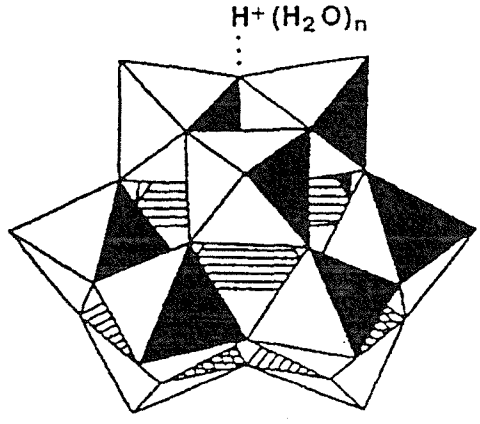

(b)

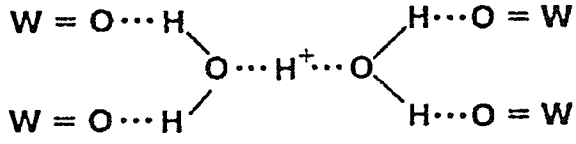

(c)

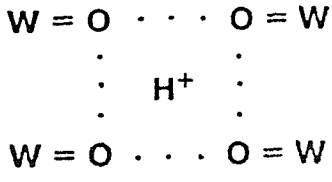

Figure 1.5 :- Proton sites in heteropolyacids: (a) HPA in solution (b) solid HPW hexahydrate (c) solid dehydrated HPW. (HPW=$H_3PW_{12}O_{40}$)

1.4.2 Supported heteropolyacids

Dispersing HPAs on solid supports with high surface areas is important for catalytic applications because the surface area of unsupported HPAs are usually low (1-10 m^2g^{-1}) [28]. The supported catalysts are characterised by various methods and the changes in the acid strength, redox properties and structure have been reported [29,30,31]. In general, HPAs strongly interact with supports at low loading levels, while the bulk properties of HPAs prevail at high loading levels. Acidic or neutral substances such as SiO_2, active carbon, acidic ion-exchange resin are suitable supports, the most frequently used support being SiO_2. Solids having basicity such as Al_2O_3 and MgO tend to decompose HPAs (note the pH range of hydrolysis of heteropolyanion) [32,33].

The high surface area of the ordered mesopores together with the presence of groups able to be functionalised have been of great use to support metal oxides and organometallic compounds achieving very high dispersions of the active phase. It was seen before that the acidity of ordered mesoporous aluminosilicates was mild and therefore, unable to catalyse reactions demanding strong acid sites. This limitation could be partially overcome using mesoporous materials as a support for strong acids such as heteropolyacids. The high surface area of this inorganic solid, coupled with its regular hexagonal array of uniform pore sizes within the mesoporous region (15-100Å), makes this material an excellent support for acid catalysis. It follows that the high acidity of HPAs well dispersed over MCM-41 should constitute a very efficient catalytic system as the two materials complement each other. There already been several reports on HPA/MCM-41 systems catalyzing reactions such as the alkylation of isobutane by butene [34] and the alkylation of 4-*t*-butylphenol (TBP) by isobutene and styrene [35]. Kozhevnikov *et al* [35] reported that HPA retained the Keggin structure on the MCM-41 surface and formed finely dispersed HPA species, without formation of HPA crystals even as HPA loadings as high as 50wt%. The most remarkable claim is that even with those high HPA contents the resultant materials presented uniformly sized mesopores of ~3.0 nm diameter. This is most surprising considering that the starting MCM-41 used has pores of 3.2 nm and since at HPA contents of 50wt% the maximum dispersion possible would be close to a monolayer, and hence it would be difficult to obtain

pores of 3.0 nm in the resultant material. The textural characterisation of the samples clearly shows that the surface area strongly decreased, indicating that some pores are blocked by the HPA, and therefore there is not a uniform distribution of the acid on the surface. Nevertheless, the resultant material was quite active as a catalyst, and in any case more active than the bulk HPA and even H_2SO_4 for the liquid phase alkylation of 4-t-butylphenol with isobutene.

1.5 Overview of Liquid Superacids

Chemists generally considered mineral acids, such as sulfuric acid, nitric, perchloric and hydrofluoric acids, to be the strongest acid systems attainable. That view has changed considerably as extremely strong acid system- hundreds of millions, even billions of times stronger than sulfuric acid have been discovered. Following Gillespie's definition, any acid may be termed a superacid when its acidity is stronger than that of 100% H_2SO_4, i.e., $H_o \leqq$ -12 [36]. Such a superacidity has been reached by a number of systems, which are generally made up by mixing a fluorine-containing Brønsted acid (HF, HSO_3F, CF_3SO_3H, etc) and a fluorinated Lewis acid (BF_3, SbF_5, TaF_5, etc.). The systems have been developed since the 1960s, when Olah's studies of obtaining stable solutions of electron deficient ions, particularly carbocations, focused interest on very high-acidity nonaqueous systems [37].

An example of a strong protic (Brønsted) superacid used in this work is the trifluoromethanesulfonic acid (triflic acid). This acid was first prepared by the oxidation of bis(trifluoromethylthio)mercury with aqueous hydrogen peroxide [38]. Commercially, it is prepared by electrochemical fluorination of methanesulfonic acid [39], and it can also be prepared from trichloromethanesulfonyl chloride (Cl_3CSO_2Cl) with HF followed by hydrolysis. It is colourless liquid that boils at 162°C, fumes in moist air and is converted to a stable monohydrate, which is a solid at room temperature. Triflic acid and its conjugate bases have extreme thermal stability and are resistant to both oxidative and reductive cleavage. Strong nucleophiles are not known to displace fluoride from triflic acid or its derivatives. It has an H_o value of –14.6 [40]. Other properties of triflic acid, such as a relatively low freezing point (< -35°C) and viscosity (2.87 centipoise) compared with

sulfuric acid, have made it a highly useful solvent for the generation of cation radicals [41] and carbocations. It is also extensively used as an acidic catalyst for chemical syntheses [40].

The astonishing acidity of related superacids allows protonation of exceedingly weak bases. Not only all conceivable π-electron donors (such as olefins, acetylenes and aromatics) but also weak σ-electron donors (such as saturated hydrocarbons including the parent alkane, methane) are protonated. The ability of superacids to protonate saturated hydrocarbons (alkanes) rests on the ability of the two-electron two-center covalent bond to share its bonded electron pair with empty orbital (*p* or *s*) of a strongly electron-deficient reagent such as a protic acid (figure 1.6).

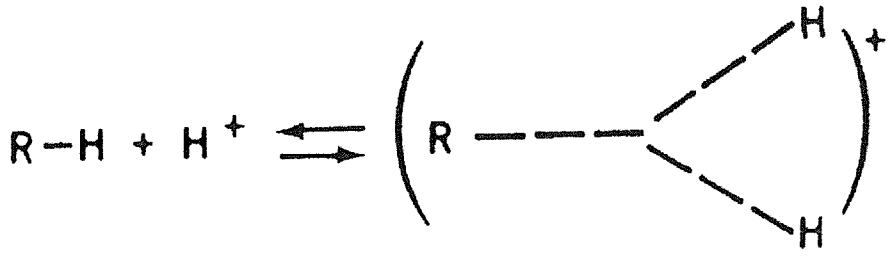

Figure 1.6 :- showing the two-electron two-center covalent bond to share its bonded electron pair with empty orbital (*p* or *s*) of a strongly electron-deficient reagent such as a protic acid.

1.5.1 Liquid Superacids supported on Solids

The preparation and the use of strong solid acids and superacids are active areas of research for isomerisation, cracking, hydrocracking, dehydration, alkylation, acylation, converting methanol to gasoline, etc. Because of the reported advantages of solid catalysts, recent research, has focused on the preparation and characterisation of stronger solid acids. Replacement of homogeneous liquid acids by heterogeneous solid acids as catalysts in the

chemical industry is expected to bring about ease of separation from the reaction mixture, which allows continuous operation, as well as regeneration and reutilisation of the catalyst. Furthermore, use of heterogeneous solid catalysts can lead to additional advantages, e.g., no corrosion of the reactor and no environmental problem in the disposal of the used catalyst.

Solid acid catalysts generally do not show intrinsic acidity comparable with liquid superacids, but high temperatures can be used to achieve catalytic activity, different from the unstable superacids. To obtain solid superacid catalysts, efforts were primarily made to bind physically or chemically the superacids to solid supports. There have been considerable difficulties in achieving this goal. For example, BF_3-based systems such as HF-BF_3 are difficult to adsorb onto solid supports because of the highly volatile BF_3, but SbF_5, TaF_5 and NbF_5 have much lower vapour pressures and are more adaptable to being attached to solids [42]. Extremely reactive HF-SbF_5 and HSO_3F-SbF_5 can also be attached preferentially to fluorinated alumina and graphite [43].

Among the strong solid acids, sulfated zirconia and related materials appear to have the greatest potential for practical applications because the materials are stable and highly reactive for paraffin conversion, for example, *n*-butane isomerisation [44]. Sulfated zirconia works as a catalyst even at room temperature, although the reactions are very slow, and promoted sulfated zirconia (containing iron and manganese) is several order of magnitude more active than unpromoted sulfated zirconia for room temperature *n*-butane iosmerisation [45]. A sulfated zirconia was prepared by acid treatment of $Zr(OH)_4$, obtained by precipitation of $ZrO(NO_3)_2$ solution with $NH_3.H_2O$ at pH=10, with 0.5M H_2SO_4 solution, followed by evaporation and drying at 100°C overnight and calcinations at 600°C for 2h. In a similar preparative method, sulfated metal oxides can be obtained by adsorbing sulfate ion onto amorphous oxides of Fe, Ti, Hf, Sn and Si followed by calcination in air.

Different catalytic systems have been studied in which triflic acid is adsorbed on various solids. For example, Topsøe *et al* [46] reported a process for liquid phase alkylation of a hydrocarbon substrate with an olefinic alkylating agent in the presence of a fluorated sulfonic acid catalyst. Benazzi *et al's* invention [47] concerns the use of a catalyst

comprising a porous organic or inorganic support, preferably silica, and at least one acid selected from acids with formula $R\text{-}SO_3H$, where R is fluorine or an alkyl group or fluorinated alkyl group in the alkylation of aliphatic hydrocarbon. However, to date there is no literature data that concerns the characteristics of these supported triflic acids.

1.6 Olefin Polymerisation

The polymerisation of olefins has evolved from 1955 when Ziegler dicovered that hydrocarbon solutions of titanium tetrachloride in the presence of triethyl aluminium give heterogeneous suspensions that polymerise ethylene at 1 atmospheric pressure [48]. This was followed closely by the discovery of Natta of polymerising propene into semi-crystalline polypropene. Long chain olefins were assembled in a stereoregular manner influencing the properties of the material formed [49]. The active metal species in the Ziegler-Natta system consists of a fibrous form of $TiCl_3$ formed *in situ* from $TiCl_4$ and $AlEt_3$. By using this catalyst, polymerisation can be carried out under relatively mild conditions from room temperature to 93°C and from atmospheric pressure to 100 atmospheres. However, Ziegler-Natta systems have a limitation where copolymerisation is concerned : while they are efficient at polymerising small monomers such as ethylene, their activity drops off when dealing with larger monomers.

The discovery by Sinn and Kaminsky of metallocene catalysts for olefin polymerisation in 1981, has opened up a new frontier in this area of organometallic chemistry [50,51]. These systems associate metallocene and methyl aluminoxane (MAO) as a co-catalyst and exhibit high activities in ethylene, propylene and higher α-olefins polymerisation.

1.6.1 Historical Interest in the Role of Cationic Species in Ziegler-Natta Olefin Polymerisation

For many years, it has been suspected that cationic d^0 metal alkyl species $Cp_2M(R)^+$ are involved in metallocene-based Ziegler-Natta olefin polymerization catalyst systems of the general type Cp_2MX_2/AlR_nX_{3-n}. In the early 1960s, Shilov proposed on the basis of

conductivity and electrodialysis experiments that the active species in the soluble Cp_2TiCl_2/AlR_nCl_{3-n} catalyst system is cationic [52]. This early work suggested that the role of the Al cocatalyst in these systems is to alkylate the transition metal and to activate the resulting $Cp_2M(R)(Cl)$ species for olefin coordination and insertion [53] by Lewis acid complexation or halide abstraction. However, it was later realised that these early studies were complicated by adventitious water, which can promote polymerization via formation of alumoxanes, $[Al(CH_3)(\mu\text{-}O)]_n$, which are extremely effective cocatalysts in Cp_2MX_2-based systems [50,54].

Several key advances in the early 1980s generated renewed interest in the proposal that $Cp_2M(R)^+$ ions are active species in the soluble catalyst systems. Watson, Marks and co-workers demonstrated that neutral group 3 and lanthanide metal systems of general type $Cp_2^*M(R)$ and $[Cp_2^*M(H)]_2$, which in monomeric form are isoelectronic (neglecting *f* electrons) with $Cp_2M(R)^+$ (M=Ti,Zr), are active ethylene polymerisation catalysts (figure 1.7) [55,56].

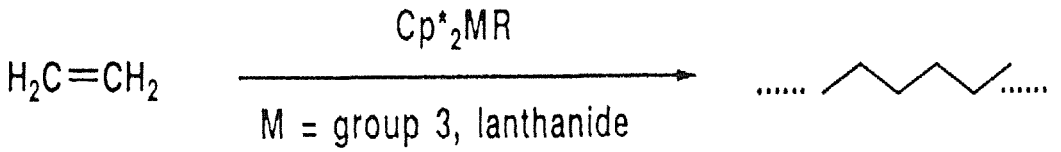

Figure 1.7 :- showing the ethylene polymerisation reaction.

Further indirect support for the cationic proposal was provided by extensive studies of early-metal metallocene alkyl complexes. In general, it was observed that four-coordinate d^0 metal alkyls $Cp_2M(R)(X)$ (M= Ti, Zr, X= alkyl, aryl, halide, etc.) [57], three-coordinate d^1 complexes $Cp_2Ti(R)$ [58] and neutral and cationic d^2 olefin alkyl complexes $Cp_2M(R)(olefin)^{n+}$ (M= group 5, 6) do not undergo olefin insertion [59]. Together these observations strongly implied that a three-coordinate, 14-electron, d^0 $Cp_2M(R)^{n+}$ species (n= 0, group 3, lanthanide; n =1, group 4) or a $Cp_2M(R)(L)^{n+}$ species containing a labile ligand L

is required for olefin insertion and polymerization in metallocene-based catalysts, and they prompted efforts to synthesise and isolate cationic group 4 metal alkyls [60].

1.7 Heterogeneous Metallocene Catalysis

The need for the heterogenisation of these metallocene systems stems from one principal problem in homogeneous catalysis: the zirconocene catalysts were so active in homogeneous catalysis that morphological control (for instance, syndiotactic or isotactic) of the polymers is very difficult. By blocking the catalyst on a support, the single site created would control better the morphology of the monomers inserted during the propagation. The polymer formed using slurry, bulk monomer, or gas phases [61] processes are usually of higher density or crystallinity (eg. high density polyethylene, linear low density polyethylene and isotactic polypropylene).

A second advantage to the heterogenisation is an economic one. Plants are already set up for the heterogeneous Ziegler-Natta sytem and for this reason, it would be cheaper to readapt them for the new heterogeneous metallocene catalyst. The development of modern gas phase [61] and slurry polymerisation processes could also prevent the problem of reactor fouling observed when using homogeneous sytems (formed polyolefin is deposited at the reactor walls). Silica supports within the system are known to fragment during the polymerisation process; therefore the optical and physical properties of the polymer formed are not altered by the heterogeneous catalysts. This fragmentation of the support material is also important because it does not hamper ethylene diffusion (the polymer being produced on the support surface) and thus leads to an increase in activity [62].

For the industrial production of polyolefins heterogeneous catalysts are generally preferred over homogeneous ones. Several studies in the literature have concentrated on the use of supported metallocene complexes in the olefin polymerisation [63,64,65]. Silica, alumina and magnesium compounds are the most used inorganic supports. The aim is to find a way to attach the metallocene to the support without losing the performance of the homogeneous complex. Three main immobilisation techniques can be classified, direct impregnation of

metallocenes on the support, pre-treatment of the support with ordinary alkylaluminiums or methylaluminoxane (MAO) followed by the reaction with the metallocene compound and the immobilisation of metallocene ligands on the supports followed by addition of transition metal salts [66]. In search of alternatives for MAO, weakly coordinating boron based cocatalysts such as $X^+[B(C_6F_5)_4]^-$(X^+= $PhN(H)Me_2^+$,Ph_3C^+) and $B(C_6F_5)_3$ have been found to effectively activate metallocenes [67]. Supported catalysts can also be activated by trialkyl aluminium [68,69]. Even though they are largely overshadowed by the more widely used MAO and fluorinated borate anion activators, single-sites catalysts activated by simple alkyl aluminiums continue to be studied because of the low cost, stability and wide availability of the co-catalyst. Much of this research focuses on modifying the activator or improve catalytic activity, especially with respect to zirconocene catalysts.

The main problems still faced in heterogenisation are lower yields and catalyst activity as compared to homogeneous system. Furthermore, a need of a threshold level of MAO to work (Al/Zr range of 50-400) [70,71] and desorption of the metallocene from the catalyst when using methylaluminoxane (MAO) as a cocatalyst [72] are serious drawbacks. The reasons for the low catalyst activities are not clear, but steric hindrance around the active site on the silica surface seems to be one constraint [73]. The introduction of a spacer molecule such as trisiloxane or pentamethylene [73] or silanes [64] between metallocene and silica have resulted in increased catalyst activity in ethene polymerisation. Also, high surface area and the presence of well-defined, stable sites for the attachment of the active component to the support have been found to be of importance [74]. The regular, cylindrical and hexagonally ordered pores of MCM-41 have been observed to suppress the formation of inactive binuclear complexes between two metallocenes or between metallocene and methylaluminoxane, resulting in stable active sites and high activity in propene polymerisation [15,75]. The pores are large (2-10 nm, depending on the alkyl chain length of surfactant) compared to e.g., zeolites, which could enable large metallocene molecules to be withheld not only on the surface but also inside the supercage of the support.

Recently, sulphated zirconia and related solid acids have received considerable attention because of their proposed "superacidity" and high catalytic activity for various hydrocarbon

transformations [43,76]. Marks *et al* reported the formation of highly electrophilic metallocene species on "superacidic" strong Brønsted sites via metal-carbon bond protonolysis and initial observations on adsorbate α-olefin/arene hydrogenation and polymerisation activities [77].

1.7.1 Metallocene Compounds of Zirconium

Until the 1950s, this was an unexplored area of chemistry but then two events occurred: ferrocene was discovered and K. Ziegler catalysed the polymerisation of ethylene using an organo-titanium derivative. The first event initiated a systematic study of cyclopentadienyl compounds, and so led to the preparation of the most stable of the organometallic compounds of the group IV, while the second event provided a strong commercial incentive for the investigation of this field.

Cyclopentadienyl zirconium compounds are known for metal oxidation states of IV, III and II. They can contain up to four cyclopentadienyl rings as ligands. However, *mono*- and *bis*(cyclopentadienyl) compounds of zirconium (IV) are the most common organozirconium compounds [78]. In this work, one of the most commonly used metallocene, dimethyl *bis*(cyclopentadienyl) zirconium (IV) was chosen for the preparation of the sandwich complexes.

1.8 Aim of the research

The main aim of the work has been the modification of silica surfaces by acids followed by incorporation of the metallocene catalyst, zirconium (IV) dimethyl to the modified silica to produce active heterogeneous catalysts for ethylene polymerisation. There has already been a vast amount of work done on the subject of heterogenisation of metallocene, with or without the presence of cocatalysts [67,68,77] but the aim of the thesis is to prepare strongly Brønsted acidic groups on the silica surface and subsequently, incorporation of metallocene to generate highly electrophilic cationic metallocene catalysts. The thesis can be divided into 3 main areas. The characterisation of the silica supports, followed by the synthesis and characterisation of supported acids and finally, the chemistry of the modified silica supports with organometallic compounds.

In chapter 3, the two types of silica support utilised were studied extensively as background work. Surface hydroxyl groups (silanols) on silica often react with various catalyst components to immobilise the species on the surface. The way in which many species react with surface silanols has been difficult to characterise and is largely unexplored. To rationally design silica supported catalysts, an important first step is to fully understand and characterise the various silanol groups present on the surface. Silanol groups present on these two surfaces were characterised qualitatively and quantitatively by various techniques which include infrared spectroscopy, MAS NMR, methane evolution titration, PXRD and BET N_2 adsorption.

In chapter 4, the strongest acid in the Keggin heteropolyacids, 12-phosphotungstic acid (HPW) was supported on both the surfaces. Typically, two types of HPW loading were prepared, a low loaded HPW (15-18wt%) and a high loaded HPW (~40wt%). These supported HPW were prepared from organic solvent which showed to produce supported HPW with better characteristics compared to preparation from aqueous solution. A wide range of characterisation techniques were applied to study the textural properties, acidities and thermal stabilities of these supported HPW and the results obtained were compared to the data in the literature.

Chapter 5 describes the synthesis and characterisation of two liquid superacids supported on silica. Methanesulfonic and trifluoromethanesulfonic acids were supported on both types of silica and their properties were investigated by a range of techniques described in chapter 2.

Finally, chapter 6 was concerned with the synthesis and characterisation of $Fe(CO)_3COT$ (where COT = cyclooctatetraene) and $Zr(Me)_2(Cp)_2$ (Cp = cyclopentadiene) supported on silica modified with liquid superacids. The ultimate study of a complex interaction was carried out by infrared, solution and solid state NMR experiments.

References

[1] G.S.Attard, J.C.Glyde, C.G.Göltner, *Nature*, **378**, 366, 1995.

[2] J.S.Beck, J.C.Vartuli, W.J.Roth, M.E.Leonowicz, C.T.Kresge, K.D.Schmitt, C.T.W.Chu, D.H.Olson, E.W.Sheppard, S.B.McCullen, J.B.Higgins, J.L.Schlenker, *J.Am.Chem.Soc.*, **114**, 10834, 1992.

[3] I.V.Kozhevnikov, *Russ.Chem.Rev.*, **56**, 811, 1987.

[4] I.V.Kozhevnikov, K.I.Matveev, *Russ.Chem.Rev.*, **52**, 817, 1983.

[5] M.Misono, *Catal.Rev.Sci.Eng.*, **29**, 269, 1987.

[6] W.Keim, *Angew.Chem.Int.Ed.Engl.*, **29**, 235, 1990.

[7] P.Behrens, G.D.Stucky, Angew.Chem.Int.Ed.Engl., **32**, 696, 1993.

[8] R.K.Iler, *The Chemistry of Silica*, Wiley, New York, 1979.

[9] M.E.Landis, *J.Am.Chem.Soc.*, **113**, 3189, 1991.

[10] Q.Huo, D.I.Margolese, U.Ciesla, P.Feng, T.E.Gler, P.Sieger, R.Leon, P.M.Petroff, P.Schuth, G.D.Stucky, *Nature*, **368**, 317, 1994.

[11] P.T.Tanev, T.J.Pinnavaia, *Science*, **267**, 865, 1995.

[12] G.S.Attard, C.G.Göltner, J.M.Corker, S.Henke, R.H.Templer, *Angew.Chem.Int.Ed.Engl.*, **36**, 1315, 1997.

[13] A.H.Whitehead, J.M.Elliot, J.R.Owen, G.S.Attard, *J.Chem.Soc., Chem.Commun.*, 331, 1999.

[14] X.Feng, G.E.Fryxell, L-Q Wang, A.Y.Kim, J.Liu, K.M.Kemmer, *Science*, **276**, 923, 1997.

[15] T.Maschmeyer, F.Rey, G.Sankar, J.M.Thomas, *Nature*, **378**, 159, 1995.

[16] M.T.Pope, A.Müller, *Angew.Chem.Int.Ed.Engl.*, **30**, 34, 1991.

[17] M.T.Pope, *Heteropoly and Isopoly Oxometalates*, Springer:Berlin, 1983.

[18] J.F.Keggin, *Proc.R., Soc.London*, **A144**, 75, 1934.

[19] T.Okuhara, N.Mizuno, M.Misono, *Adv.Catal.*, **41**, 113, 1996.

[20] H.Wu, *J.Biol.Chem.*, **43**, 189, 1920.

[21] G.A.Tsigdinos, *Ind.Eng.Chem.Prod.Res.Dev.*, **13**, 267, 1974.

[22] M.Misono, N.Mizuno, K.Katamura, A.Kasai, Y.Konishi, K.Sakata, T.Okuhara, Y.Yoneda, *Bull.Chem.Soc.Jpn.*, **55**, 400, 1982.

[23] M.Misono, *Catalysis by Acids and Bases*, B.Imelik, Ed., Elsevier:Armsterdam, p147,1985.

[24] I.V.Kozhevnikov, *Chem.Rev.*, **98**, 171, 1998.

[25] L.P.Kazanskii, M.A.Fedotov, V.I.Spitsyn, *Dokl.Akad.Nauk.SSSR*, **233**, 152, 1977.

[26] W.G.Klemperer, W.Shum, *J.Am.Chem.Soc.*, **99**, 3544, 1977.

[27] G.M.Brown, M-R Noe-Spirlet, W.R.Bushing, H.A.Levy, *Acta Crystallogr.Sect.B*, **33**, 1038, 1977.

[28] N.Mizuno, M.Misono, *Chem.Rev.*, **98**, 199, 1998.

[29] I.V.Kozhevnikov, K.R.Kloetstra, A.Sinnema, H.W.Zandbergen, H. van Bekkum, *J.Mol.Catal.*, **114**, 287, 1996.

[30] Y.Wu, X.Ye, X.Yang, X.Wang, W.Chu, Y.Hu, *Ind.Eng.Chem.Res.*, **35**, 2546, 1996.

[31] F.Marme, G.Coudurier, J.C.Védrine, *Microporous Mesoporous Mater.*, **22**, 151, 1998.

[32] K.Nowinska, R.Fiedorow, J.Adamiec, *J.Chem.Soc., Faraday Trans*, **87**, 749, 1991.

[33] K.M.Rao, R.Gobetto, A.Lannibello, A.Zecchina, *J.Catal.*, **119**, 512, 1989.

[34] W.Chu, Z.Zhao, W.Sun, X.Ye, Y.Wu, *Catal.Lett.*, **55**, 57, 1998.

[35] I.V.Kozhevnikov, A.Sinnema, R.J.J.Janse, K.Pamin, H van Bekkum, *Catal.Lett.*, **30**, 241, 1995.

[36] R.J.Gillespie, *Acc.Chem.Res.*, **1**, 202, 1968.

[37] G.A.Olah, *Angew.Chem.Int.Ed.Engl.*, **12**, 173, 1973.

[38] R.N.Hazeldine, J.M.Kidd, *J.Chem.Soc.*, 4228, 1954.

[39] T.Gramstad, R.N.Hazeldine, *ibid*, 173, 1976.

[40] R.D.Howells, J.D.McCown, *Chem.Rev.*, 69, 1977.

[41] G.C.Yang, A.E.Pohland, *J.Phys.Chem.*, **76**, 1504, 1972.

[42] G.A.Olah, G.K.S.Prakash, J.Sommer, *Science*, **13**, 206, 1979.

[43] K.Arata, *Adv.Catal.*, **37**, 165, 1990.

[44] M.Hino, K.Arata, *J.Chem.Soc., Chem.Commun.*, 851, 1980.

[45] C-Y Hsu, C.R.Hemibuch, C.T.Armes, B.C.Gates, *J.Chem.Soc., Chem.Commun.*, 1645, 1992.

[46] H.Topsoe, S.Hommeltoft, *Eur.Pat.*, 0433 954 A1, 1991.

[47] E.Benazzi, J-F Joly, *U.S.Pat.*, 5 906 957, 1999.

[48] K.Ziegler, E.Holzkamp, H.Breiland, H.Martin, *Angew.Chem.*, **67**, 541, 1955.

[49] G.Natta, *J.Polym.Sci.*, **16**, 143, 1955.

[50] H.Sinn, W.Kaminsky, *Adv.Organomet.Chem.*, **18**, 99, 1980.

[51] W.Kaminsky, *J.Chem.Soc., Dalton Trans.*, 1413, 1998.

[52] A.K.Zefirova, A.E.Shilov, *Dokl.Acad.Nauk.SSSR*, **136**, 599, 1961.

[53] P.Cossee, *J.Catal.*, **3**, 80, 1964.

[54] W.P.Long, D.S.Breslow, *Liebigs Ann.Chem.*, 463, 1975.

[55] P.L.Watson, G.W.Parshall, *Acc.Chem.Res.*, **18**, 51, 1985.

[56] G.Jeske, H.Lauke, H.Mauermann, P.N.Sweptson, H.Schumann, T.J.Marks, *J.Am.Chem.Soc.*, **107**, 8091, 1985.

[57] D.J.Cardin, M.F.Lappert, C.L.Raston, *Chemistry of Organozirconium and hafnium Compounds*, Ellis Horwood, Ltd., West Sussex, England, 1986.

[58] J.H.Teuben, *Fundamental and Technological Aspects of Organo-f-Element Chemistry*, T.J.Marks, J.L.Fragala, eds., p195, Reidel, Dordrecht, The Netherlands, 1985.

[59] F.W.S.Benfield, N.J.Cooper, M.L.H.Green, *J.Organomet. Chem.*, **76**, 49, 1974.

[60] R.F.Jordon, P.K.Bradley, R.E.Lapointe, D.F.Taylor, *New.J.Chem.*, **14**, 505, 1990.

[61] D.F.Oxley, *Chem.Ind.*, 305, Apr. 1998.

[62] J.H.Z.dos Santos, S.Dorneles, F.C.Stedile, J.Dupont, M.M.De Camargo Forte, I.J.R.Baumvol, *Macromol.Chem.Phys.*, **198**, 3529, 1997.

[63] R.Duchateau, R.A van Santen, G.P.A.Yap, *Organometallics*, **19**, 809, 2000.

[64] J.H.Z. dos Santos, P.P.Greco, F.C.Stedile, J.Dupont, *J.Mol.Catal.A*, **154**, 103, 2000.

[65] H.Rahiala, I.Beurroies, T.Eklund, K.Hakala, R.Gougeon, P.Trens, J.B.Rosenholm, *J.Catal.*, **188**, 14, 1999.

[66] G.G.Hlatky, Chem.Rev., 100, 1347, 2000.

[67] G.G.Hlatky, D.J.Upton, H.W.Turner, *PCT Int.Appl.*91/09982, 1991.

[68] J.C.W.Chien, J.T.T.Hsieh, *J.Polym.Sci., Polym.Chem.*, **14**, 1915, 1976.

[69] D.Slotfeldt-Ellingsen, I.M.Dahl, O.H.Ellestad, *J.Mol.Catal.*, **9**, 423, 1980.

[70]T.J.Burkhardt, J.L.Brinen, G.G.Hlatky, W.S.Spaleck, A.Winter, *World Pat.*, 94 28034, 1994.

[71] M.C.Sacchi, D.Zucchi, J.Tritto, P.Locatelli, T.Dall'Occo, *Macromol.Rapid Commun.*, **16**, 581, 1995.

[72] N.V.Semikolenova, V.A.Zakharov, *Macromol.Chem.Phys.*, **198**, 2889, 1997.

[73] D-H Lee, K-B Yoon, *Macromol.Rapid Commun.*, **18**, 427, 1997.

[74] F.Ciardelli, A.Altomore, M.Michelotti, *Catal.Today*, **41**, 149, 1998.

[75] L.K.Van Looven, D.F.Geysen, K.A.Vercruysen, B.H.Wouters, P.J.Grobet, P.A.Jacobs, *Angew.Chem.Int.Ed.*, **37**, 517, 1998.

[76] A.Corma, *Chem.Rev.*, **95**, 559, 1995.

[77] T.J.Marks, H.Ahn, *J.Am.Chem.Soc.*, **120**, 13533, 1998.

[78] P.C.Wailes, R.S.P.Coutts, H.Weigold, *Organometallic Chemistry of Titanium, Zirconium and Hafnium*, Academic, London, 1974.

Chapter 2

Experimental Techniques

2.1 Introduction

A range of techniques to characterise silica modified with acids has been attempted. This chapter will outline the theory and experimental for each technique.

2.2 Experimental for Gas Evolution Titration by Grignard Method

The principle of this quantitative method is to measure the pressure of methane evolved during reaction 2.1 and relate it back to the hydroxyl group concentration. This is valid for the reaction of the OH which reacts stoichiometrically with the Grignard reagent:

$$\text{Si-OH} + \underset{\text{excess}}{\text{CH}_3\text{MgBr}} \longrightarrow \text{CH}_4 + \text{Si-OMgBr} + \Delta \qquad \textbf{2.1}$$

The closed system employed for this study consists of a round bottom flask connected to a CG 16K manometer from Edwards. As the reaction is carried out under vacuum, it was essential to get a seal strong enough to prevent any gas leaking in the closed system. The aluminium compression fitting used allows the perfect glass-metal connection. When the subaseal is not in use, the vacuum tap is always shut. The dry solvent introduced has to be degassed before titration, to prevent any pressure reading due to the solvent. After the addition of the Grignard reagent, it is important to constantly monitor the temperature and pressure change and consider that equilibrium is reached when the temperature is back to its initial value. When samples studied are loaded in the glove box, the gauge is easily linked to the rest of the body by simply pushing both parts together with the help of 'O' rings.

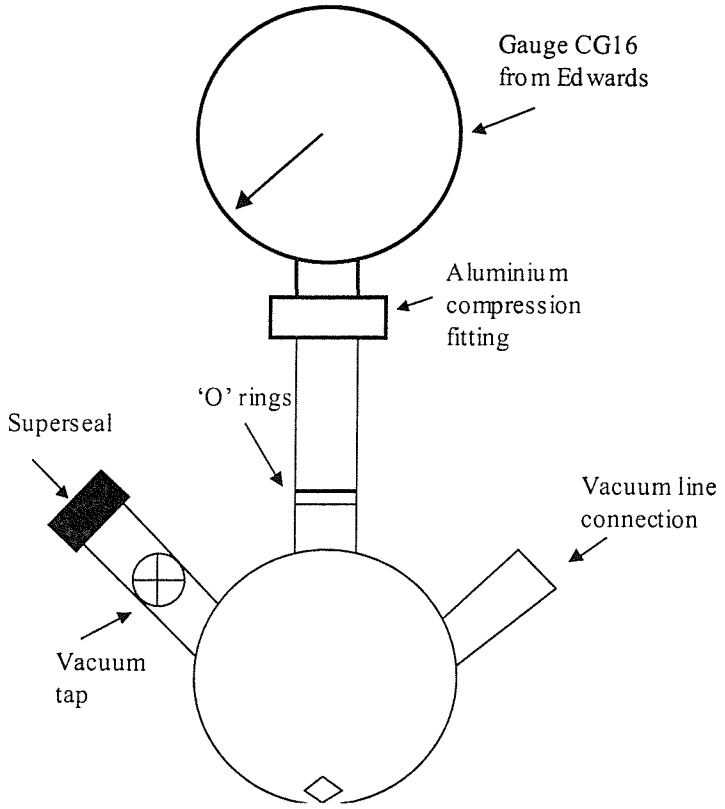

Figure 2.1 :- Gas titration apparatus used to determine the concentration of the hydroxyl groups on the silica supports.

2.3 Theory of UV-Visible Spectroscopy

Ultraviolet-visible absorption usually corresponds to excitation of an electron from the ground electron state to a higher electron state. Each photon of the incident radiation must possess energy that corresponds to the energetic difference between the electron levels. The energetic transition can occur from any of the rotational and vibrational levels that are associated with the lower electron state to any of the rotational and vibrational levels that are associated with the higher electron state.

Because many vibrational and rotational levels can be simultaneously occupied in different molecules and because the incident radiation that is used in most spectrophotometers contains a large number of photons, many vibrational and rotational levels that are associated with the higher electron state can be simultaneously populated in different molecules. As the wavelength of the incident radiation is altered (scanned), a molecule can be excited from the same electron, vibrational and rotational levels to a single excited electron level, but to different vibrational and rotational levels. Because the energetic differences between the vibrational and rotational levels that are associated with a particular electron level are small, the many possible changes in energy between the vibrational and rotational levels of the two electron levels overlap, causing broad absorptive bands in the ultraviolet-visible region for polyatomic species.

The portion of a molecule that absorbs radiation is a chromophore. In the ultraviolet-visible region, strong chromophores contain some degree of unsaturation. Because different chromophores have uv-visible absorptive maxima at different wavelengths, it sometimes is possible to identify the absorbing molecule by comparing the wavelength of the absorptive maximum from the spectrum of a sample with the wavelengths of the absorptive maxima of known substances. Generally, a spectrum consisting of a plot of absorbance, percent transmittance or log of absorbance as a function of wavelength is automatically obtained using a scanning spectrophotometer.

2.3.1 Experimental for Solid State Diffuse Reflectance UV-Visible Spectroscopy

DRS spectroscopy were recorded on a Lambda 19 UV/Vis/NIR spectrometer. All the silica samples were insoluble and therefore can only be analysed in this mode. The sample is always presented as a finely ground powder to the beam using the integrating sphere of the instrument. The sample is placed in quartz solid cells and the spectra are recorded in Kubelka-Munk mode, which attempts to compensate for the effects on sample particle size on the scattering, as the wavelengths get shorter. It is difficult to get reliable information on intensities from solid state spectra – only relative intensities of the bands from a single spectra can be compared.

2.4 Theory of Diffuse Reflectance Infrared Fourier Transform Spectroscopy (DRIFTS)

Diffuse reflectance occurs when light impinges on the surface of a material and is partially reflected and transmitted. Light that passes into the material may be absorbed or reflected out again. Hence, the radiation that reflected from an absorbing material is composed of surface-reflected and bulk re-emitted components, which summed are the diffuse reflectance of the sample. The particular sensitivity of diffuse reflectance spectroscopy to surface structures, is due to the usually multiple reflection and diffraction of radiation at the surfaces of the scattering particles. Therefore, catalytic processes and chemically modified surfaces are frequently studied in this way.

With a strongly scattering sample, the reflected radiation is spread over the entire hemisphere above the sample. With the same optical throughput the spectrometer provides, only a small fraction of the scattered radiation would be collected, therefore losses are inevitable. The adequate detection system is the integrating sphere which in its ideal form would reflect each ray without loss again and again until it happens to fall onto the detector. In infrared, however, the ideal situation is by no means given, and instead mirrors covering large solid-angle are used. Efficiency is in the order of 0.1 only [1]. For particulate samples, and even more for compact samples exhibiting a smooth surface, it is crucial to prevent

specularly reflected radiation from being detected together with the diffusely reflected component. To avoid this, the solid angle into which the incident radiation is specularly reflected should be excluded. Advantageously, irradiation normal to the surface or out of plane configurations are used as depicted in Figure 2.2.

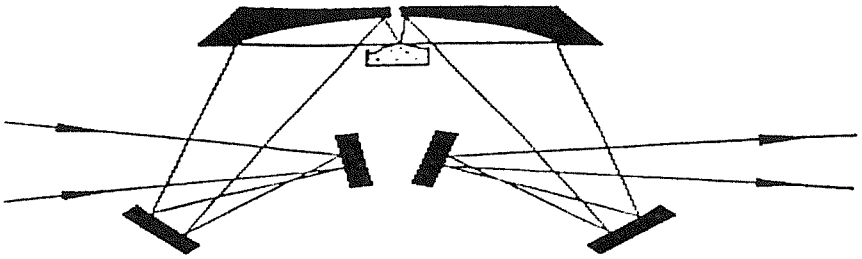

a)

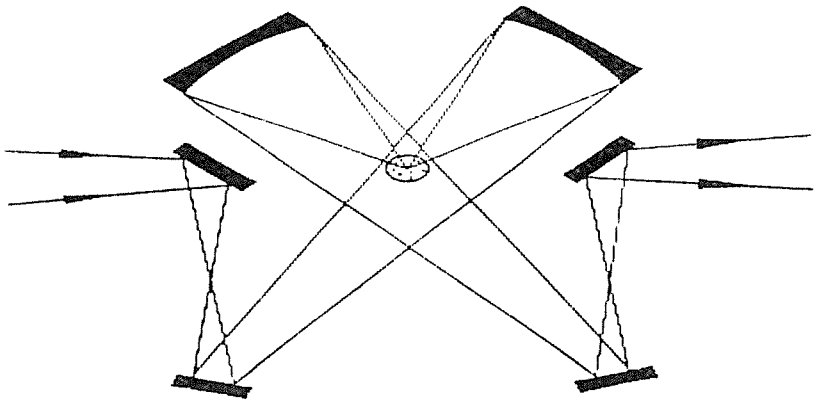

(b)

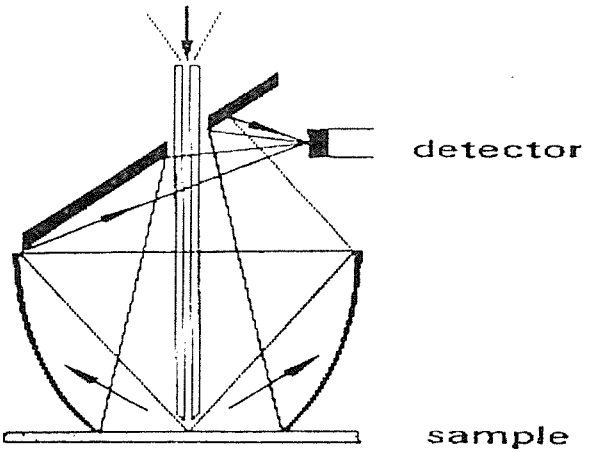

c)

Figure 2.2 :- Optical schemes of different diffuse-reflectance accessories a) in-plane configuration, usable with blocker; b) out-of-plane configuration; c) attachment for large samples.

2.4.1 Experimental for DRIFTS

DRIFTS studies were carried out using a Perkin Elmer 1710 FTIR spectrometer, equipped with a TGS detector and an in-plane configuration for the optical system (Figure 2.2a). The solid samples were loaded into a stainless steel crucible and placed in the DRIFTS cell. In this work, difference spectra were recorded with the modified silica samples as the background before spectra of pyridine loaded samples were obtained. Typically, the number of scans recorded was at least 200 and at 2 or 4 cm^{-1} resolution.

2.5 Determination of the specific surface area, pore size distribution and pore volume

The most widespread method in determining the specific surface area of solid substrates is without doubt the Brunauer-Emmet-Teller (BET) method [2]. Application of the BET method involves the determination and interpretation of an adsorption isotherm, usually that of nitrogen at the boiling point of liquid nitrogen (77 K). Gas adsorption data, if determined under appropriate conditions, may also be employed to provide an assessment of the pore size distribution in the solid. In addition, useful information may be obtained concerning the chemical nature of the solid surface by the analysis of the gas-solid interactions which control the adsorption process. The interpretation of the adsorption isotherm is not always straightforward, however, and it is now evident that the calculation of surface area and pore size distribution is justified only when the adsorption mechanism is adequately characterised.

Adsorption isotherms can be classified into five characteristic types shown in figure 2.3 [3]. Type I isotherms show a fairly rapid rise in the amount of adsorption with increasing pressure up to a limiting value. They are referred to as Langmuir-type isotherms and are obtained when adsorption is restricted to a monolayer. Type II isotherms are frequently encountered and represent multilayer physical adsorption on non-porous solids. They are often referred to as sigmoid isotherms. For such solids, point B represents the formation of an adsorbed monolayer. Type IV isotherms level off near the saturation vapour pressure and are considered to reflect capillary condensation in porous solids. The upper limit of adsorption is mainly governed by the total pore volume. Type III and V show no rapid initial

uptake of gas and occur when the forces of adsorption in the first monolayer are relatively small. These isotherms are rare. Many adsorption isotherms are borderline cases between two or more of the above types.

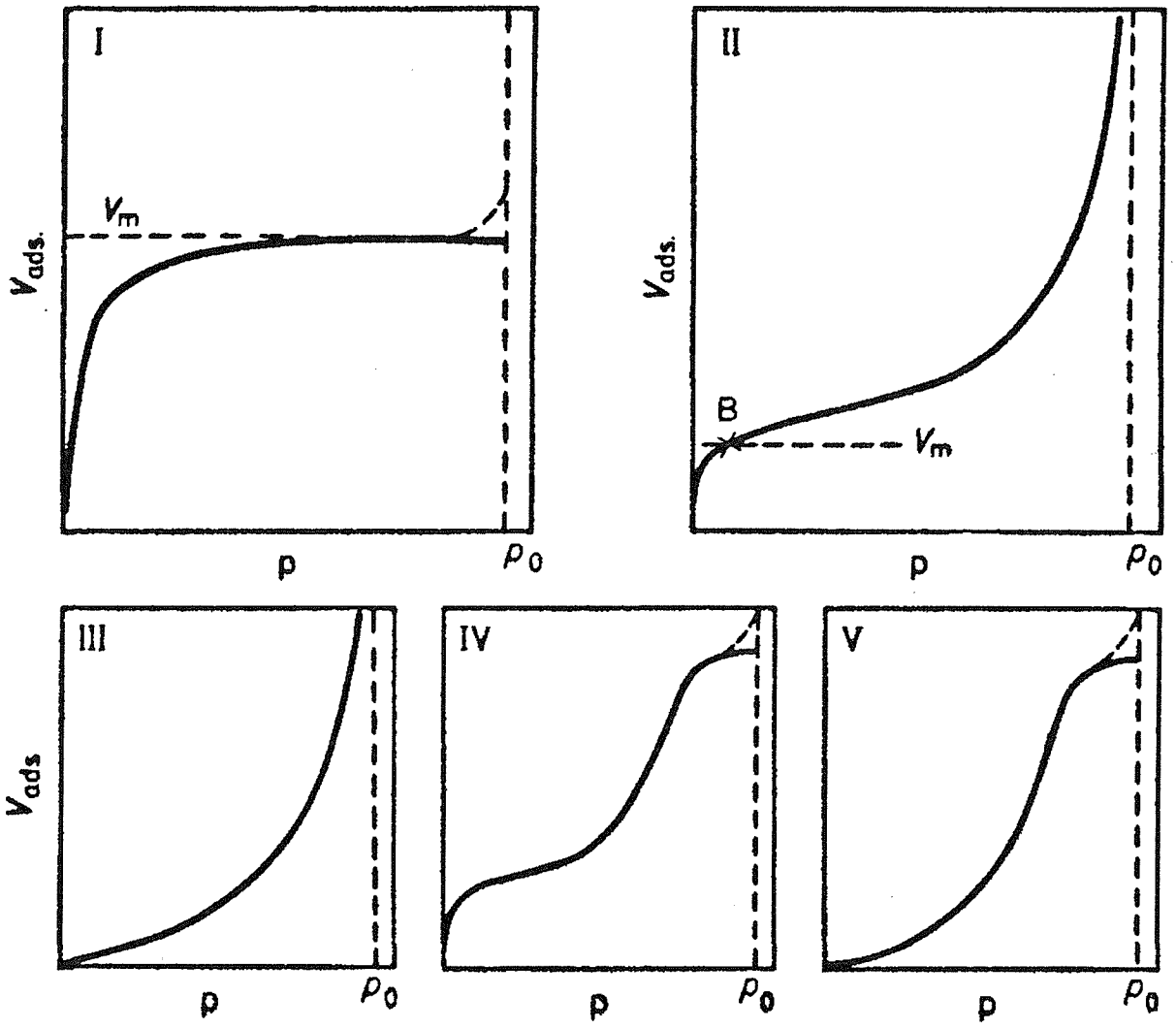

Figure 2.3 :- Brunauer's classification of adsorption isotherms [3]. (p_o = saturated vapour pressure)

By the introduction of a number of simplifying assumptions, the BET theory provides an extension of the Langmuir monolayer model to multilayer adsorption. As with the Langmuir monolayer theory, adsorption of the first layer is assumed to take place on an array of surface sites of uniform energy. Molecules in the first layer then act as sites for multilayer adsorption which, in the simplest case, leads to the development of an infinite number of layers at the saturation pressure, p_o.

Under equilibrium conditions, the rates of condensation and evaporation are equated for each adsorbed layer. It is assumed that the evaporation-condensation constants for all layers above the first are identical and that the corresponding heats of adsorption are equal to the heat of condensation of the adsorptive. Summation of the amount adsorbed in all layers then gives the BET equation, which is usually expressed in the linear form

$$\frac{p}{x(p_o - p)} = \frac{1}{x_m c} + \frac{(c-1)}{x_m c}\frac{p}{p_o} \qquad \textbf{2.2}$$

where x is the amount adsorbed at the equilibrium relative pressure p/p_o, x_m is the monolayer capacity and c is a constant, which is related exponentially to the first layer heat of adsorption. Equation 2.2 demands a linear relation between $p/x(p_o - p)$ and p/p_o. With all known experimental isotherms the range of linearity of the BET plot is restricted to a limited part of the isotherm, usually within the p/p_o range of 0.05-0.30.

In spite of some grounded criticisms e.g. the BET model assumes energetically identical adsorption sites, neglects lateral interactions and assumes identical behaviour in all layers of the multilayer adsorption and the proposal of alternative models, the BET equation has retained its utility. It is a relatively easy approach and the method is applicable to a great variety of adsorption isotherms.

It is obvious that the pores in a solid material are unlikely to be all of exactly the same size. Indeed, the fact that capillary condensation takes place over a range of relative pressure demonstrates that the mesopore volume is distributed over a range of effective pore radius. Many attempts have been made to calculate the pore size distribution from the course of an

adsorption isotherm [4-9]. They are based on different pore models (cylindrical, ink bottle, packed sphere,...). Even the so-called 'modelless' calculation methods do need a pore model in the end to convert the results into an actual pore size distribution. Very often, the exact pore shape is not known, or pores are very irregular, which makes the choice of the model rather arbitrary. The model of Barrett, Joyner and Halenda (BJH) model [2] is based on calculation methods for cylindrical pores. The method uses the desorption branch of the isotherm. The desorbed amount of gas is due either to the evaporation of the liquid core, or to the desorption of a multilayer. Both phenomena are related to the relative pressure, by means of the Kelvin equation.

2.5.1 Experimental for BET surface area measurements

Surface area measurements were determined following the BET method for nitrogen adsorption at 77K, the data being collected with a Micrometric GEMINI III 2375 surface area analyser. The principle of the method is that the precise amount of gas required to cover the surface of a particular sample with a single complete monolayer of adsorbate can be estimated, then the surface area of the material can be calculated if the area occupied by a single adsorbate is known. The sample was placed in a sample tube that was attached to the analyser.

2.6 Theory of Powder X-Ray Diffraction [10-12]

A monochromatic beam of X-rays strikes a finely powdered sample that, ideally, has crystals randomly arranged in every possible orientation. In such a powder sample, the various lattice planes are also present in every possible orientation. For each set of planes, therefore, at least some crystals must be oriented at the Bragg angle, θ, to the incident beam and thus, diffraction occurs for these crystals and planes. The angle at which the beam is diffracted (θ) can be related to d-spacing and the wavelength of the X-rays (λ) by the Bragg equation [13] ($n\lambda=2d\sin\theta$, where n is an integer). A crystal should display diffraction data from each lattice plane which gives rise to the observed 2θ values on the diffraction pattern.

The diffracted beams may be detected either by surrounding the sample with a strip of photographic film or by using a movable detector, such as a scintillation counter.

Powder X-ray diffraction is a technique of use in the characterisation of any material with inherent long range order. It is routinely used for the identification of unknown powders, with the use of a diffraction peak database. It is also widely used for ascertaining the purity of a compound with respect to any other diffracting phase. Each crystalline phase has a characteristic powder pattern which can be used as a fingerprint purposes. The two variables in powder pattern are peak position, i.e. d-spacing, which can be measured very accurately if necessary, and intensity, which can be measured either qualitatively or quantitatively. However, it is by no means a straightforward exercise to obtain reliable powder X-ray intensity data. Sample preparation is very important as it may be difficult if not impossible to avoid preferred orientation of crystals within the powder specimen. Powder should be ground down, preferably to size of 1 to 10 μm, and it may be worthwhile to sieve samples prior to X-ray diffraction. One or two large (e.g. 1 mm) diameter crystals in an otherwise fine powder can cause havoc with intensity measurements. Intensities are normally measured by diffractometry, as peak heights or peak areas at slow scanning speeds.

2.6.1 Experimental of Powder X-Ray Diffraction

The technique involves a beam of X-rays being directed onto finely powdered sample mounted in a flat aluminium holder. Copper $K_{\alpha 1}$ radiation is provided by an X-ray tube fitted with a primary monochromator. The radiation is collimated through an aperture diaphragm onto the sample and will be diffracted according to which plane of the crystal it strikes. The powder X-ray diffraction patterns were recorded on a Siemens θ-2θ D5000 diffractometer and the diffracted beam is detected with a scintillation counter in which the counter is scanned across the diffraction pattern in a conventional diffractometer. The diffraction is continuously transferred onto a computer where a plot of diffracted intensity (counts/s) is plotted against the angle 2θ is displayed. The schematic representation of Siemens D5000 diffractometer is shown in figure 2.4.

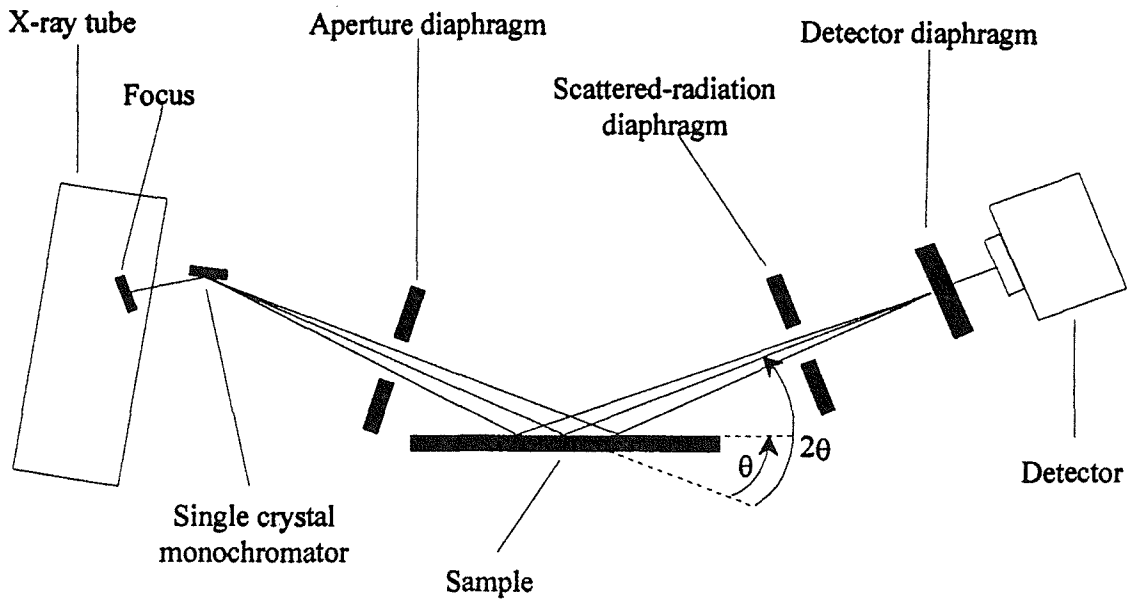

Figure 2.4 :- Schematic representation of Siemens D5000 diffractometer.

2.7 Electron Microscopy

Scanning electron microscopes are useful for displaying images of surface structures, which are generated by secondary electrons. The transmission electron microscope relies on the primary electrons passing through the specimen to give high resolution images of internal structures of samples (which must be less than 1×10^{-7} μm thick).

The incident electrons are usually generated by passing an electric current through a tungsten filament at the top of a column. A voltage, usually in the range 300 V to 40 kV, is applied between the electron source (the cathode) and the rest of the column (the anode). This voltage accelerates the electrons down the column, towards the specimen.

Secondary electrons are usually used to provide the image in SEM and this type of electron is generated as a result of inelastic scattering of the incident electrons. Secondary electrons are useful for high resolution imaging. They are attracted by a grid, typically set at +200 to +600 V potential, in front of a scintillation detector. They are further accelerated by a

potential of about 10 kV onto the scintillation detector surface, where their energy is converted to visible light. The light emitted passes down a perspex light guide to a photomultiplier tube where it is converted to an electrical current. This signal can be amplified to produce an image on a cathode ray tube (a television screen). A large number of secondary electrons results in a bright image on the screen.

The electron beam used in TEM is typically generated at 100-200 kV affording a resolution of 0.2 nm and a magnification of 1×10^6. On passing through a specimen, the primary electrons may be transmitted without being deflected or elastically scattered or inelastically scattered (losing energy). The image formed by the TEM is produced by the transmitted electrons which helps form a bright field image. Scattering of the primary electrons of the beam by the specimen gives rise to the contrast in this image. This image darkens when the inelastic scattering increases which occurs when the mean atomic number and thickness of the sample increases. A dark field image can also be produced by selecting a diffracted beam rather than the transmitted beam which is not deflected. Once the electron beam has been passed through the specimen it is magnified and focused by an image forming electromagnetic lens (the objective lens). It then strikes a fluorescent screen where the energy of the electrons is converted to visible light, forming an image. Alternatively, the screen can be replaced by a camera so that a photographic image is recorded.

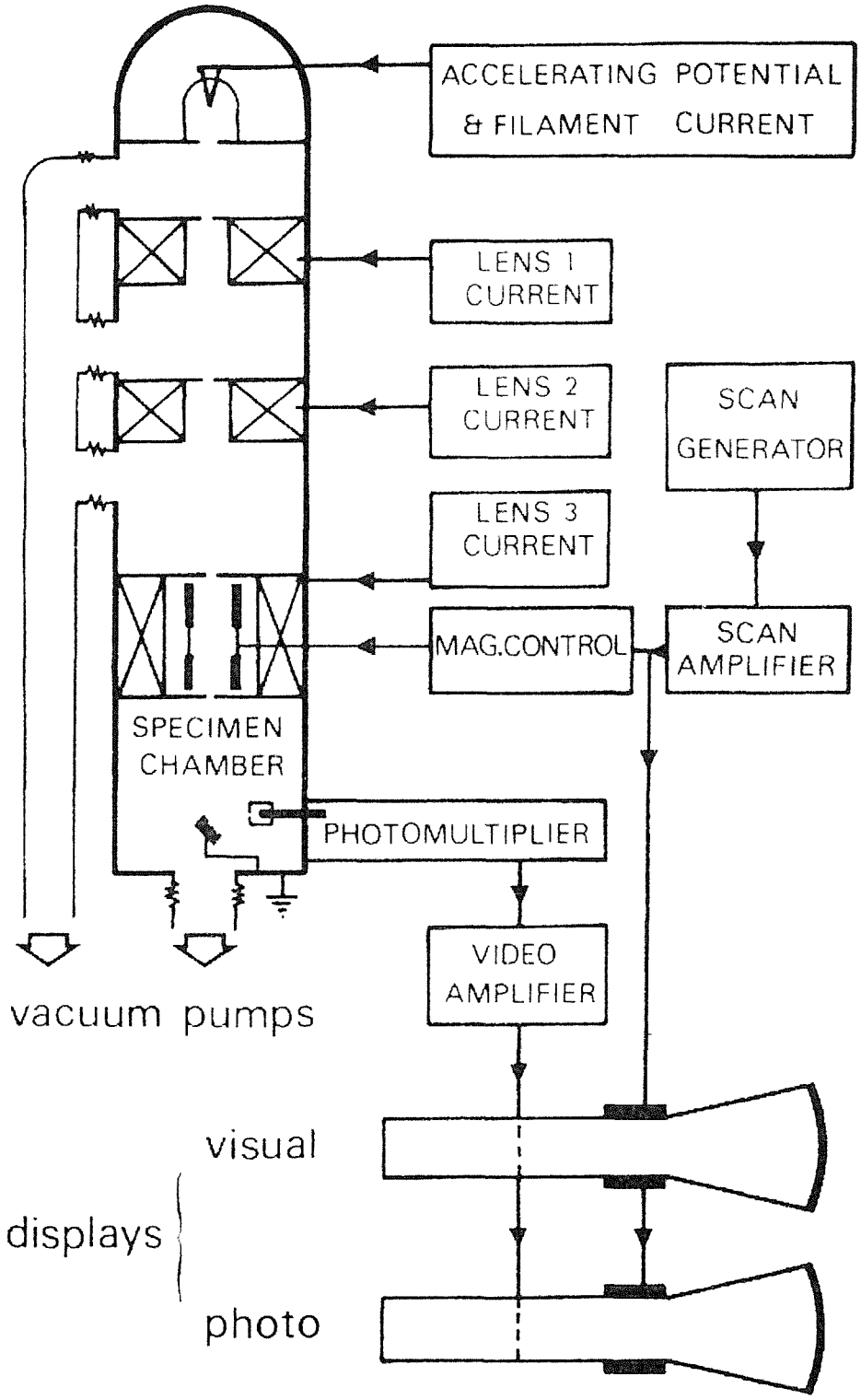

Figure 2.5 :- Schematic diagram of a scanning electron microscope. The details (for example, the number of lenses) vary between different manufacturers.

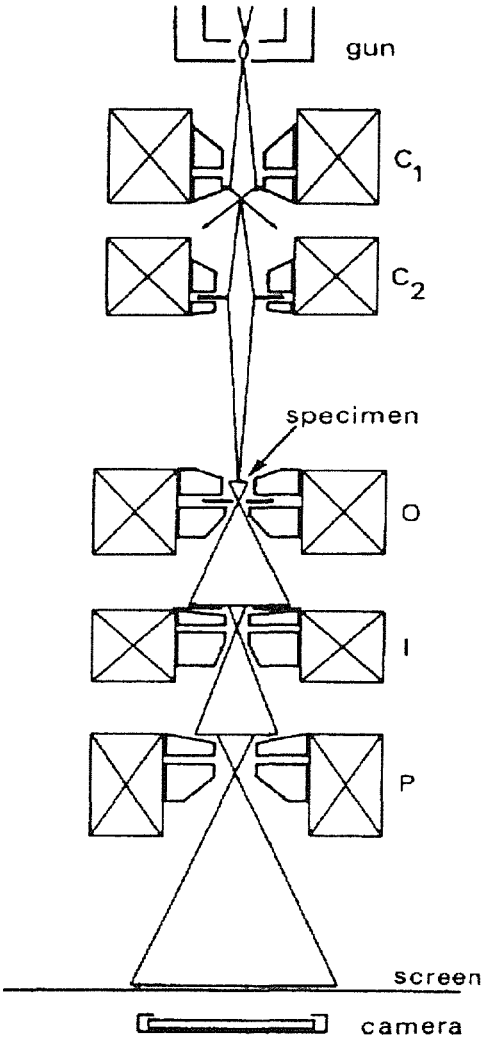

Figure 2.6 :- A schematic representation of the layout of the main components of a typical transmission electron microscope. The electron gun is at the top of the column and C_1 and C_2 are the two condenser lenses. The second condenser lens has a variable aperture. The specimen sits in a holder that is inserted into the microscope through the airlock which lies between the second condenser lens and the objective lens O. This lens also has a variable aperture and there is another variable aperture in the object plane of the intermediate lens I. The projector lens P forms the final image on the fluorescent screen, which is observed through a glass window in the column. A plate or film camera below the screen enables the image to be recorded.

2.7.1 Experimental of Electron Microscopy

SEM images were obtained with JEOL scanning electron microscope. Solid samples were crushed and mounted on aluminium stubs. Silica samples which are non-conductors of electricity have to be treated before they can be studied with the SEM. A plasma of gold ions is sputtered onto the sample at very low pressure and a thin film of gold forms on its surface. This coating inhibits image distortion by sample charging, and does not normally affect surface detail because the gold coating can only be detected at relatively high magnifications. Gold is often used because it is an excellent electrical conductor and being a heavy metal, has a high secondary and back scattering electron yield.

TEM images of silica samples were carried out on a JEOL FX 2000 transmission electron microscope. The samples were prepared as follows. A small amount of sample (typically 10^{-4} g) was crushed with a pestle and mortar for *ca.* 5 minutes. Then the sample was transferred to a sample vial and distilled water was added into the vial. The closed sample vial which contains the silica sample suspension is then placed in an ultrasonic bath and left for ca. 5 minutes. A small drop of the fine suspension (always taken from the top of the tube) is dropped onto a copper disc with a fine carbon grid. The sample was then left to evaporate depositing the silica sample onto the copper disc/carbon grid.

2.8 Solid State NMR

The development of NMR spectroscopy of solids has been much slower than that of fluids, because of three major difficulties (for spin ½ nuclei), all associated with the immobility of the nuclei in solids. However, advances have been made which make it possible to obtain high resolution spectra, more or less routinely, and so the potential of NMR for solving structural problems can be applied to solid materials.

The first major difficulty with solids is that dipolar couplings are not averaged to zero by molecular tumbling, and that long range couplings are also important because the material is not fluid. The combined effect of the many couplings is to give very broad resonances, often tens of kHz wide. Secondly, the chemical shift of a nucleus depends on the orientation of the molecule with respect to the magnetic field, and in solids the effect of this chemical shift anisotropy is not averaged out by molecular tumbling, and so leads to line broadening, again of thousands of Hz. Finally, again because of the immobility of the nuclei, the relaxation time T_1 is very long, and this means that multipulse methods are not very efficient. It is therefore very difficult to get spectra with good signal to noise ratios. The difficulties mentioned are only for the case where the spin of the nuclei is ½. If the nuclear spin is greater than ½, there are also quadrupolar splittings from the varying orientation of the nucleus with the electric field gradient at the nucleus.

Several methods are available that can decrease band broadening in solids. Use of one or more of the methods can result in nmr spectra of solids that are nearly as well resolved as those of liquids. Nearly all anisotropic effects can be eliminated by rapidly rotating the sample in the magnetic field. Dipolar interactions between two nuclei are proportional to $3\cos^2\theta-1$. Consequently, anisotropic effects can be eliminated by spinning the sample at an angle θ, relative to the magnetic field, at which $3\cos^2\theta-1=0$. That angle is 54°44' and is termed the magic angle. The technique by which the sample is rotated in the magnetic field at the magic angle is magic angle spinning (MAS).

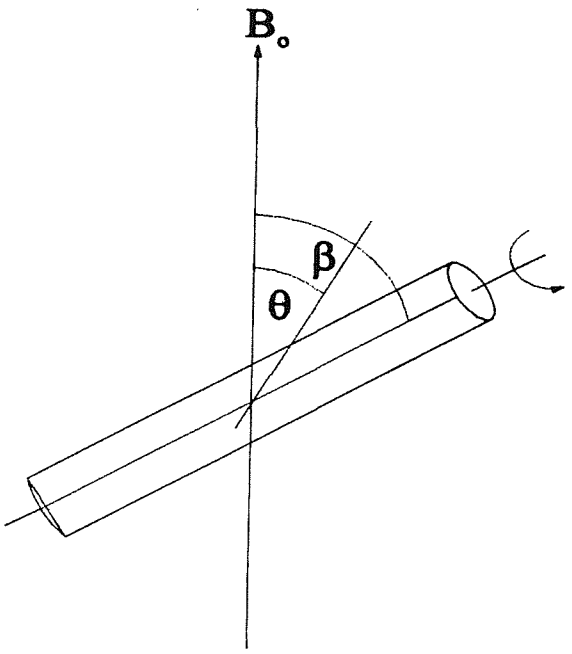

Figure 2.7 :- The magic angle at β= 54°44' to the applied magnetic field B_0.

Double resonance can be used to cause spin decoupling in solids. For studies of nuclei in solids at low concentration or weakly magnetic nuclei, cross polarisation (CP) is valuable. Cross polarisation is a technique for transferring magnetism from a relatively abundant nucleus, such as protons, to a less abundant nucleus, such as ^{13}C. It is often used in combination with MAS to provide structural information from ^{13}C NMR data on solids. Cross polarisation shortens the spin-lattice relaxation time in solids and allows multiple Fourier transform spectra to be obtained in a reasonable time. CP differs from most NMR methods in that it uses a pulse rather than a continuous wave (CW). The entire spectral range is simultaneously recorded as a function of time after each pulse instead of recording the spectrum by scanning the magnetic field or the radio frequency separately.

2.8.1 Experimental of Solid State NMR

All the modified silica samples were sent to Industrial Research Laboratories, University of Durham for MAS NMR analysis. All the NMR spectra were recorded on a Varian UNITY *plus* with a 7.05 T Oxford Instruments magnet. The resonance frequency for hydrogen is 300 MHz.

The ^{1}H, ^{13}C and ^{29}Si chemical shifts are reported relative to tetramethyl silane ($Si(CH_3)_4$). ^{31}P chemical shifts are reported relative to 85% H_3PO_4.

2.9 Temperature Programmed Desorption (TPD) with a Plug Flow Microreactor

The weight of the modified silica charge, typically ~20mg, is loaded into the centre of a 200mm long quartz tube with an internal diameter of 3mm. The powdered sample is held in place with two plugs of quartz wool, to give a catalyst bed length of 8-10mm. On each end of the quartz tube is glued a ⅛" push on fitting. This allows the tube to be attached to the gas line without the need for screw threads, which would result in frequent breakage of the brittle quartz. One end is attached to the outlet from the solenoid valves, and through the other a type K thermocouple is simultaneously introduced to the centre of the catalyst bed as the seal with the second push on fitting is made.

The vast majority of the gas exiting from the reactor bed passes out through the flow meter, and the total gas flow may be determined in this way. However, a proportion of the gas effluent may be allowed to enter the UHV chamber via the stainless steel capillary and the leak valve, where its composition can be analysed with the use of the mass spectrometer.

All couplings and tubing throughout the system are of minimum volume. For example, 1/16"fittings are used wherever possible; the stainless steel capillary is of 0.25mm internal diameter and is coupled to the reactor bed exit via a zero volume T-piece. This is done in order to minimise the dead volume of the microreactor, and thus reduce the extent to which a short pulse of gas entering the catalyst bed will lose time resolution as it travels through

the system and into the mass spectrometer analyser. The capillary is differentially pumped, to prevent poor conductance through it increasing the response time of the mass spectrometer. The result is that a two-second pulse, at a total gas flow of 20ml/min, has a peak width at half peak height of approximately 20 seconds at the mass spectrometer.
The mass spectrometer used is a Fisons Quartz 200AMU VG quadrupole instrument. There are two different methods available for the detection of ions. The simplest of the detectors is the Faraday plate. Ions exit the mass analyser, pass through a collimating slit, and strike a metallic plate. The current caused by this ionic bombardment is converted to a potential, amplified electronically, and transmitted to the readout device. The Faraday plate has the advantages of being very simple and dependable. The second detector available is an electron multiplier. This is based on a dynodic strip, where a potential difference is maintained across the strip by a regulated power supply. The potential drop across the strip is typically about 2kV. Ions from the analyser bombard the cathode at one end of the strip, inducing the emission of electrons. A magnetic field is used to direct the emitted electrons in a cycloidal path back towards the dynodic strip. Upon striking the strip, the current is further amplified by the emission of several electrons for each impinging electron. The process is repeated many times along the length of the strip toward the anode, where the resulting current flow is monitored on an external circuit. The electron multiplier is the more sensitive of the two detectors, and has routinely been the detector of choice throughout this work.

The heating system for this microreactor is a simple arrangement of twelve ¼", 75W cartridge heaters inserted into a brass block. The brass block is actually in two pieces that are screwed together, with a groove cut in each half to accommodate the quartz tube. A ceramic insulating hood is then placed over the block to reduce temperature fluctuation on heating, and allow higher temperatures to be achieved. An Eurotherm 902 series temperature controller is used to control the power output to these heaters, in order to achieve the desired heating rate. A maximum catalyst bed temperature of approximately 700°C is obtainable.

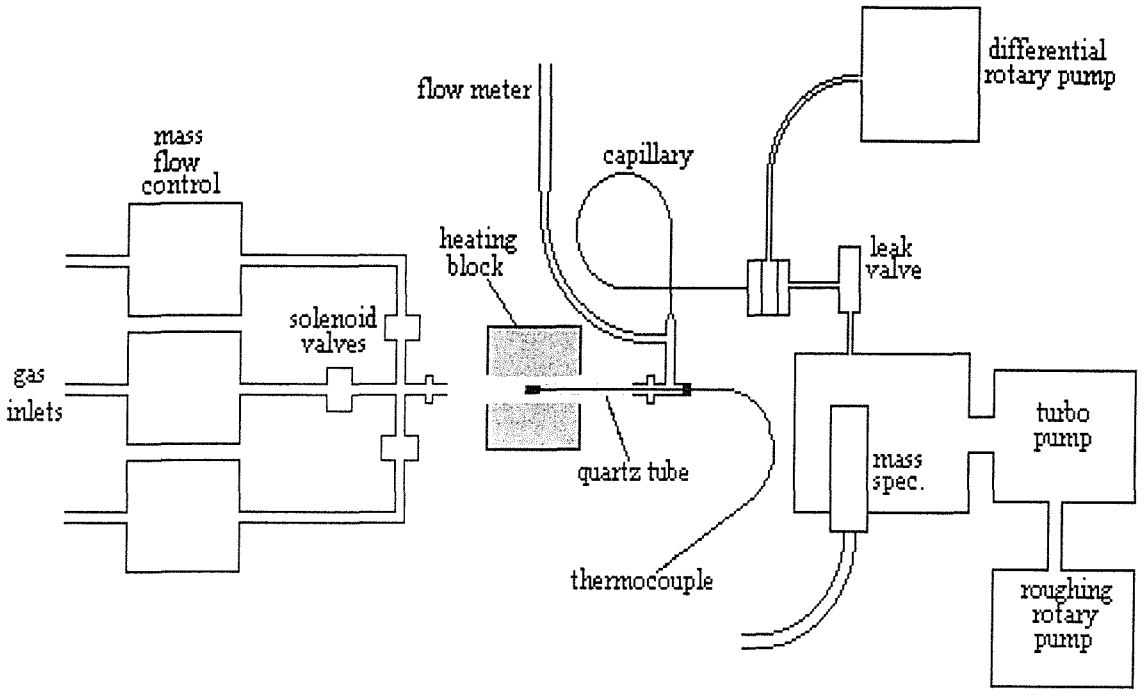

Figure 2.9 :- A schematic diagram of a plug flow microreactor system

References

[1] E.H.Korte, *Appl.Spectrosc.*, **42**, 428, 1988.

[2] S.Brunauer, P.H.Emmett, E.J.Teller, *J.Am.Chem.Soc.*, **60**, 309, 1938.

[3] S.Brunauer, *Physical Adsorption of Gases and Vapours*, Oxford University Press, 1944.

[4] D.Dollimore, G.R.Heal, *J.Colloid Interface Sci.*, **42**, 57, 1973.

[5] C.Pierce, *J.Phys.Chem.*, **57**,149,1953.

[6] E.P.Barrett, L.G.Joyner, P.P.Halenda, *J.Am.Chem.Soc.*, **73**, 373,1951.

[7] M.M.Dubinin, *Zh.Fiz.Khim.*, **30**, 1652, 1956.

[8] C.G.Shull, *J.Am.Chem.Soc.*, **70**, 1405, 1948.

[9] M.Kruk, M.Jaroniec, *Langmuir*, **13**, 6267, 1997.

[10] G.H.Stout, L.H.Jensen, *X-Ray Structure Determination, A Practical Guide*, MacMillan, New York, 1968.

[11] M.M.Woolfson, *An Introduction to X-ray crystallography*, Cambridge University Press, 1970.

[12] P.H. Klug, L.E.Alexander, *X-ray Diffraction Procedures for Polycrystalline and Amorphous Materials*, John Wiley and Sons, New York, 1974.

[13] A.K.Cheeham, P.Day, *'Solid State Chemistry Techniques'*, Oxford University Press, 1988.

Chapter 3

Synthesis and Characterisation of the Silica Supports

3.1 Introduction

Silica is probably the most widely employed oxide in catalysis; two forms, gels and sils, differ in their morphology [1]. The former are highly porous materials, and probably are less suitable for surface organometallic chemistry. There is a doubt over the accessibility of large organometallics to pores and also some metal cations can be present as contaminants from the hydrolysis procedures used in their production. Sils, on the other hand, are essentially non porous and derive their high surface areas from small particle sizes [2] (5-40 nm diameter); generally they are also of higher purity, with some residual chloride (from the $SiCl_4$ precursor) being the most likely contaminant.

Since 1957, the surface hydroxyl groups of these silica supports have been characterised and analysed by numerous studies especially using infrared spectroscopy [3,4]. This study has been repeated more recently by Morrow *et al* [5] and has shown that degassing silica under vacuum during 6 hours could create new active sites on the silica surface, strained siloxane bridges acting as a weak Lewis acid centres. Their reaction with organosiloxanes, organosilanes and water has been studied [6]. Silica gel and its various active sites have also been characterised by solid state ^{29}Si NMR [7,8,9] and quantification of surface hydroxyl groups has been determined [10] using chemical modification with trichlorosilane.

The ultimate particles which make up the silicas can be regarded as polymers of silicic acid, consisting of interlinked SiO_4 tetrahedra. At the surface, the structure terminates in either a siloxane group (Si-O-Si) with the oxygen on the surface, or one of several forms of silanol groups (Si-OH). The silanols can be divided into isolated groups (or free silanols), where the surface silicon atom has three bonds into the bulk structure and the fourth bond attached to a single OH group (cf. figure 3.1I), and vicinal silanols (or bridged silanols), where two single silanol groups, attached to different silicon atoms, are close enough to hydrogen bond (cf. figure 3.1II). A third type of silanols, geminal silanols, consist of two hydroxyl groups, that are attached to one silicon atom (cf figure 3.1.III).

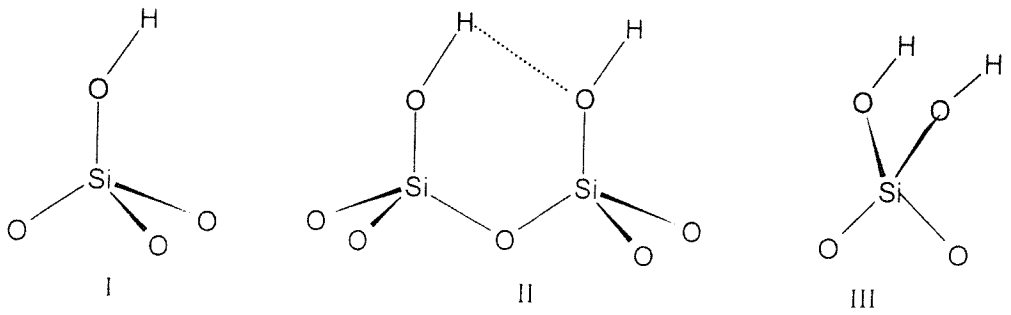

Figure 3.1 :- Three different types of silanol groups on the silica surface: isolated silanols(I), vicinal silanols or bridged silanols(II) and geminal silanols(III).

The inorganic supports that were chosen for this study is an amorphous silica, Aerosil 200, produced by Degussa AG [11] and a mesoporous silica prepared using the method proposed by Attard *et al* [12]. Before modifying and using these silica materials, it is important to have a clear understanding of their structure and dimensions, since once the materials have been modified, they become even more complex in nature. Various characterisation techniques are utilised including methane gas titration, PXRD, BET surface area measurements, TEM, SEM, ^{29}Si MAS NMR and IR spectroscopy.

3.2 Experimental

3.2.1 Pretreatment of silica, Aerosil 200

Presented as white fluffy powder, Aerosil 200 silica contains surface impurities and hydroxyl groups and, therefore, to eliminate the former and control the latter, it is calcined overnight under a flow of oxygen before its utilisation. Aerosil 200 was placed in two procelain boats inside a quartz tube and calcined under oxygen at 480°C overnight. Then, it was transferred to a Schlenk tube and dehydroxylated under vacuum at 480°C for at least 6 hours in a high temperature oven. The silica was kept under N_2.

3.2.2 Preparation of mesoporous silica, H_1SiO_2

Mesoporous silica, H_1SiO_2 was prepared according to the literature [12]. Typically Brij 76 ($C_{18}H_{37}(OCH_2CH_2)_nOH$, n~10, 10g) and tetramethoxysilane (TMOS, 20g) were first weighed into a round bottom flask. The composition ratio of the chemicals used were 1:2:1 for Brij 76, TMOS and diluted HCl (10g) respectively .The pH of the diluted HCl was adjusted to ~1.3. After making sure the Brij 76 was completely dissolved in HCl, the mixture obtained was then evaporated under vacuum for about 20-30 minutes to remove the methanol generated in the reaction. After rotary evaporation, the mixture was left in the oven for 24 hours at ~40°C. Finally, calcination was carried out under N_2 gas for 3-4 hours, followed by calcination under O_2 gas for 8 hours at 470°C. The mesoporous silica was vacuum dehydrated at 300°C for 4 hours before use. The silica was kept in the dessicator.

3.2.3 Titration of hydroxyl groups on the silica surface by a Grignard method

The principle of this method followed that used by BP Chemicals was to measure the pressure of the CH_4 evolved during the following reaction, where the hydroxyl groups react stoichiometrically with the Grignard reagent:

$$\text{Si-OH} + \underset{\text{excess}}{CH_3MgBr} \longrightarrow CH_4 + \text{Si-OMgBr} + \Delta \qquad \textbf{3.1}$$

The apparatus employed was a round bottom flask with a manometer on top. Details of the experimental set up for this titration are given in chapter 2. The silica sample was loaded in a glove box and after addition of butyl ether (10ml) and methylmagnesium bromide (5ml, 5mmol), an important stirring was maintained within the round bottom flask. However, before proceeding to the titration, a calibration of the manometer CG 16K from Edwards has been carried out using methanol such as:

$$\text{Me-OH} + \underset{\text{excess}}{CH_3MgBr} \longrightarrow CH_4 + \text{Me-OMgBr} + \Delta \qquad \textbf{3.2}$$

3.2.4 Calibration of the manometer CG16 from EDWARDS

With reference to the above equation 3.2, the formula used for this particular reaction was the following:

$$n_{CH3MgBr} = (P_e - P_o)*(V_{tot} - V_{methanol} - V_{gri})/(RT)$$

Using different theoretical amounts of Grignard (3.0 ml, 2.0 ml and 5.0 ml) these amounts can be calculated from the CH_4 partial pressures resulting from the experiment. The results of this titration are presented in the following table.

	N_{gri} = 3.0 mmol	N_{gri} = 2.0 mmol	N_{gri} = 5.0 mmol
Temperature	293 K	292 K	293 K
CH_4 partial pressure	240 mbar	170 mbar	390 mbar
amount of Grignard	(3.2 ± 0.2) mmol	(2.3 ± 0.2) mmol	(5.1 ± 0.2) mmol

As a conclusion, the pressures measured during the experiment, after calculation, were found to correspond to the starting amount of Grignard added. Therefore, the manometer can be seen to suit the actual titration.

3.2.5 Principle of calculation of the hydroxyl group concentration by a Grignard method.

From the reaction (3.1),

$n_{OH} = n_{CH4}$

$C_{OH} = n_{OH} / m_{silica}$

Ideal gas equation,

$n = PV / RT$

Therefore,

$C_{OH} = n_{CH4} / m_{silica} = P_{CH4}V / RTm_{silica}$

Where

$P_{CH4} = P_e - P_o$ and $V = V_{tot} - V_{gri} - V_{solv} - V_{silica}$

I.e.

$C_{OH} = (P_e - P_o)*(V_{tot} - V_{gri} - V_{solv} - V_{silica})/ (m_{silica} * RT)$

Moreover

$V_{silica} = m_{silica} / \rho$

Therefore

$$C_{OH} = (P_e - P_o) * (V_{tot} - V_{gri} - V_{solv} - m_{silica} / \rho) / (m_{silica} * RT) \quad \textbf{3.3}$$

Where

C_{OH}, in $mol.kg^{-1}$

P_o, the pressure observed on the manometer before the injection of Grignard has been done (in bar)

P_e, pressure when equilibrium is reached (after 12 minutes) in bar

V_{tot} of the apparatus is 330 ml = $330*10^{-6}$ m^3 (where 160 ml is the internal volume of the manometer and 170 ml is the glassware volume measured)

V_{gri}, volume of Grignard reagent injected (5 ml of CH_3MgBr in butyl ether, 5mmol)

V_{solv}, volume of solvent injected (10 or 15 ml of butyl ether)

m_{silica}, the mass of silica weighed in the glove box (in kg)

ρ, the density of the silica (2300 $kg.m^{-3}$)

R = 8.10047385 * 10^{-5} $bar.m^3.mol^{-1}.K^{-1}$

T, the starting temperature (at equilibrium T is reached again)

3.2.6 Calculation of the systematic error due to this titration [13].

Considering equation 3.3, the relative standard deviation of the hydroxyl groups amount is given by the following equation:

$$\delta n_{OH}/n_{OH} = \sqrt{((\sqrt{(\delta P_e^2 + \delta P_o^2)}/(P_e - P_o))^2 + (\sqrt{(\delta V_{tot}^2 + \delta V_{solv}^2 + \delta V_{gri}^2 + (\delta m_{silica}/\rho)^2)}/ (V_{tot} - V_{solv} - V_{gri} - m_{silica}/\rho) + (\delta T/T)^2 + (\delta m_{silica}/m_{silica})^2)}$$

Where

$\delta P_e = \delta P_o$, the standard deviation of the pressures read on the manometer

δV_{tot}, the standard deviation due to the measurement of the total volume of the apparatus

$\delta V_{solv} = \delta V_{gri}$, the standard deviation due to the syringes

δm_{silica}, the standard deviation due to the weight of the silica in the glove box

δT, the standard deviation for the temperature

The errors due to the gas titration method are *ca.* 3-5 % for a standard pressure change. However, the error is inversely proportional to the concentration in hydroxyl groups. When samples have a low hydroxyl group content, the pressure difference read is small implying a major error on this value, the error due to the method then increases to ca. 15 %.

3.3 Results and Discussion

3.3.1 Grignard Titration

Since the discovery of surface hydroxyl groups on silica in 1936, many studies on the quantification of the silanol number (α_{OH}:number of hydroxyl groups per nm^2) and on the characterisation of the different hydroxyl types have been published [14,15]. The studies can be divided into theoretical calculations, physical methods and chemical methods. For physical methods, infrared spectroscopy [16] is the most commonly applied technique for monitoring and controlling the surface hydroxylation of silica. Chemical methods are generally based on the reaction of surface hydroxyl groups with a selectively reacting compounds to form covalently bonded surface species of well known composition. As

reactive compounds, diborane, boron trichloride, diazomethane, organosilanes and organometallic compounds have been employed. The number of hydroxyl groups per nm^2 is then derived from the amount of the chemisorbed species as well as the amount of volatile reaction products.

In this work, a chemical method, a Grignard titration is employed. The titration proceeds by reaction of methylmagnesium bromide with the surface hydroxyls, which generates one mole of methane per mole of hydroxyl groups. The pressure of the evolved methane is measured, and this value can be used to determine the number of moles of hydroxyl groups in a given mass of silica. If the surface area of the silica is known, then this may be used to generate the number of hydroxyl groups per nm^2. The hydroxyl concentrations were calculated for both types of silica, Aerosil 200 and H_1SiO_2.

The results are displayed in Table 3.1 and 3.2 respectively.

Table 3.1 :- Grignard titration results for Aerosil 200, calcined and vacuum dehydroxylated at 480°C.

Titration number	1	2	3
Mass silica weighed	0.930 g	0.875 g	0.820 g
Volume solvent	15.0 ml	15.0 ml	15.0 ml
Volume Grignard(1M)	5.0 ml	5.0 ml	5.0 ml
Temperature	291 K	291 K	291 K
Partial pressure observed	90 mbar	80 mbar	80 mbar
OH concentration	(1.2±0.1) mol/kg	(1.2±0.2) mol/kg	(1.2±0.2) mol/kg
OH surface content	(3.8±0.2) OH/nm^2	(3.5±0.3) OH/nm^2	(3.8±0.3) OH/nm^2

Table 3.2 :- H_1SiO_2 vacuum dehydrated at 300°C for 3-4 hours.

Titration number	1	2	3
Mass silica weighed	0.550 g	0.610 g	0.600 g
Volume solvent	10.0 ml	10.0 ml	10.0 ml
Volume Grignard(1M)	5.0 ml	5.0 ml	5.0 ml
Temperature	293 K	291 K	291 K
Partial pressure observed	80 mbar	90 mbar	90 mbar
OH concentration	(1.9±0.2) mol/kg	(2.1±0.2) mol/kg	(2.2±0.2) mol/kg
OH surface content	(1.7±0.4) OH/nm^2	(1.9±0.4) OH/nm^2	(1.9±0.4) OH/nm^2

The wall structures of mesoporous silica is thought to be amorphous [17]. Therefore, it is not unexpected that the surface chemistry of siliceous H_1SiO_2 is similar to that of silica. All SiOH groups, i.e. single, hydrogen bonded and geminal SiOH groups, which could be observed on silica surfaces are also observed on H_1SiO_2 surfaces. However, from the results reported here, the number of SiOH groups/nm^2 over H_1SiO_2 surface is ~2, which is far less than on Aerosil 200 (~4/nm^2) in spite of the lower dehydroxylated temperature used in H_1SiO_2 pretreatment. This difference is expected since H_1SiO_2 is better ordered than amorphous silica and therefore a highly condensed surface with less SiOH groups.

3.3.2 Transmission Electron Microscopy

Shown in figure 3.2 (top) is representative TEM image of Aerosil 200 and the TEM images for mesoporous silica H_1SiO_2 are shown in figure 3.2 (bottom) and figure 3.3. It is evident from the TEM micrograph that particles of Aerosil 200 are essentially non porous and small "ultimate" particles attached together to form chains are observed. In reference [2], high resolution electron micrograph of Aerosil 300 could be interpreted as of overlapping plates. The range of the particle size has been showed to be in the region of 10-40 nm in diameter [2,18].

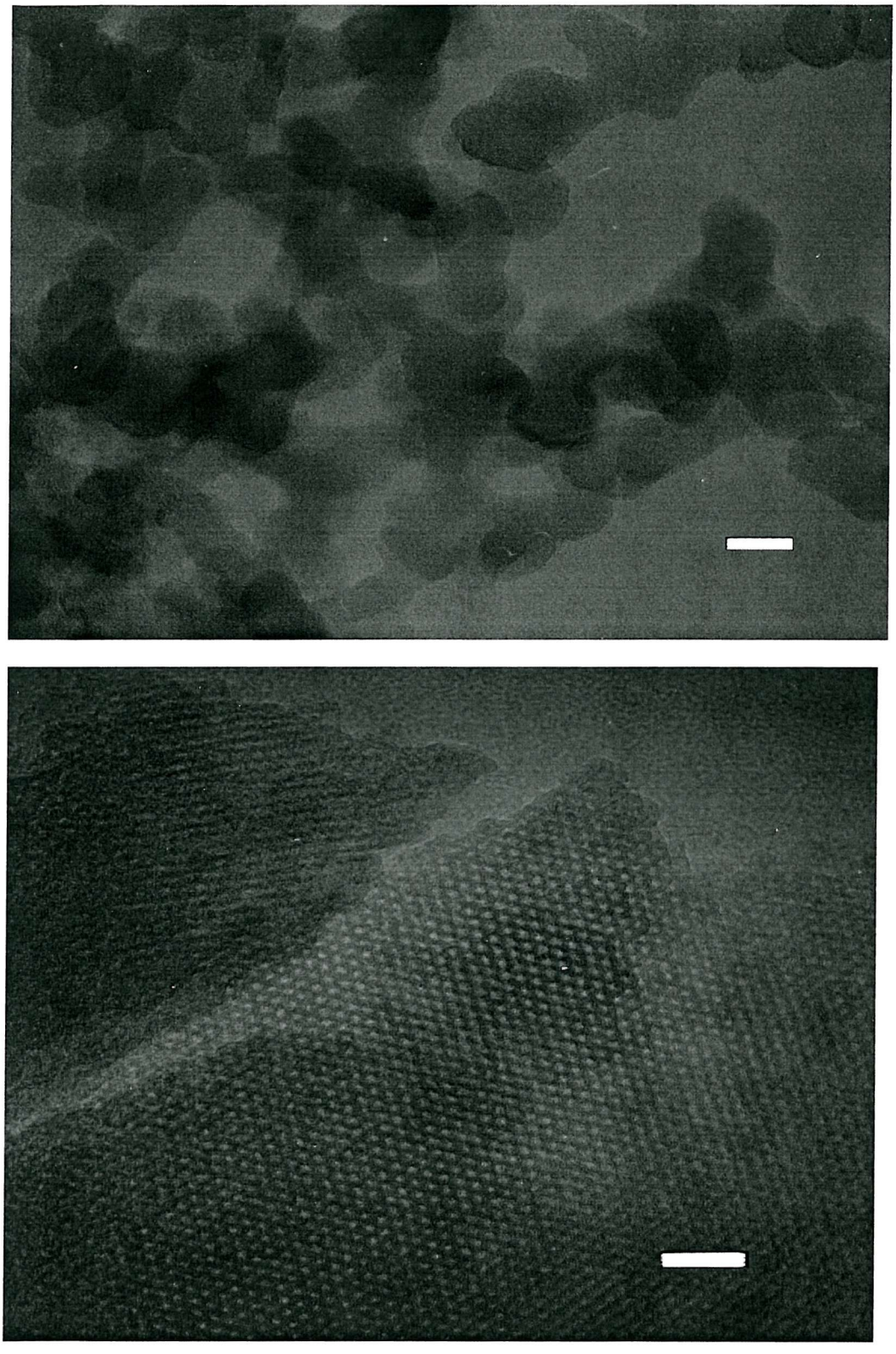

Figure 3.2 :- TEM image of Aerosil 200(top) and H_1SiO_2 (bottom), showing the hexagonal pore structure(bottom). Scale bar = 20 nm

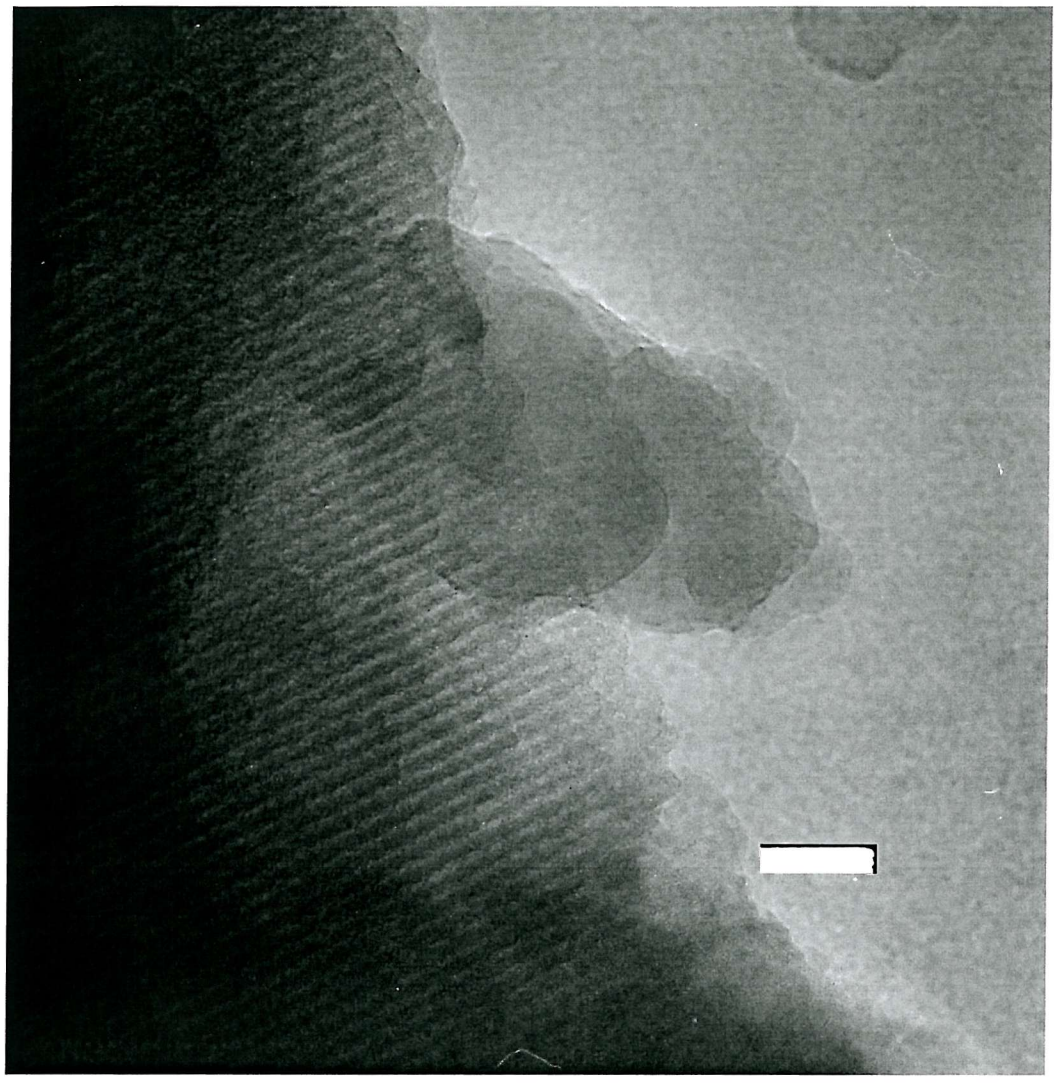

Figure 3.3 :- TEM image of H_1SiO_2 showing the equidistant parallel lines. Scale bar = 20 nm.

To elucidate the pore structure of mesoporous materials, transmission electron microscopy is commonly used. Figure 3.2 (bottom) shows a TEM image of the hexagonal arrangement of uniformly sized pores of a sample of H_1SiO_2. Equidistant parallel lines observed in figure 3.3 are shown to be related to the hexagonal repeat between tubules. The honeycomb array is sufficiently regular to give fringes in projection under proper orientation of the specimen. A schematic drawing of parallel channels is given in figure 3.4.

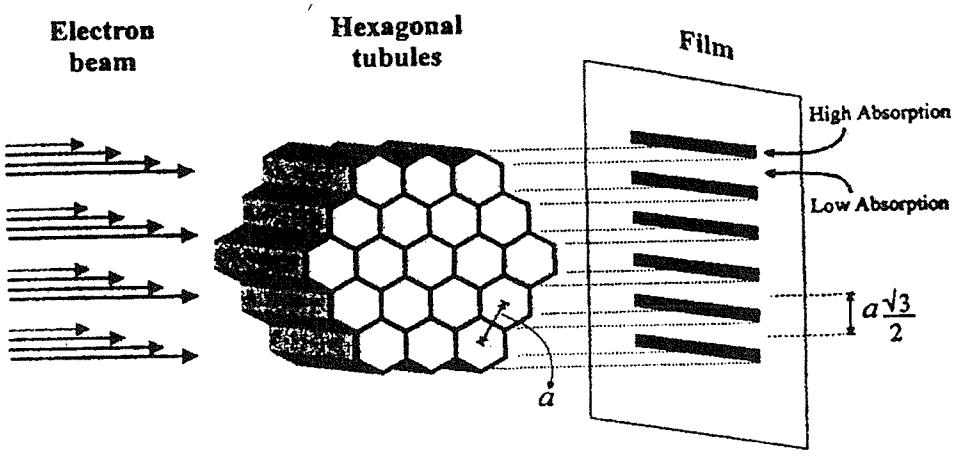

Figure 3.4 :- Schematic model showing apparent "lamellar structure" from a projection of a hexagonal array of tubules.

With TEM, the image contrast in a non crystalline sample below atomic resolution arises from differences in transmission caused by interaction with a different number of atoms in the path of electrons. With this model, the aspect of micrographs will depend on the orientation of the channels with respect to the electron beam direction. A lamellar appearance is expected for beam directions in the plane defined by the perpendicular to one family of channel walls and the length of tubules, because the projected scattering density is higher along the bands corresponding to a zigzag walls, than in between them, where half the number of walls in the zigzag equidistance between darker regions is $a\sqrt{3}/2$, where a is the distance from tube centre to tube centre and also the unit cell dimension in hexagonal plane. For beam directions outside this plane, this structure disappears because the projection of scattering density is not periodic. When the electron beam propagates along the channel direction, the hexagonal structure is observed, with the distance between the centres of hexagons related to that separating the lines.

The exact analysis of pore sizes and thickness of the pore walls from TEM images is very difficult and not really possible without additional simulations because of the focus problem. The orientation of a particular particle of the specimen will also affect the results of these parameters, if the particle is not horizontal, measurements of pore sizes and wall thickness will give rise to errors. Chen et al [19] showed for MCM-41 that the thickness of the features, the pore sizes and wall thickness, depend strongly on the focus conditions, and careful modeling is necessary for precise analysis.

The wall thickness can be calculated by determining the difference between the lattice parameter ($a=2d_{(100)}/\sqrt{3}$) determined by x-ray diffraction and the pore size obtained by nitrogen adsorption analysis. However, one should bear in mind that the values are only estimates because so far no reliable means for pore size analysis exists. Moreover, the lattice parameters are often calculated from quite broad reflections and therefore do not correspond to an exact value. However, independent studies showed that in the case of the original MCM-41 synthesis that the wall thickness of around 1.0 nm remains constant if the pore sizes are varied in the range from 2.5 to 10.0 nm [20].

3.3.3 BET surface area measurements

Adsorption of probe molecules has been widely used to determine the surface area and to characterise the pore size distribution of solid catalysts. Soon after the preparation of MCM-41 the physisorption of gases such as N_2, O_2 and Ar had been studied to characterise the porosity [21,22].

Low temperature nitrogen adsorption isotherms allow the calculation of the specific surface area, pore volume and the distribution of pore diameters. Figure 3.5 and figure 3.6 shows the N_2 adsorption-desorption isotherm and pore size distribution respectively. The specific surface area of the calcined mesoporous silica, H_1SiO_2 was found to be 700(±25) m^2g^{-1} from nitrogen adsorption measurements which is in the range expected for this type of material. Nitrogen adsorption/desorption curves showed only slight hysteresis, indicating a highly uniform pore size with no pore blocking effects from narrow pores during desorption. The mesoporous silica H_1SiO_2 gives a type IV isotherm, typical of mesoporous solids. Adsorption at low pressures ($p/p_o<0.3$) is accounted for by a thin layer of adsorbed gas on the walls of the mesopores. As the relative pressure

increases ($p/p_o>0.3$), the isotherms show an inflection characteristic of capillary condensation within the mesopores and the p/po position of the inflection point is related to the pore diameter. The sharpness in this step indicates a very uniform pore diameter.

To determine the pore size distributions in cylindrical pores, several methods are known based on geometrical considerations [23], thermodynamics or statistical thermodynamic approach. From the BET surface area measurements, it is possible to calculate a pore size distribution curve which helps to indicate the mean pore diameter which is important to know, when depositing organometallics onto the external and more importantly internal surfaces of this type of material. The method used in this work for analysing pore size distributions in the mesopore range is the Barrett-Joyner-Halenda(BJH) method [24] which is based on the Kelvin equation and thus, has a thermodynamic origin. Figure 3.6 exhibits narrow pore size distribution curve that is obtained from the adsorption/desorption data, which peaks at 3.5 nm. However, compared with new methods that rely on more localized descriptions such as density functional theory(DFT) and Monte Carlo simulation (MC), the thermodynamically based methods overestimate the relative pressure at desorption and therefore underestimate the calculated pore diameters by *ca.*1.0 nm [25]. Anyhow, pore sizes calculated by the BJH method are still probably in the right range. However, one should bear in mind that the values are only estimates, because so far no reliable means for pore size analysis exists.

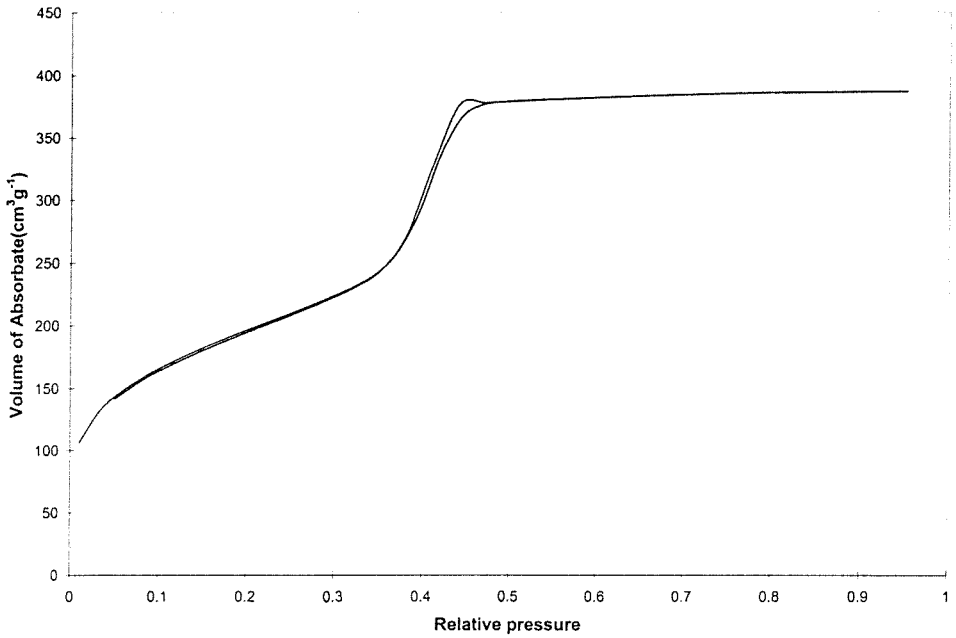

Figure 3.5 :- N_2 adsorption-desorption isotherm for the calcined H_1SiO_2 at 470°C.

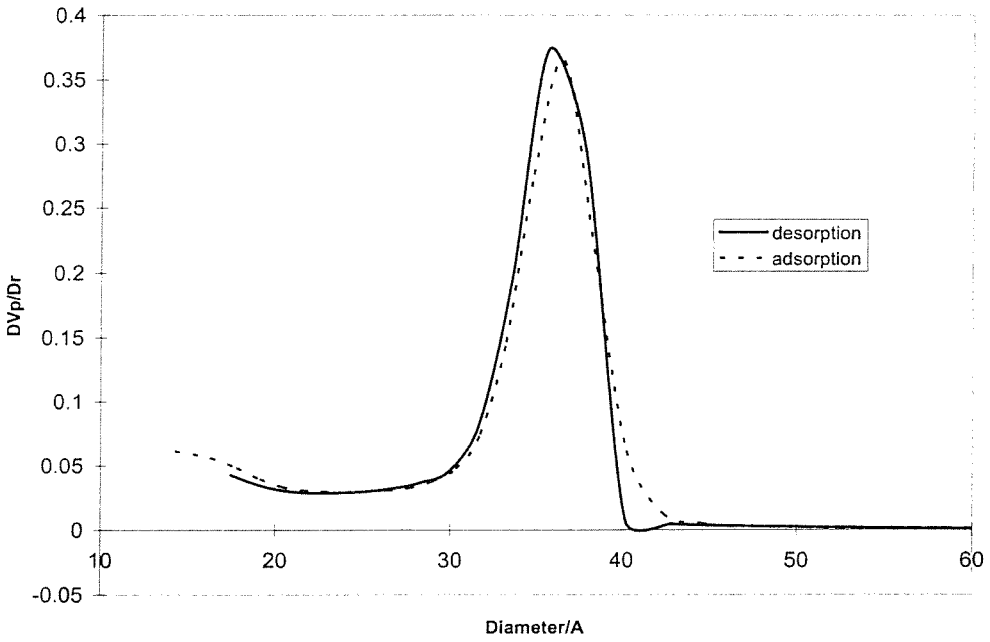

Figure 3.6 : Pore size distribution for the calcined H_1SiO_2 at 470°C.

3.3.4 Powder X-Ray Diffraction

The long range order in these silicas may be readily investigated by X-ray powder diffraction, as the ordered pore structure results in low angle reflections due to the very large repeat distances. Figure 3.7 shows the PXRD pattern of calcined H_1SiO_2. The XRD pattern shows typically 3 reflections at 42.4 Å, 25.3 Å and 22.2 Å respectively. The reflections are due to the ordered hexagonal array of parallel silica tubes and can be indexed assuming a hexagonal unit cell as (100), (110) and (200). The (110) and (200) reflections are not always observed for hexagonal mesoporous materials and its clear presence, in this case, demonstrates that this material has a good degree of long range ordering. Since the mesoporous silica is not crystalline at atomic level, no reflections at higher angles are observed.

Figure 3.8 shows a schematic representation of the hexagonal arrangement of pores observed for mesoporous materials, together with the periodicity corresponding to the d_{100} reflection and the relationship between the d_{100} reflection and a, the hole to hole distance. Therefore, from figure 3.8, it can be seen that the equation relating the d_{100} reflection and a can be written as: $a = d_{100} \times \sin 60°$. However, this expression can be simplified further as $\sin 60° = 2/\sqrt{3}$, leading to the equation: $a = 2d_{100}/\sqrt{3}$. From the formulae $a=2d_{(100)}/\sqrt{3}$, the thickness of the pore walls, calculated by substracting the pore diameter from the unit cell parameter, is ca 14 Å, comparable to the reported value by Attard et al [12]. Using this relationship, the hole to hole distance can be estimated to be 48.5Å for this material.

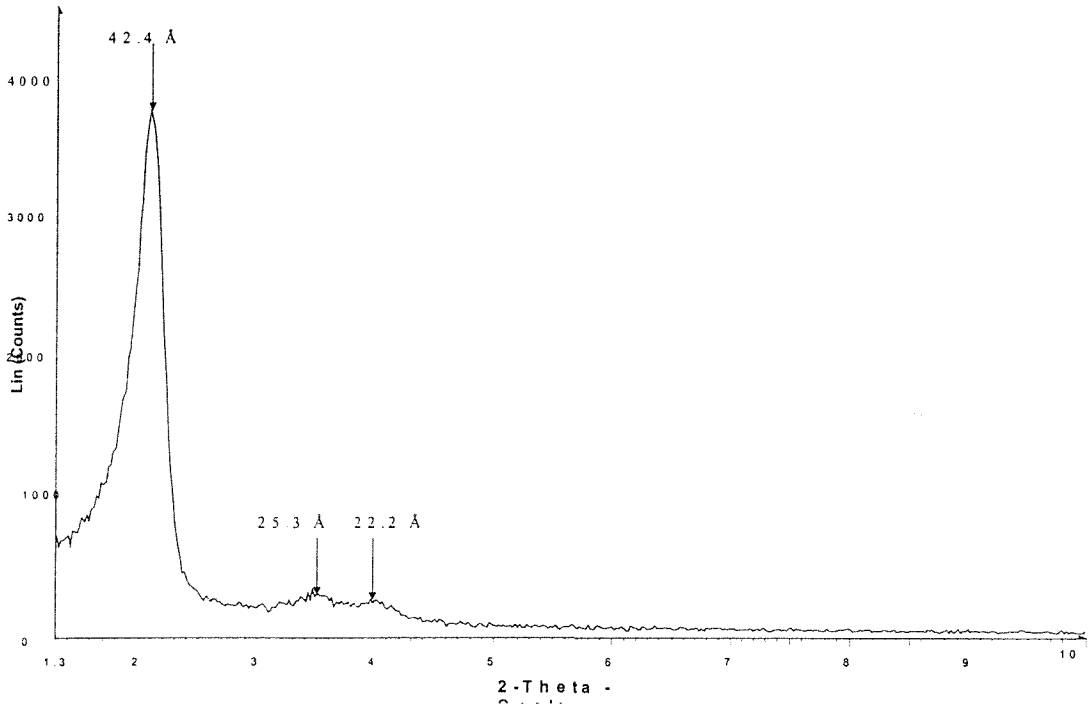

Figure 3.7 :- PXRD patterns of calcined H_1SiO_2, showing the main reflection and 2 other reflections of much lower intensities.

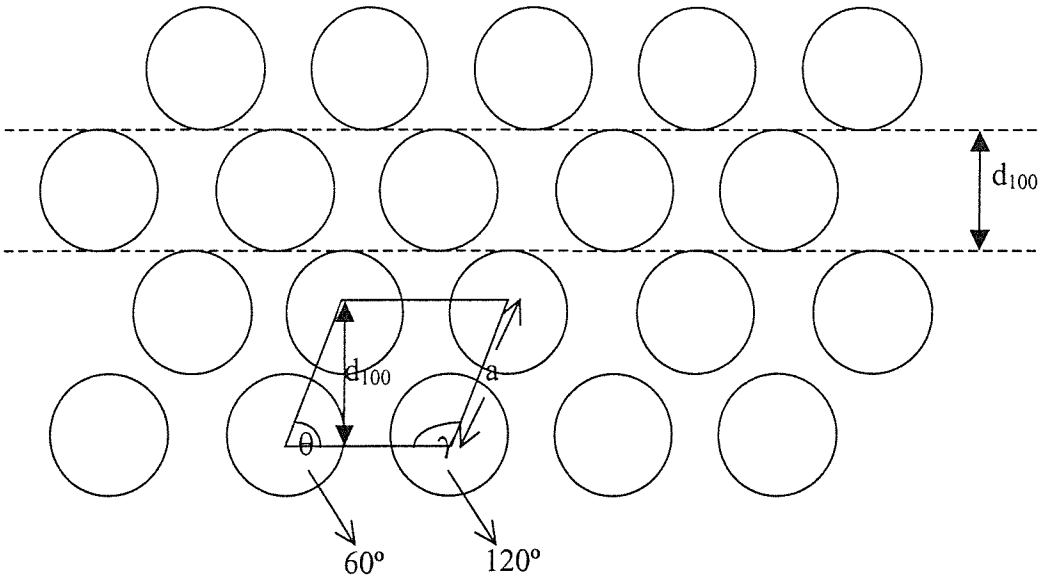

Figure 3.8 :- Schematic representation of the hexagonal pores observed for H_1SiO_2 mesoporous silica.

3.3.5 IR spectroscopy

Figure 3.10 shows the FTIR spectra of Aerosil 200 before and after vacuum dehydration at 480°C. There are several differences between the two spectra that are worth noting. At room temperature, a sharp absorption band at ~3740 cm^{-1} ascribed to free SiOH groups and another broad absorption band centered at 3400 cm^{-1}, together with bands positioned at 1600 cm^{-1} and 1800 cm^{-1} are assigned to hydrogen bonded SiOH groups perturbed by physically adsorbed water, respectively are observed. More interesting in terms of structural information are the absorption bands in the Si-OH stretching region from 3800 to 3000cm^{-1}. After vacuum dehydration at ~480°C, bands due to physically adsorbed water were removed or intensities of the bands were reduced.

Figure 3.11 shows the IR spectra of H_1SiO_2 before and after vacuum dehydration for 3-4 hours at 300°C. With increasing temperature, dehydroxylation of hydrogen bonded and geminal SiOH groups take place to form siloxane bonds (rf. figure 3.9) and simultaneously more free SiOH groups are generated. That is why the intensity of the absorption band at 3740 cm^{-1} increased gradually at higher outgassing temperatures as compared to the absorption band at 3400 cm^{-1}. The very broad band at 3400cm^{-1} in both spectra is due to hydrogen bonded hydroxyl groups and adsorbed water [26]. This suggests that, despite calcination at 470°C, the dehydroxylation of the surface is not complete. Generally, both types of silica exhibit almost identical IR spectra with prominent bands at ~1080 cm^{-1} and ~800 cm^{-1} which are attributed to Si-O bulk mode seen in spectrum 3.11 b and ~1080 cm^{-1} in spectrum 3.11 a.

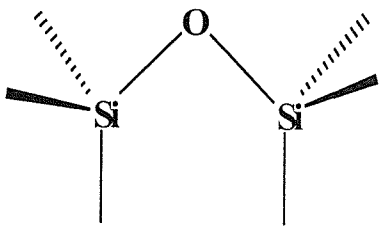

Figure 3.9 :- A siloxane bridge

Dehydroxylation of single SiOH groups is considered to be impossible since they are too far apart (0.5 nm) [27] and such a process would necessarily involve the unfavourable

formation of highly strained bridged structures [28]. Dehydroxylation from geminal groups could also probably be very difficult since silicon does not form =Si=O links readily [29].

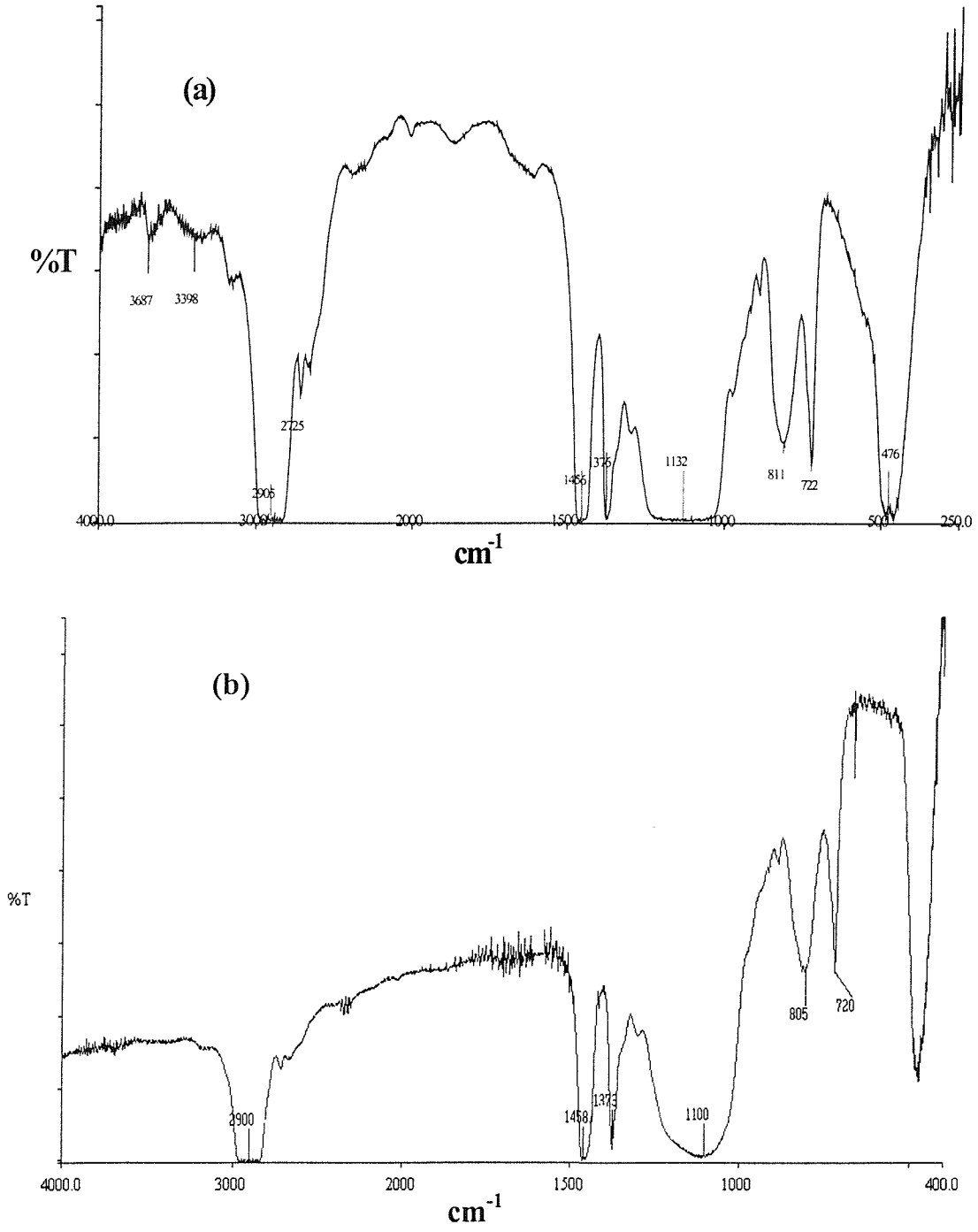

Figure 3.10 :- FTIR nujol mull spectra of Aerosil 200 before (a) and after (b) vacuum dehydration at 480°C.

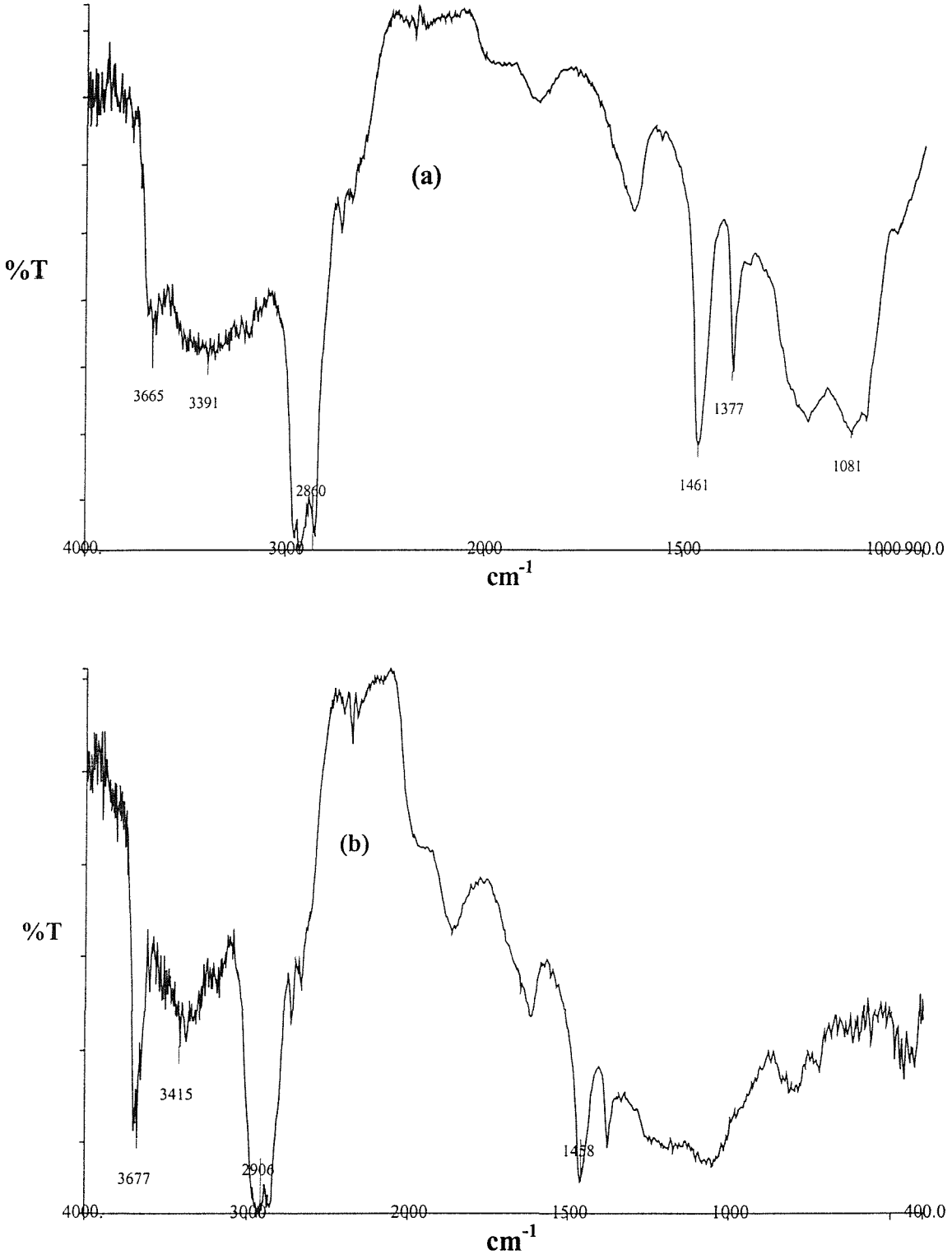

Figure 3.11 :- IR nujol mull spectra of H_1SiO_2 (a) before and (b) after vacuum dehydration at 300°C for 3-4 hours.

3.3.6 Solid State NMR

Solid State ^{29}Si nuclear magnetic resonance (^{29}Si NMR) experiments employing magic angle spinning (MAS) with or without cross polarisation (CP) has been shown previously to be reliable means for quantitatively characterising the nature of various solid surfaces, in particular that of amorphous silica [9]. The fact that the CP process discriminates against ^{29}Si nuclei far away from protons makes this technique a sensitive method for measuring SiOH groups. The nature of the cross polarisation experiment makes this a surface sensitive technique, or, more accurately, the technique is sensitive to silicon nuclei in close proximity to hydrogen atoms. These silicon nuclei also have a faster relaxation mechanism due to their hydrogenous environment, and so by using short relaxation times between pulses the signal from the bulk silicon nuclei, which take much longer to relax back to the ground state, is negligible. This is important to note, as it means that the spectra obtained cannot be used to estimate the average silicon environment within the bulk.

NMR spectra of silica consist typically of a number of broad resonances, which are assigned with respect to a well-established nomenclature. Silicon environments in these types of systems may be readily divided into five groups, denoted Q branches. A Q^4 environment pertains to a silicon in the centre of an SiO_4 tetrahedron that is linked to four other silicons. In a Q^3 environment the SiO_4 tetrahedron is directly bonded to three other silicon atoms plus one other, often a hydrogen atom. In this notation, Q represents a silicon atom bonded to 4 oxygen atoms forming a tetrahedron. The superscript *n* indicates the connectivity: the number of other Q units attached to the SiO_4 tetrahedron under study (rf. table 3.3).

Table 3.3 :- Description of Q^n environments

Q^0	Q^1	Q^2	Q^3	Q^4
$Si(OH)_4$	$Si(O\text{-}Si)(OH)_3$	$Si(O\text{-}Si)_2(OH)_2$	$Si(O\text{-}Si)_3(OH)$	$Si(O\text{-}Si)_4$

Figure 3.12 shows the CP MAS ^{29}Si spectra for Aerosil 200 and H_1SiO_2 respectively. Both spectra show Q^4, Q^3, and Q^2 resonances centred at –109, -101, and –90 ppm respectively. The CP MAS NMR spectra of both spectra are dominated by the Q^4 peak at around –109 ppm accompanied by a shoulder at around –101 ppm which may be assigned as Q^3 silicon. The first observation is that the peaks in calcined H_1SiO_2 are broad and closely resemble those of amorphous silica, which is a strong indication that the pore walls are actually amorphous, with a wide range of O-Si-O angles [30]. The broad ^{29}Si band can be deconvulated into 3 main peaks in both spectra. The low intensity peak at –90 ppm is assigned to geminal-hydroxyl silanol sites (Q^2), peak at –101 ppm to single hydroxyl silanol sites (Q^3) and the peak at –109 ppm to surface silicons which are not bonded to any hydroxyl groups (Q^4). However, ^{29}Si solid state NMR is unable to distinguish between the two types of Q^3 environment, the isolated silanols and the vicinal silanols (rf. figure 3.1 I and II). After calcinations of H_1SiO_2, Q^4 environments are formed at the expense of Q^3 and/or Q^2. The degree of this transformation depends on the severity of reaction conditions applied to the condensation of Si-OH groups.

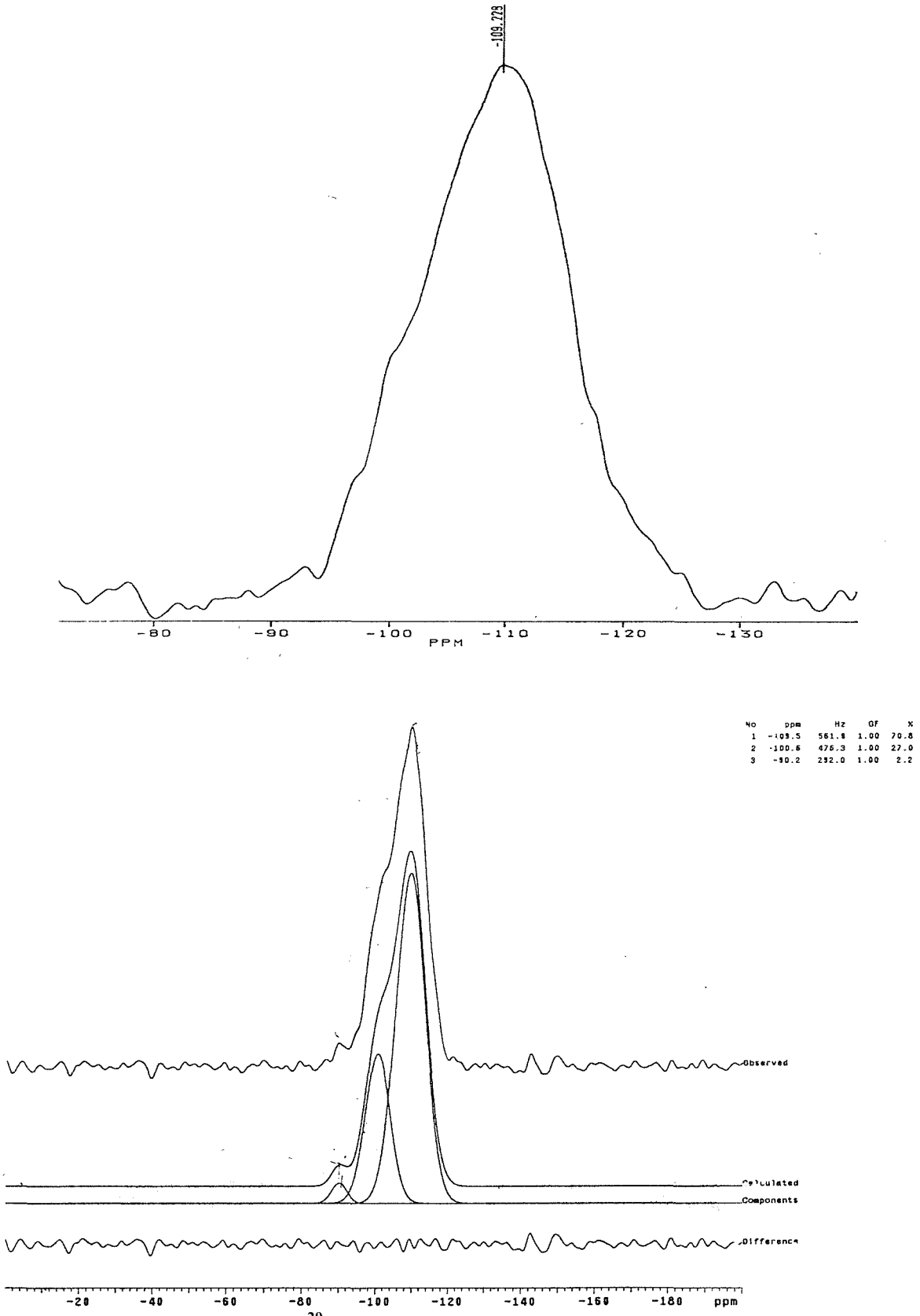

Figure 3.12 :- CP MAS ^{29}Si NMR of Aerosil 200(top), vacuum dehydroxylated at 480°C and H_1SiO_2(bottom), calcined at 470°C respectively.

3.4 Conclusions

Both types of silica have been characterised in detail. Table 3.4 shows all the measured parameters performed on these silicas.

Table 3.4 :- Physical properties of Aerosil 200 and H_1SiO_2.

	Aerosil 200	H_1SiO_2
calcination temperature/°C	480	470
surface area/ nm^2	200	700
OH groups/nm^2	~4.0	~2.0
hole to hole distance/Å		48.5
wall thicknessÅ		14
average pore diameter/Å		34
lattice parameter/Å		42.4

The three observed types of SiOH groups have the following characteristics, single SiOH groups with an IR absorption band at ~3740 cm^{-1} and and ^{29}Si NMR peak at –101 ppm which generally thought to be Q^3, hydrogen bonded SiOH groups with the IR absorption band at 3200-3600 cm^{-1} and ^{29}Si NMR peak at –101 ppm and geminal SiOH groups with an IR absorption band at ~3738 cm^{-1} and ^{29}Si NMR peak at –90 ppm respectively. The value of the OH groups/nm^2 has contributions from all these three groups on both the external and internal surfaces for H_1SiO_2.

References

[1] E.F.Vansant, P V D Voort, *Stud.Surf.Sci.Catal.*, **93**, 120, 1995

[2] G.D. Parfitt, K.S.W.Sing, *Characterisation of Powder Surfaces*, Academic Press, New York, 1976.

[3] H.A.Benesi, A.C.Jones, *J.Phys.Chem.*, **63**, 179, 1959.

[4] M.L.Hair, *Chemically Modified Surfaces: Silanes, Surfaces and Interfaces*, Gordon and Breach, 1985, London and references therein.

[5] B.A.Morrow, I.A.Cody, *J.Phys.Chem.*, **80**, 1995, 1976.

[6] A.Grabbe, T.A.Michalske, W.L.Smith, *J.Phys.Chem.*, **99**, 4648, 1995.

[7] G.Engelhardt, D.Michel, *High Resolution Solid State NMR of Silicates and Zeolites*, Wiley, 1987, Chichester and references therein.

[8] D.W.Sindorf, G.E.Maciel, *J.Am.Chem.Soc.*, **103**, 4263, 1981.

[9] D.W.Sindorf, G.E.Maciel, *J.Am.Chem.Soc.*, **105**, 1487, 1983.

[10] P V D Voort, I Gillis-D'Hamers, E.F.Vansant, *J.Chem.Soc.Faraday Trans.*, **89**, 3751, 1990.

[11] Degussa Safety Data Sheet (91/155/EEC)

[12] G.S.Attard, J.C.Glyde, C.G.Göltner, *Nature*, **378**, 366, 1995.

[13] J.C.Miller, J.N.Miller, *Stastistics for Analytic Chemistry*, Ellis Horwood, Chichester, 1988.

[14] C.W.Chronister, R.S.Drago, *J.Am.Chem.Soc.*, **115**, 4793, 1993.

[15] B.A.Morrow, I.A.Cody, *J.Phys.Chem.*, **77**, 1465, 1973.

[16] A.Jentys, K.Kleestorfer, H.Vinek, *Microporous and Mesoporous Mater.*, **27**, 321, 1999.

[17] C.Y.Chen, H.X.Li, M.E.Davis, *Microporous Mater.*, **2**, 27, 1993.

[18] J-M Basset, B.C.Gates, J-P Candy, A.Choplin, M.Leconte, F.Quignard, C.Santini, Eds, *Surface Organometallic Chemistry: Molecular Approaches to Surface Catalysis*, Kluwer Academic Publishers, 1988.

[19] C.Y.Chen, S-Q Xiao, M.E.Davis, *Microporous Mater.*, **4**,1, 1995.

[20] J.S.Beck, J.C.Vartuli, W.J.Roth, M.E.Leonowicz, C.T.Kresge, K.D.Schmitt, C.T.W.Chu, D.H.Olson, E.W.Sheppard, S.B.McMullen, J.B.Higgins, J.L.Schlenker, *J.Am.Chem.Soc.*, **114**, 10834, 1992.

[21] P.J.Branton, P.G.Hall, K.S.Sing, *J.Chem.Soc., Chem.Commun.*, 1257, 1993.

[22] P.J.Branton, P.G.Hall, K.S.Sing, H.Reichert, F.Schüth, K.K.Unger, *J.Chem.Soc.,*

Faraday Trans., **90**, 2956, 1994.

[23] S.J.Gregg, K.S.W.Sing, *Adsorption, Surface and Porosity*, Academic Press, New York, 2nd edn, 1982.

[24] E.P.Barrett, L.G.Joyner, P.P.Halenda, *J.Am.Chem.Soc.*, **73**, 373, 1951.

[25] U.Ciesla, F.Schüth, *Microporous and Mesoporous Mater.*, **27**, 131, 1999.

[26] H.Landmesser, H.Kosslick, W.Storek, R.Fricke, *Solid State Ionics*, **101**, 271, 1997.

[27] D.W.Sindorf, G.E.Maciel, *J.Phys.Chem.*, **87**, 5516, 1983.

[28] J.P.Peri, A.L.Hensley, *J.Phys.Chem.*, **72**, 2926, 1968.

[29] R.K.Iler, *The Chemistry of Silica*, Wiley, New York, 1979.

[30] A.Sayari, *Stud.Surf.Sci.Catal.*, **102**, 1, 1996.

Chapter 4

Synthesis and Characterisation of 12-phosphotungstic acid supported on silica

4.1 Introduction

This chapter concerns the investigation of silica based supports loaded with various amounts of HPA. The supported acid was prepared by adsorption from organic solvents which is different from the method commonly used in the literature to prepare the supported heteropolyacids. As a support, an amorphous silica (Aerosil 200) and a liquid crystal templated mesoporous silica of Attard et al [1] were utilised. The HPA used in these studies is 12-phosphotungstic acid (HPW), the strongest acid in the Keggin series of HPA. The amount of supported HPW was determined with EDX-SEM analysis. Characterisation of the solid acids were performed by Powder X-Ray Diffraction (PXRD), sorption of N_2, electron microscopy, uv-visible and solid state NMR spectroscopy. The formation of acidic sites resulting from the deposition of HPW on the silica was investigated by following the adsorption of pyridine using Diffuse Reflectance Infra-Red spectroscopy (DRIFTS). The strength of the acid centres presents was studied by ^{31}P solid state NMR of chemisorbed triethylphosphine oxide (TEPO). Finally, the thermal stability of the supported HPW will be probed by temperature programmed desorption (TPD) study.

4.2 Experimental

4.2.1 Preparation of 12-phosphotungstic acid (HPW)

$H_3PW_{12}O_{40}.nH_2O$ was prepared according to the literature [2]. Sodium tungstate dihydrate (40 g, 0.121 mole) and disodium phosphate (6.4 g, 0.045 mole) were dissolved in boiling water (60 ml). 32 ml of concentrated hydrochloric acid was added dropwise with constant stirring .

Phosphotungstic acid begun to separate when about half of the acid was added. Since the precipitated acid must be purified, it was not necessary to filter it. When the solution had been cooled, ether, was added until, after shaking, 3 layers remain. The acid-ether complex, which constituted the lower layer, was washed twice with water to which enough ether was added to form a third layer. After washing, the 3 layers remained clear.

The acid-ether layer was evaporated until dryness using a rotoevaporator and recrystallised from water giving white powder as the product.

4.2.2 Preparation of silica modified with 12-phosphotungstic acid

Several methods of preparing silica supported heteropolyacids are known from the literature. For example, the supported HPW were prepared by mounting HPW on supports by impregnation from aqueous solutions, with subsequent drying and calcination at elevated temperature [3]. Most of the supported heteropolyacids were prepared by impregnating a support with aqueous HPA. Kozhevnikov *et al* [4] followed a procedure where the catalysts comprising of 10 to 50wt% HPA on a siliceous support were prepared by shaking a suspension of Aerosil 380 or MCM-41 (0.5-1 g) in an aqueous (3-5 ml) or methanol (around 30 ml) solution, containing a certain amount of HPA, in a glass vessel from 1 to *ca.* 20 h (overnight) at room temperature.

In the present work, DMSO was used as the solvent to prepare low loaded (15-18%) solid acids and methanol was used instead for high loaded samples. In a typical preparation, 1 gram of silica were used. The amount of HPW utilised were in excess as compared to the silanol number of the silicas. The weighed HPW was first dissolved in the solvent. After complete dissolution of the heteropolyacid, the HPW solution was added to the silica in a round bottom flask equipped with a magnetic stirrer. The mixture was left to stir for a varying period depending on the loading of the samples. After the reaction, the mixture was filtered through a fritted disc (low loaded samples) and vacuum evaporated (high loaded samples). The solid acids obtained were washed several times with the solvent and dried under suction at room temperature.

4.2.3 Acidity Determination by Basic Indicators

Basic indicators of varying strength were used. These include neutral red (pKa= +6.8), methyl yellow (pKa= +3.3), crystal violet (pKa= +0.8), dicinnamalacetone (pKa= -3.0), benzalacetonephenone (pKa= -5.6) and anthraquinone (pKa= -8.2). Approximately 0.1% of each indicator was prepared in dry toluene. About 0.1g of the modified silicas with HPW were tested with each of these indicators in test tubes.

4.3 Results and Discussion

4.3.1 Acidity Determination by Basic Indicators

The concept of measuring the acid strength of a surface by the observation of the colours of basic indicator molecules adsorbed from a non-aqueous medium was proposed by Walling in 1950 [5] who applied the Hammett function, H_o, to surfaces. This function, Ho, is defined on the basis of the ability of the acid to donate a proton to a non-ionised or neutral substance, i.e. a simple basic indicator (equation 4.1) where f_B, f_{BH+} are respective activity coefficients and a_{H+} is the hydrogen ion activity of the surface acid [6]. It can be seen from equation 4.1 that H_o is equivalent to the well known acidity function pH only if dilute aqueous solutions are involved.

$$B + H^+ \rightleftharpoons BH^+ \qquad 4.1$$

$$Ho = - \log [a_{H+}.(f_B/f_{BH+})]$$

The acid strength found from indicator adsorption is relative to the pK_a of the indicator, and this provides a sound basis for comparing surface acidities. The acid strength of a solid catalyst can be estimated by noting which members of a series of Hammett indicators are adsorbed in the acid form. Thus, provided that those indicators are chosen whose acid colours are intense enough to mask their basic colours, the determination can be carried out in the following way: each of a series of Hammett indicators in dry toluene is added to separate samples of the dried solid and the resulting colours are noted. The results for the 4 silica samples are tabulated in Table 4.1.

Table 4.1 :- Results of the indicators test (+ indicates colour change observed).

Sample	pK_a value of indicators			
	+6.8	+3.3	+0.8	-3.0
HPW/H_1SiO_2 (15wt%)	+	+	+	+
HPW/H_1SiO_2(40wt%)	+	+	+	+
HPW/Aerosil 200 (18wt%)	+	+	+	+
HPW/Aerosil 200(30wt%)	+	+	+	+

The HPW supported silicas does not change the colour of other indicators with $pK_a < -3.0$. Therefore, no colour change were observed for basic indicators like benzalacetophenone and anthraquinone. The pK_a of the basic indicator may be reported relative to sulphuric acid-water mixtures and therefore the acidic strength is often expressed as a weight percentage of H_2SO_4 [7]. The results obtained suggests that HPW supported on both types of silica are at least equivalent to 50% of concentrated sulphuric acid [7,8].

However, there are a few limitations involved with this indicator test method. An indicator will be converted into its conjugate acid only by acid sites which have an acid strength equal to or higher than that of the indicator. Thus, by the use of indicators alone, only the limiting strength for the strongest acid sites on a given surface can be determined, expressed as a range between two indicators of different pK_a, e.g. H_o lies between +0.8 and –3.0. The limit for the weakest strength of acid sites cannot be found, since indicators of more positive pK_a values will be converted into their conjugate acids by all of the stronger sites. Another problem arises from the visual determination of the colour change, which could be even more subjective when coloured or dark samples are used.

4.3.2 EDX-SEM analysis

EDX-SEM analysis has been performed on various particles and various places of the same particle at low magnification (<500X) with a JEOL scanning electron microscope. Several measurements for the W content in normalised weight percent have been made for all the silica samples. Modified silica samples obtained by filtration could only be achieved a maximum loading around 15-18wt% of tungsten. Increasing the amount of heteropolyacid used (several folds) and reaction time (1-5 days) did not increase the loading of the HPW significantly. Modified silica samples obtained by vacuum evaporation gave high loaded HPW.

A series of silica-based supports (Aerosil 200 and H_1SiO_2) modified with 12-phosphotungstic acid (HPW) have been prepared. The capacity of the silica supports to HPW was examined by increasing the amount of acid used and reaction time.

Two high loaded samples for each type of silica have been prepared. Aerosil 200 modified with HPW has loading about ~30wt% and H_1SiO_2 has loading of ~40wt% of tungsten.

4.3.3 UV-Visible Spectroscopy

In the diffuse reflectance uv-visible spectra of supported HPW as shown in figure 4.1, one broad absorption band and a shoulder were observed at ~268 nm and ~350 nm respectively. It has been found that both types of silica also have broad absorption bands in the same region around ~260nm. The diffuse reflectance spectrum for the HPW displayed a broad band around ~268 nm and a shoulder at ~350 nm which are probably due to a charge transfer band arising from the polytungstate lattice [9]. Both the supported HPW and unsupported HPW displayed similar bands at ~260 nm and ~350 nm in their respective uv-visible spectra. Therefore, it can be concluded that the integrity of HPW supported on silica was maintained upon immobilisation on both types of silica supports.

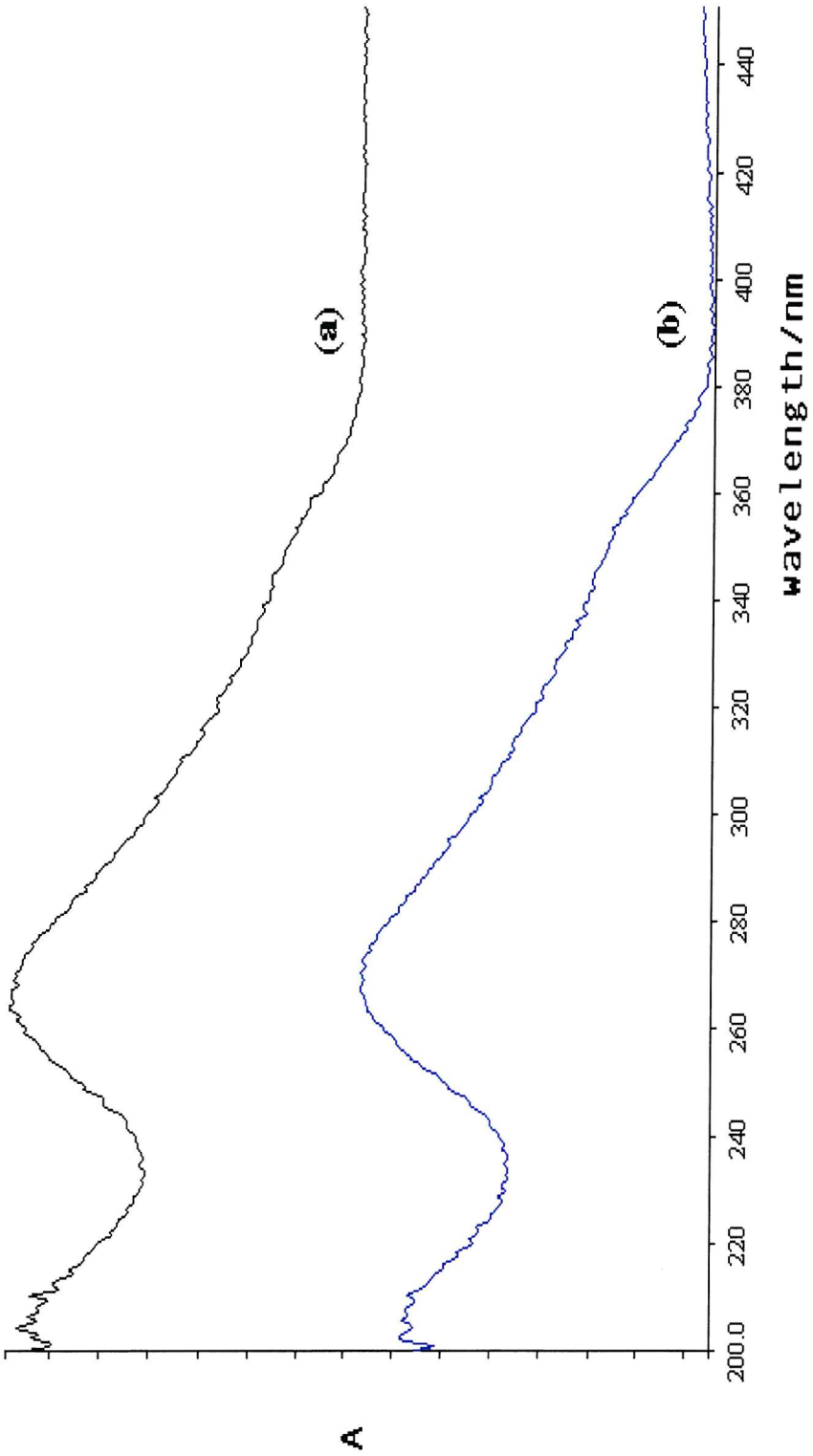

Figure 4.1 :- UV-Visible spectra of HPW supported on a) H_1SiO_2 and b) Aerosil 200

4.3.4 Electron Microscopy (SEM & TEM)

Scanning electron microscopy was applied to study the morphology of the modified silica with HPW while performing the EDX analysis. Figure 4.2 illustrates the general overview (at low magnification) and details of H_1SiO_2 modified with HPW. The surface structure of Aerosil 200 modified with HPW is shown in Figure 4.3. In conclusion, no morphology modification was observed by SEM after immobilisation with HPW.

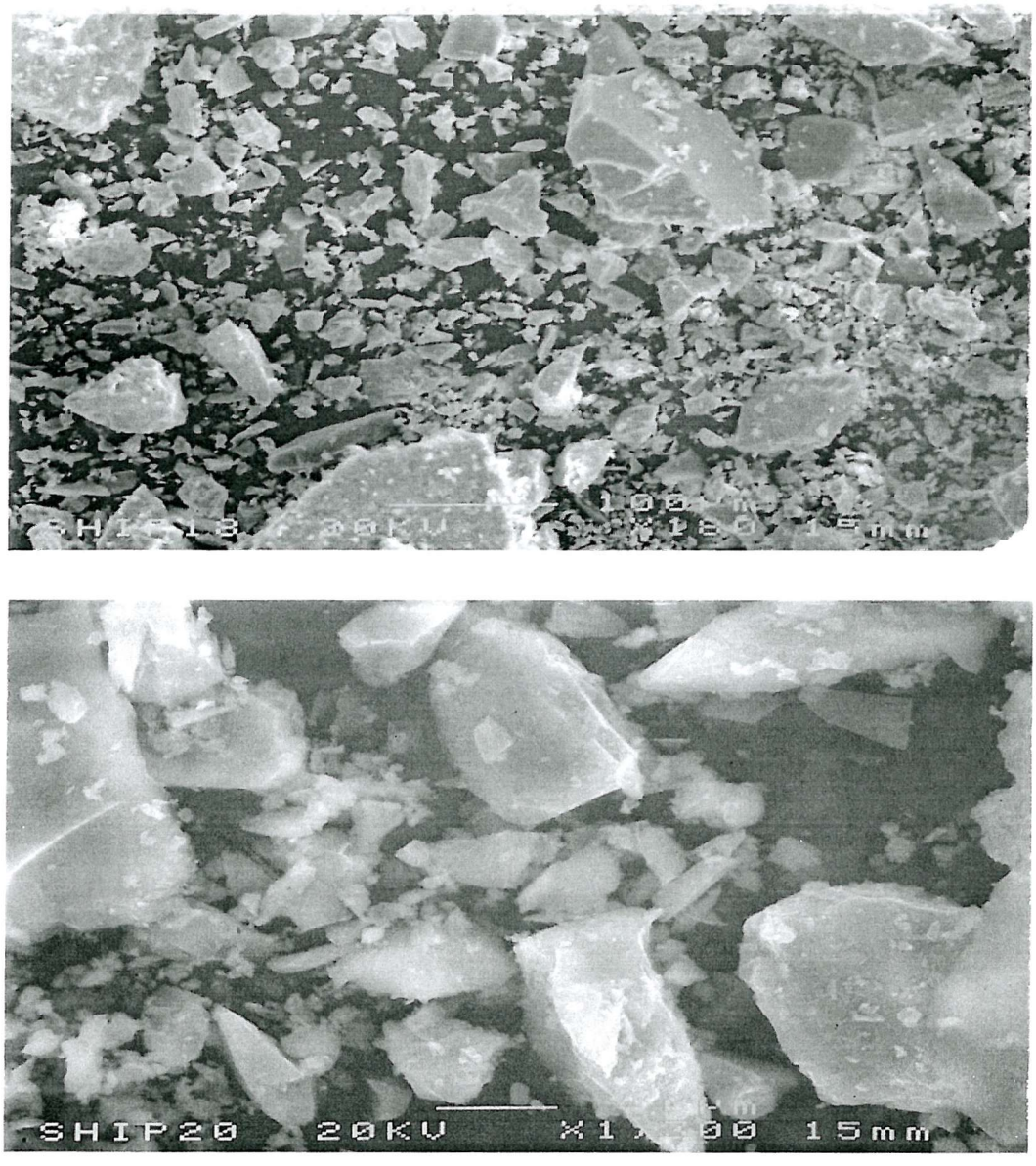

Figure 4.2 :- SEM images of H_1SiO_2 modified with HPW at low (X180,top) and high (X1300,bottom) magnifications. Scale bar 100µm (top), 10µm (bottom).

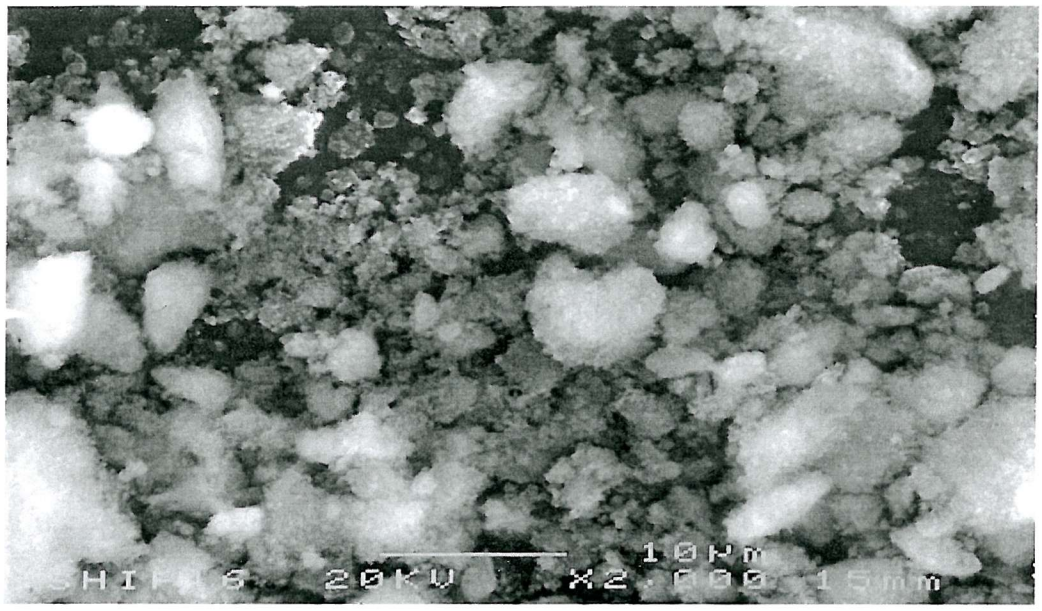

Figure 4.3 :- SEM image of Aerosil 200 modified with HPW at high magnification (X2000). Scale bar 10µm.

There is only one publication in the literature by Kozhevnikov *et al*[4] who carried out TEM analysis on HPW supported on MCM-41 molecular sieve and amorphous silica, Aerosil 380. Hence, Transmission Electron Microscopy (TEM) was performed on some HPW/Aerosil 200 and HPW/H_1 SiO_2 with the aim of determining the location and the size of the HPW species which can be distinguished as dark dots in the TEM images. However, the rather dominant mesostructure of H_1SiO_2 makes it difficult to detect the supported HPW species.

Figure 4.4 shows the dark field micrograph of a high loaded HPW on H_1SiO_2 (~40wt%). The same images that were obtained before and after amorphization indicating that the dark lines were due to the presence of the HPW species in the pores. The absence of clusters, formed by heteropolyacid (50-100Å) or crystalline heteropolyacid was confirmed for both silica supports modified with HPW. The presence of HPW species on amorphous silica, Aerosil 200 could not be ascertained from the TEM images due to the absence of any distinct dark dots. EDX-TEM analysis of thick and thin parts of the modified silica with the aim of providing some information on the location of the heteropolyacid, whether in the pore or on the surface of the support, has also been

performed on the high loaded HPW (~40wt%) on H_1SiO_2. However, very low intensity W Kα peak with energy at 69.5 keV as compared to Si Kα peak with corresponding energy at 1.84 keV made it impossible to carry out any meaningful comparison of W/Si ratio of the different parts of a particle.

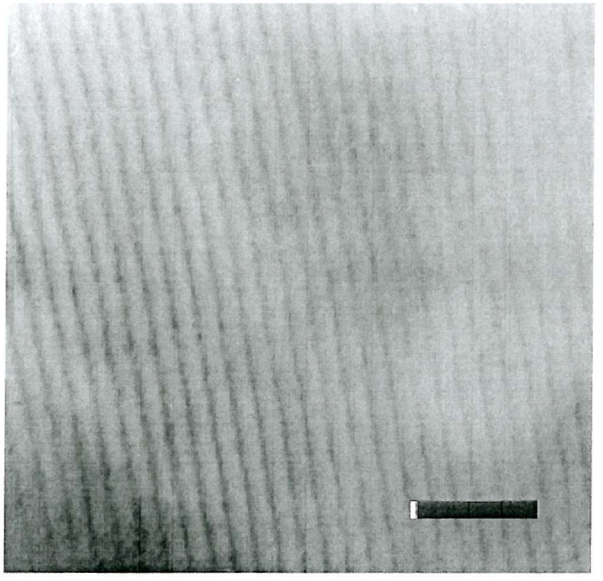

Figure 4.4 :- TEM micrograph of high loaded HPW on H_1SiO_2 (~40wt%).The horizontal dark bar indicates 20 nm.

4.3.5 Powder X-Ray Diffraction

Figure 4.5 illustrates the PXRD patterns of HPW supported on H_1SiO_2. No HPW crystals were observed in the PXRD patterns of both loading of HPW on H_1SiO_2. This result can be explained by the easy excess of HPW molecules to the H_1SiO_2 pores and the high surface area of the material. Previous results [10] has showed that crystalline HPW can only be seen at 70wt% HPW loading.

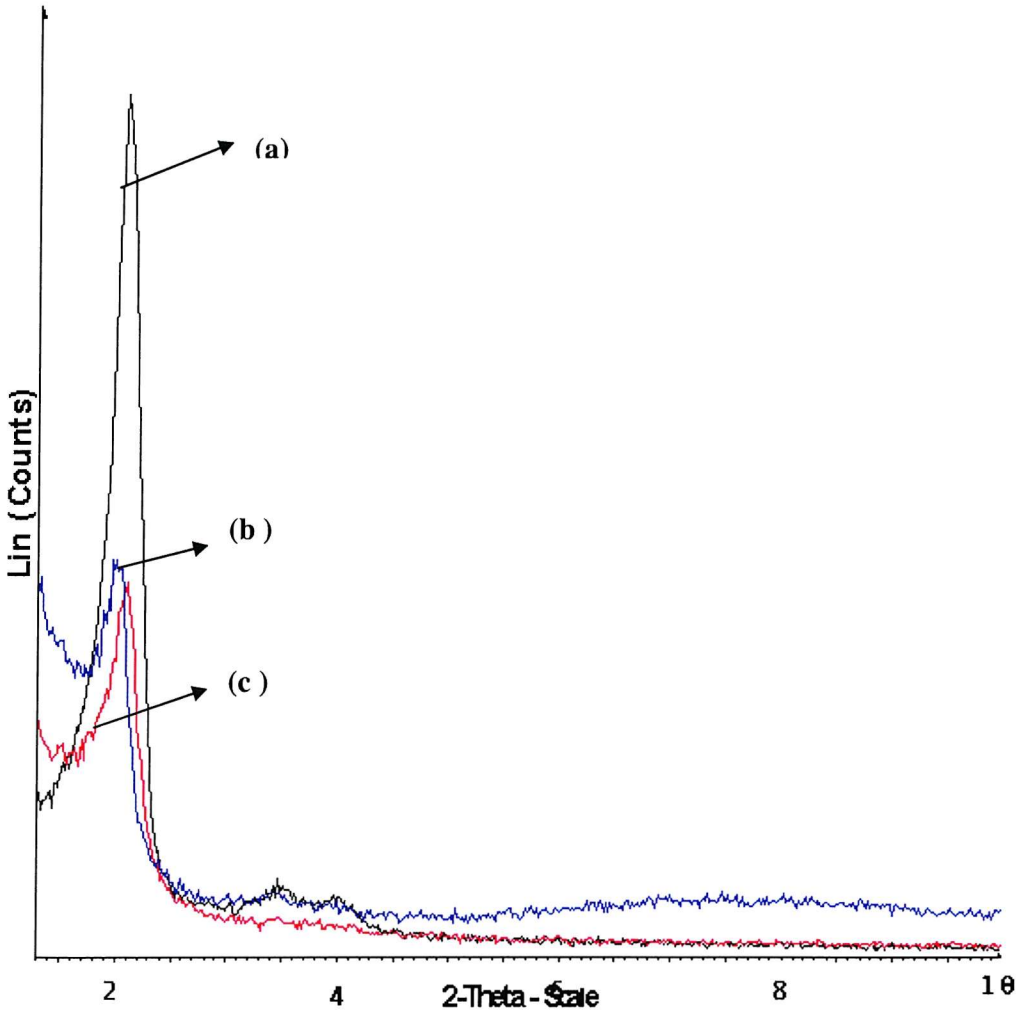

Figure 4.5 :- PXRD patterns of HPW supported on H_1SiO_2, a) H_1SiO_2 b) HPW(40wt%)/H_1SiO_2 and c) HPW(15wt%)/H_1SiO_2.

On HPW loading, the intensity of the main peak which corresponds to the [100] reflection, decreases, as expected. This suggests that the long range order of H_1SiO_2 is decreased noticeably by the presence of HPW. On the high loaded HPW on H_1SiO_2, a featureless broad bump appears in the region of XRD patterns of 2θ~10°. There is a slight shift of the XRD main peak to a lower angle. The corresponding 2θ angle has been shifted to 44.6Å from 42.1Å. This indicates that the unit cell of the H_1SiO_2 material expanded slightly after the incorporation of HPW. This is evident from the formulae $a= 2d_{100}/\sqrt{3}$ (where a is the unit cell dimension in hexagonal plane), where an increase in d value will give rise to a corresponding increment in a. No crystal phases were observed in both XRD patterns for HPW supported on H_1SiO_2. Preparation of the supported HPW by impregnation from water/aqueous solution gives rise to HPW crystalline phase in the XRD patterns at loadings over 23wt% as shown by Dwyer *et al* [11].

On the amorphous silica, no distinct diffraction peaks were observed even at loading as high as 30wt% of tungsten. It can be concluded that supported HPW obtained from organic solvents provides a better dispersion of HPW on the silica compared to preparation by impregnating a support with aqueous solution of HPW. It has been found when the content exceeded about 20wt% of HPW, broad diffraction peaks appeared at ~2θ=10°, which is characteristic to solid state HPW [12].

4.3.5 BET surface area measurements

Table 4.2 shows BET surface areas(A_{BET}), mean pore diameters(d) and pore volumes(V_P) for silica supports and silica modified with HPW.

Table 4.2 :- Physical measurements for HPW supported on both types of silica.

Sample	no. of HPW/nm^2	A_{BET}/m^{2}g^{-1}	d/Å	V_P/cm^{3}g^{-1}
Aerosil 200		~200		
H_1SiO_2		~700	35	0.59
HPW/H_1SiO_2(15wt%)	~0.06	580	28	0.32
HPW/H_1SiO_2(40wt%)	~0.16	550	30	0.36
HPW/Aerosil 200(18wt%)	~0.24	~120		
HPW/Aerosil 200(30wt%)	~0.40	~104		

The specific surface area A_{BET}, was determined from the linear part of the BET equation. The estimated coverage of HPW per nm^2 is also tabulated in Table 4.1. At similar loading, the HPW coverage is greater on Aerosil 200 silica as compared to on mesoporous silica, H_1SiO_2. The analysis of the pore size distribution was performed using the adsorption and/or desorption isotherm based on Dollimore and Heal [13] formulae. Figure 4.6 shows the pore size distribution curve centred around 30Å for the high loaded HPW on H_1SiO_2. For the low loaded HPW(15%)/H_1SiO_2, the corresponding pore size distribution is showed in figure 4.8. Both of these supported HPW shows a narrow pore size distribution with no large reduction in the pore diameter measurements.

A high level of adsorption is a characteristic property of the mesoporous silica H_1SiO_2. The adsorption-desorption isotherm for the high loaded HPW (40%) and low loaded HPW (15%) on mesoporous silica are shown in figure 4.7 and 4.9, respectively. Both isotherms can be characterised as type-IV according to the classification of Brunauer *et al* [14]. Compare to the unsupported H_1SiO_2, there was a drop in the adsorption capacity, as seen in both isotherms. There were two contributing factors to this drop in the

capacity, one was due to the weight factor of the HPW and the other was due to the reduction in the pore volume of the mesoporous silica as a result of the volumetric presence of the HPW.

For the H_1SiO_2 support, the difference between pore diameter calculated from nitrogen adsorption and that obtained from PXRD suggests a wall thickness of about 10-12Å. After HPW loading, the surface area, pore size and pore volume all decrease. The results presented show that even if the intensity of the XRD peaks of H_1SiO_2 decreases after supporting the heteropolyacid, the mesostructure is preserved and the modified materials still have rather large surface areas. The decrease in the surface area of Aerosil 200 is about 30% as compared to H_1SiO_2 which is about 15%. TEM micrographs of bare Aerosil 200 showed that the shape of the silica particles is non-spherical and this may explained the decrease in the surface area of the Aerosil 200. However, pore blocking is not expected to occur from these results since there is no sharp decrease in all the parameters measured. A.Corma *et al* [15] observed that there was a sharp decrease of surface area and pore volume in the HPW/MCM41 catalysts which is produced by blocking of the monodimensional channels of MCM-41 by small aggregates of HPW.

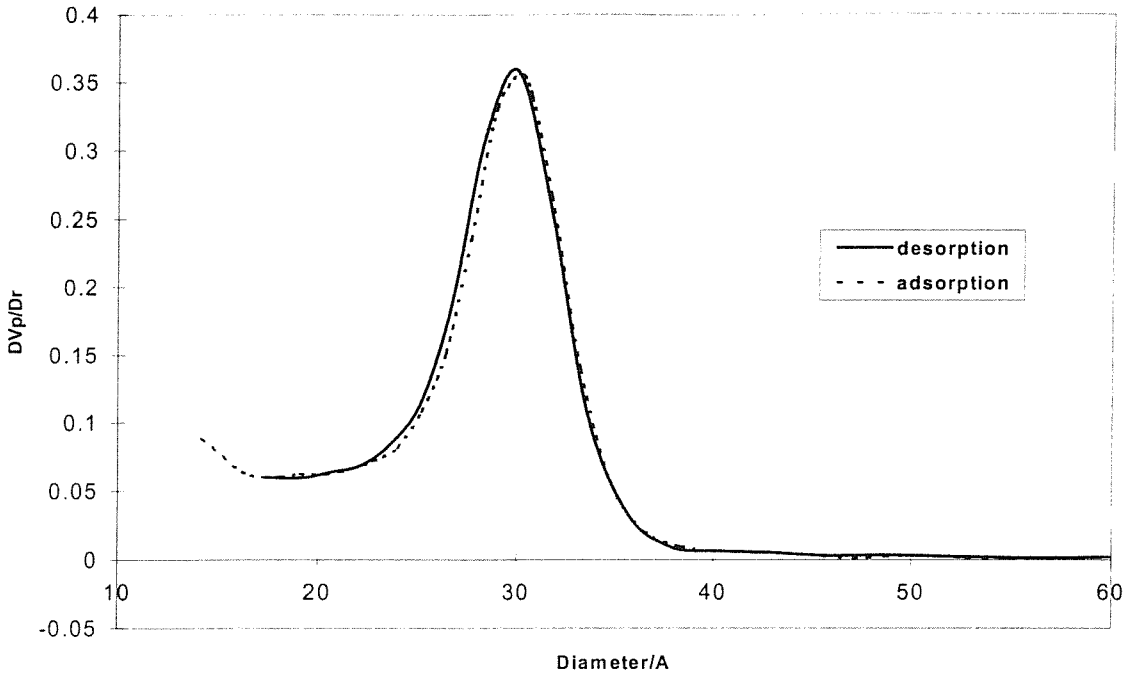

Figure 4.6 :- Pore size distribution of HPW(40wt%)/H_1SiO_2.

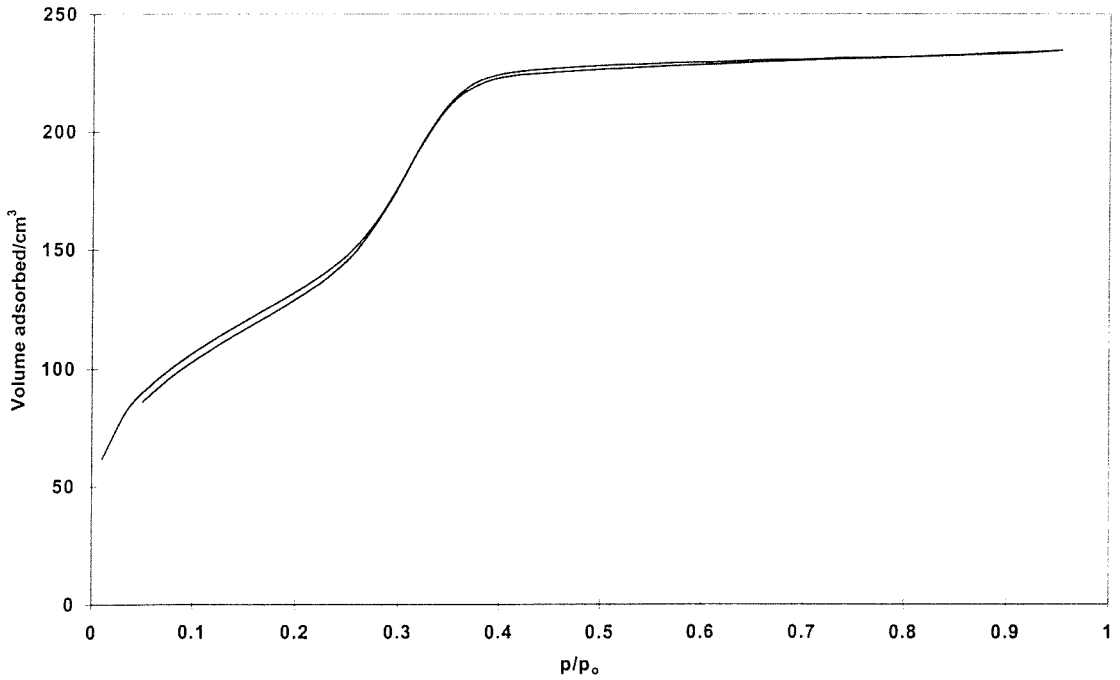

Figure 4.7 :- N_2 adsorption-desorption isotherm for HPW(40wt%)/H_1SiO_2.

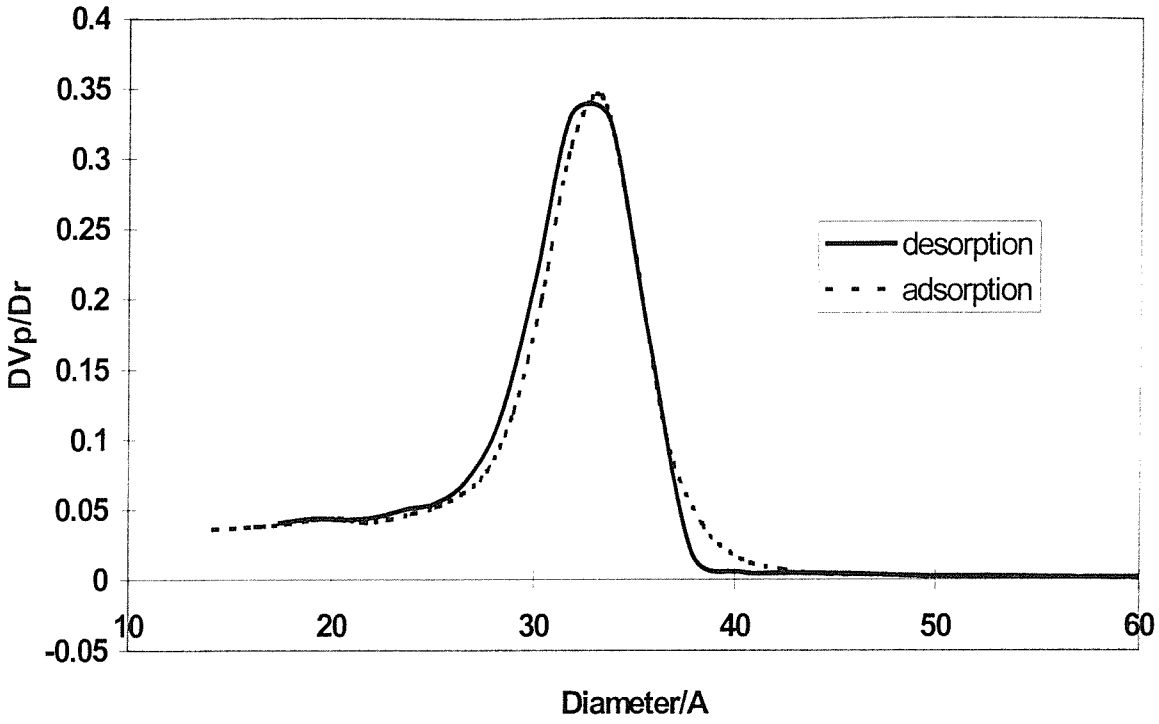

Figure 4.8 :- Pore size distribution for HPW(15%)/H_1SiO_2.

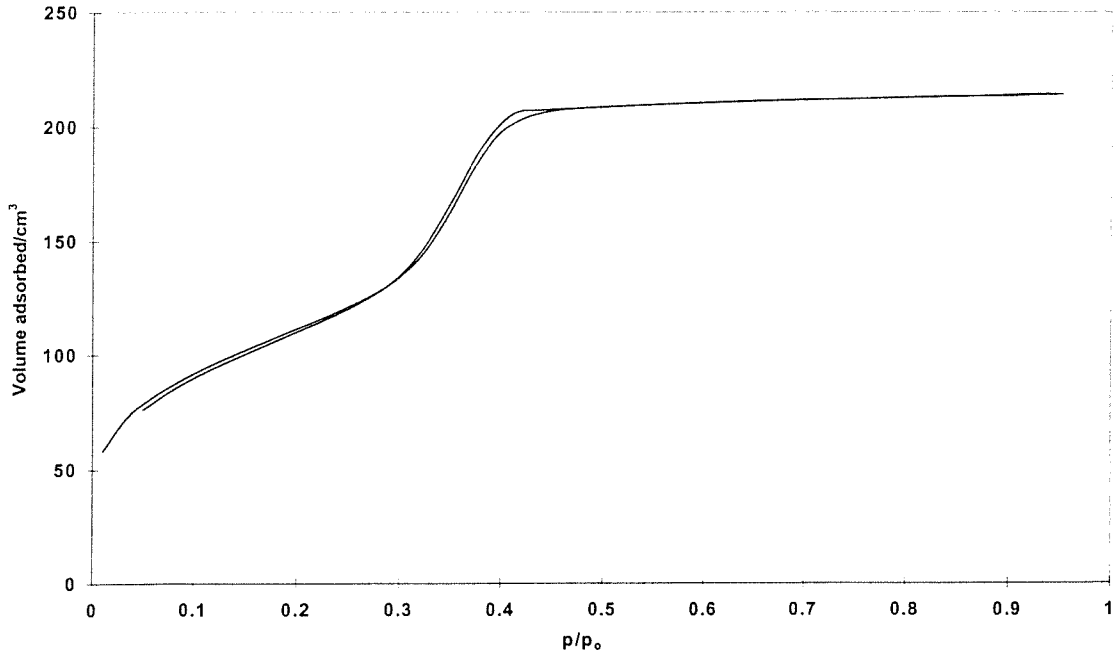

Figure 4.9 :- N_2 adsorption-desorption isotherm for HPW(15%)/H_1SiO_2.

4.3.6 Pyridine Adsorption by DRIFTS

Only very limited information on the acidic properties of the supported heteropolyacids system can be found in the literature [16,17]. In most of these studies, the acidic properties of the supported heteropolyacids were tested in an acid-catalysed reaction [18]. Systematic study on the pyridine adsorption of the supported HPW/SiO_2 system has never been reported. In the present work, the acidic properties of the supported HPW have been investigated in more details by DRIFTS and TPD of the chemisorbed pyridine. It has been found that considerable information can be obtained about the acidity of various solids by studying changes in the "ring" vibrations of pyridine and other bands in the region of 1700cm^{-1} to 1400cm^{-1}.

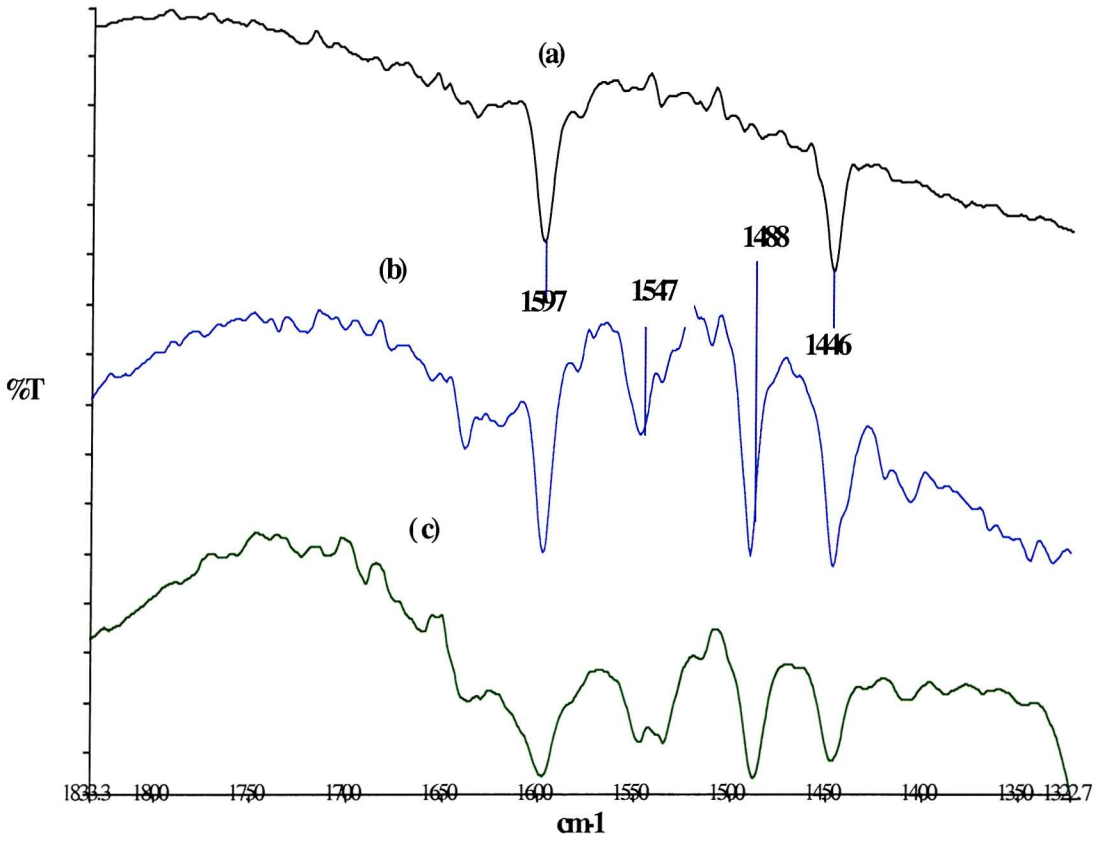

Figure 4.10 :- DRIFTS difference spectra of pyridine adsorbed on HPW supported on Aerosil 200, a) Aerosil 200 b) HPW (18wt%)/Aerosil 200 c) HPW (30wt%)/Aerosil 200.

The IR spectra of pyridine adsorbed on HPW supported on Aerosil 200 are presented in Figure 4.10. All the diffuse reflectance spectra obtained were differences spectra with the untreated silica as the background. The observed peak positions at room temperature were ~1446, ~1488, ~1547 and ~1597 cm^{-1}. A weak peak around ~1650 cm^{-1} could also be seen in spectra b and c. These positions are in good agreement with the data reported for pyridine adsorbed on acidic solids by Parry [19]. The spectrum of pyridine co-ordinately bonded or hydrogen bonded to the surface is markedly different from that of the pyridinium ion. Unmodified silica surface only shows two bands at 1447cm^{-1} and 1599cm^{-1} which indicates hydrogen bonded pyridine. The peak positions at ~1489, ~1538 and ~1650 cm^{-1} are assigned as pyridinium ion.

A pyridine desorption study at elevated temperature was undertaken to elucidate the strength of the acidic sites present. The effect of evacuation temperature on HPW (18wt%)/Aerosil 200 is displayed in Figure 4.11. The hydrogen bonded pyridine peaks were removed at evacuation temperature about ~200°C (duration 1-1½ hours). A new Brønsted acid band positioned at ~1631 cm^{-1} was observed at elevated temperature besides the appearance of the isolated hydroxyl group at ~3739 cm^{-1}. This showed that the remaining pyridine at higher temperature only adsorbed on the acid sites generated by the supported HPW.

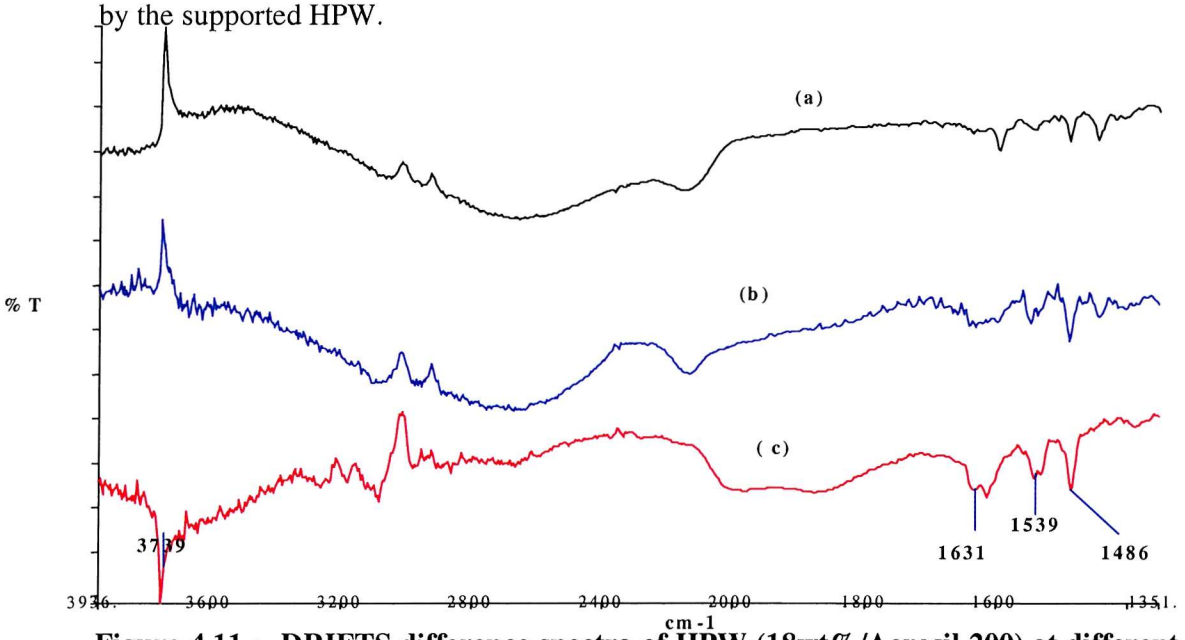

Figure 4.11 :- DRIFTS difference spectra of HPW (18wt%/Aerosil 200) at different evacuation temperature, a) room temperature b) 100°C c) 200°C.

After removal of the weakly bonded pyridine, HPW (18wt%)/Aerosil 200 was studied by Temperature Programmed Desorption (TPD) in the temperature range of 300-800K. However, no pyridine desorption could be observed. Masses due to the decomposition of the Keggin acid and pyridine were observed instead. One reason would be the acid interaction with the base, pyridine was too strong that the adsorbate decomposes before it desorbs. J.B.Moffat *et al* [20] have claimed that pyridine was desorbed into the gas phase only in conditions such that more than *ca.*1 pyridine molecule had been adsorbed per Keggin unit. When smaller quantities were adsorbed at 298K decomposition products only were detected. By increasing the evacuation temperature to 250°C, bands due to pyridine adsorption had disappeared completely from the IR spectrum.

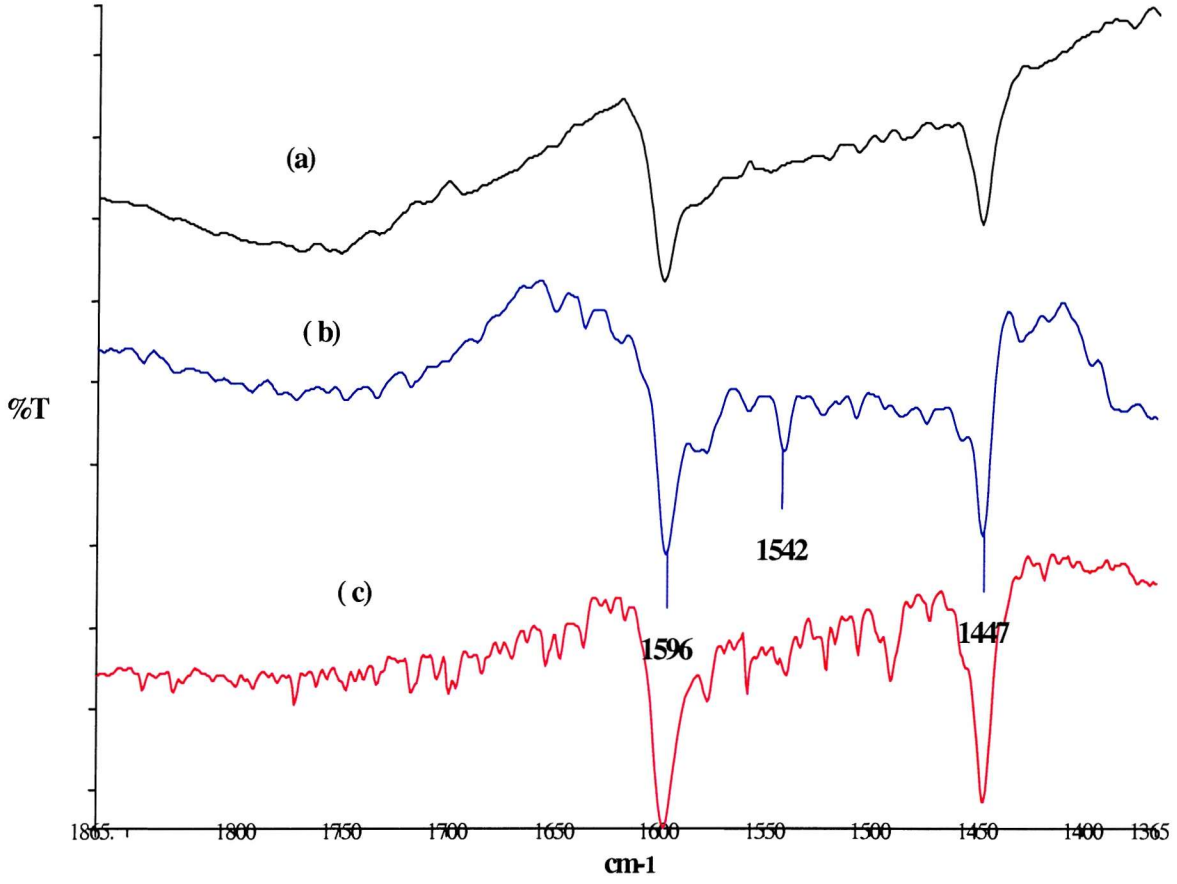

Figure 4.12 :- DRIFTS difference spectra of pyridine adsorbed on HPW supported on H_1SiO_2, a) H_1SiO_2 b) HPW (15wt%)/H_1SiO_2 c) HPW (40wt%)/H_1SiO_2.

Figure 4.12 illustrates the IR spectra of pyridine adsorbed on HPW supported on H_1SiO_2. Hydrogen bonded pyridine at ~1447 cm^{-1} and 1596 cm^{-1} were observed in addition to a peak due to Brønsted acidity around ~1542 cm^{-1}. It is clear from these spectra that HPW supported on Aerosil gives intense absorption peaks due to Brønsted acidity as compared to HPW on H_1SiO_2. One reason which accounts for this observation is the very low loading of HPW on mesoporous silica per nm^2. Under comparable conditions, the loading was 0.24 molecules/nm^2 for HPW(18wt%)/Aerosil 200 but only 0.06 molecules/nm^2 for HPW(15wt%/H_1SiO_2). There is a presence of peaks which were attributed to Brønsted acidity that can be clearly observed in the IR spectrum for high loaded HPW on H_1SiO_2. By comparison, the increase in HPW loading on H_1SiO_2 did not increase the Brønsted acidity significantly.

4.3.7 Solid State NMR

^{31}P Solid State NMR is a valuable tool for the investigation of solid as well as supported catalysts based on heteropolyacids [21,22]. There were a number of solid state NMR studies in the literature which focused on the supported heteropolyacids system. F.Lefebvre [23] has studied a series of HPW/SiO_2 catalysts with various polyanion contents (ranging from 13 to 87wt%) by ^{31}P MAS NMR spectroscopy. Two peaks were detected, corresponding to the bulk HPW and the other to $(\equiv SiOH_2^+)(H_2PW_{12}O_{40}^-)$. A.Corma *et al* [15] used ^{31}P MAS NMR relaxation time as a probe to study the dispersion and state of the Keggin anions in the HPW/SiO_2 with different loadings.

Figure 4.13 shows ^{31}P MAS NMR spectra for (a) HPW(18wt%)/SiO_2 (b) HPW(15wt%)/H_1SiO_2 and (c) HPW(40wt%)/H_1SiO_2. All the 3 NMR spectra have a single peak ~15 ppm which is similar to the ^{31}P chemical shift of bulk HPW. The spectrum for bulk HPW agrees well with the literature value [21] which showed that the chemical shift depends on the water content in the sample, ranging from –11.0 to –15.8 ppm. The chemical shifts were -15.1 ppm for highly hydrated sample, -15.6 ppm for hexahydrate sample and –11.1 ppm for anhydrous one. The results obtained indicates unambiguously that the Keggin structure is retained upon loading HPW on silica.

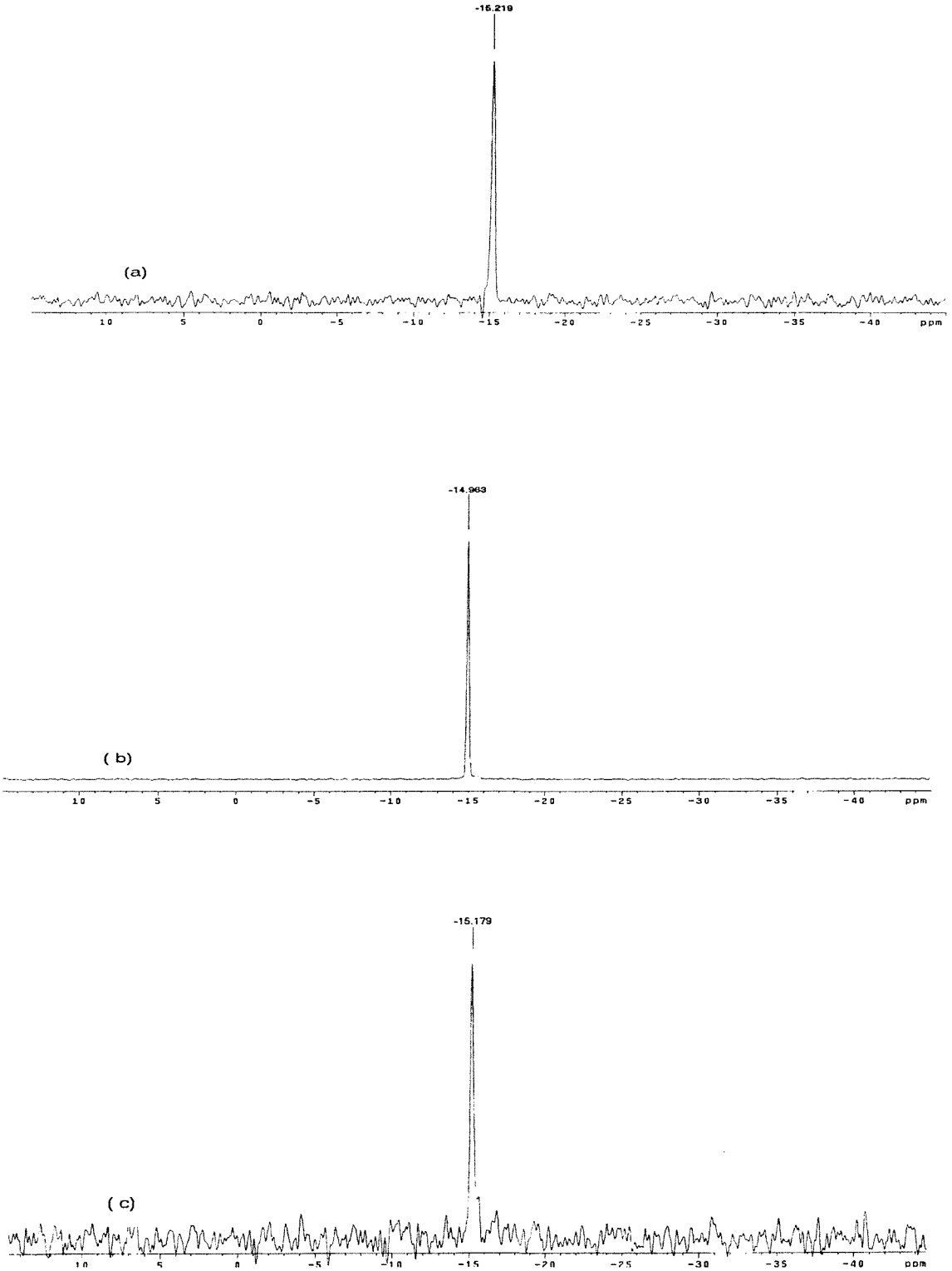

Figure 4.13 :- ^{31}P MAS NMR spectra of a) HPW(18wt%)/SiO_2 b)HPW(15wt%)/H_1SiO_2 c) HPW(40wt%/H_1SiO_2).

In contrast, HPW supported on pure siliceous supports, amorphous silica SiO_2 or mesoporous molecular sieve MCM-41 [4] which were prepared by conventional impregnation with aqueous HPW solution include at least two HPW forms, which can well be discriminated by ^{31}P MAS NMR. One (A) with intact Keggin structure and the other (B) with a different structure. The relative amount of the two depends on the HPA loading and the preparation procedure. Besides the intense line of HPW, there is another resonance of lower intensity at –13.3 ppm which can be assigned to lacunary(defect) heteropoly anions formed via the decomposition of the HPW Keggin structure. It is known that the anion decomposes in aqueous solution at pH ≥2 to form the lacunary anions [10].

Figure 4.14 displayed the ^{29}Si MAS NMR spectrum of HPW/H_1SiO_2 loaded with 15wt% of tungsten. The deconvolution of this spectrum depicted in Figure 4.14 b reveals 3 resonances at –109.4, -100.2 and –91.2 ppm. Compared to unmodified H_1SiO_2, the ratio of Q^4:Q^3 is slightly higher in the HPW/H_1SiO_2 loaded with 15wt%. Chemical shifts at –91.2 ppm (Q^2) is attributable to silicon atoms, carrying geminal silanols, -100.2 ppm (Q^3) is attributed to silicon atoms carrying single hydroxyl groups, being either isolated or vicinal silanols while –109.4 ppm (Q^4) is due to silicon atoms not bonded to any silanol groups [24]. The results obtained may implied that there is some interactions of HPW with the isolated or vicinal silanols of the silica surface. This is not surprising since it has been demonstrated [4] that the ^{31}P MAS NMR of the species $(\equiv SiOH_2)^+(H_2PW_{12}O_{40})^-$ and the bulk HPW are unlikely to be significantly different.

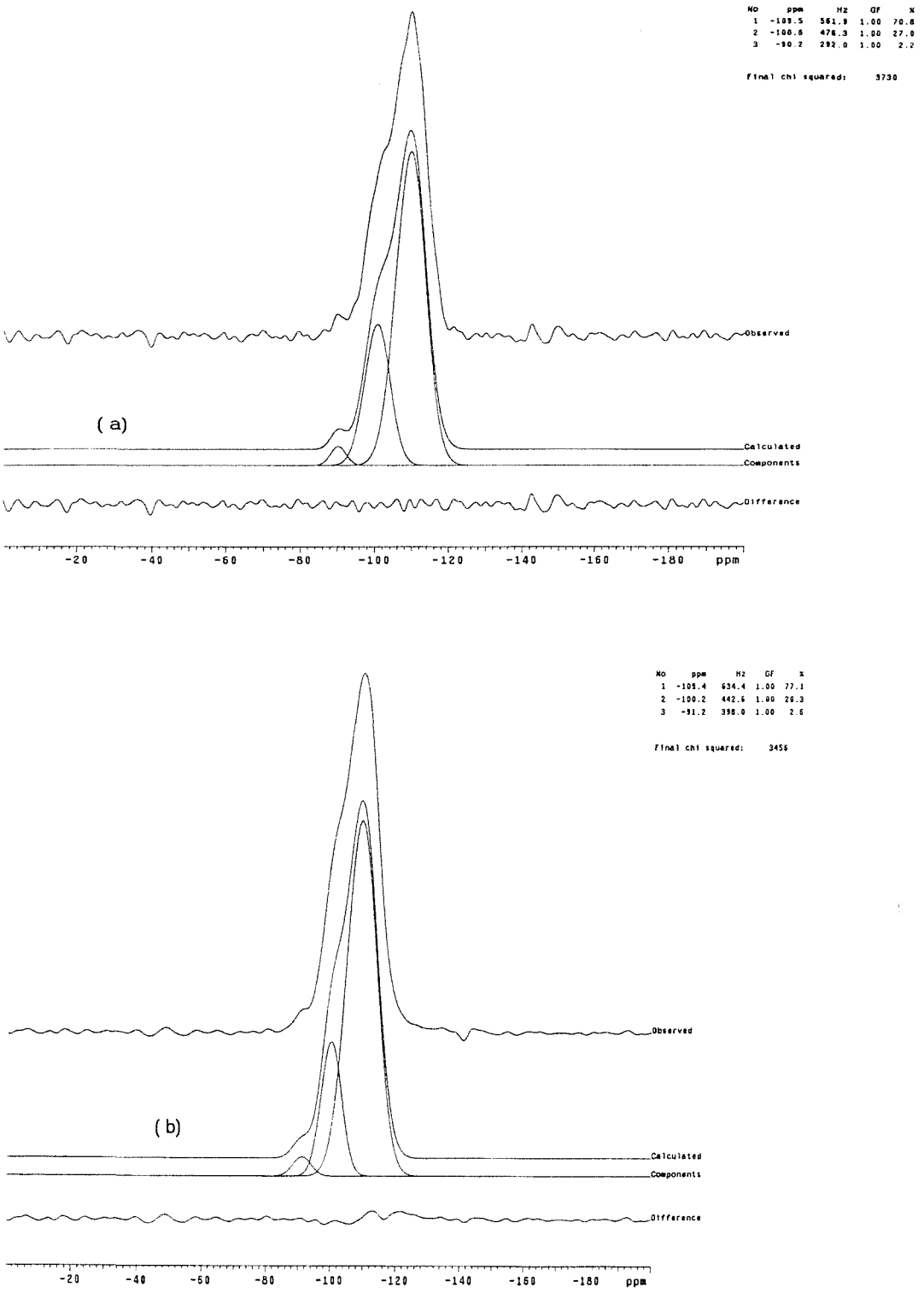

Figure 4.14 :- ^{29}Si MAS NMR spectra of a) H_1SiO_2 b) HPW(15wt%)/H_1SiO_2.

4.3.8 ^{31}P Solid State NMR of TEPO (triethylphosphine oxide)

Several probe molecules have been used to study solid acids including ^{13}C acetone, ^{13}C mesityl oxide and ^{15}N pyridine [25,26]. Unfortunately, due to the low population of probe molecules adsorbed on the acid sites of a surface, the low sensitivity of these nuclei requires either extensive signal averaging or the use of labeled materials. To avoid both of these problems, an ideal replacement probe would be ^{31}P. The gyromagnetic ratio and natural abundance of ^{31}P are much greater than those of either ^{13}C or ^{15}N resulting in an order of magnitude increase in the NMR signal that can be observed.

Previously reported ^{31}P MAS NMR studies over the past decade have focused primarily on trimethylphosphine as the adsorbate of choice. Unfortunately, the small variation of the ^{31}P chemical shift of trimethylphosphine probe for the determination of acidity limits the utility of this probe for the determination of acidity. Drago and Osegovic [27] have demonstrated that the ^{31}P isotropic chemical shift of the probe triethylphosphine oxide (TEPO) can be used to identify the acidity of multiple acid sites on the surface. The difference in the ^{31}P chemical shift of chemisorbed TEPO with respect to physisorbed TEPO, $\Delta\delta$ (where the range is between 2-70), establishes a scale of solid acidity that can be validated by comparison to enthalpies of calorimetric methods [28].

The same methodology has been applied to study the acidities of the supported heteropolyacid/HPW system in this work. Figure 4.15 depicts the ^{31}P MAS NMR spectra for (a) HPW(18wt%)/Aerosil 200 (b) HPW(30wt%)/Aerosil 200, both treated with TEPO. As can be seen from both spectra, the bulk of the acidic sites presence were only weakly acidic with $\Delta\delta$= ~13. A shoulder and a small peak around ~80 ppm and ~110 ppm respectively could be observed in the high loaded sample. This indicates the presents of a few sites with strong acidity with $\Delta\delta$ > 30 ppm. These results may complement the results obtained with the acidity determination experiment with basic indicators which suggests the presence of acid sites of at least equivalent to 50% of concentrated sulphuric acid. Stronger acid sites will cause greater interaction with the

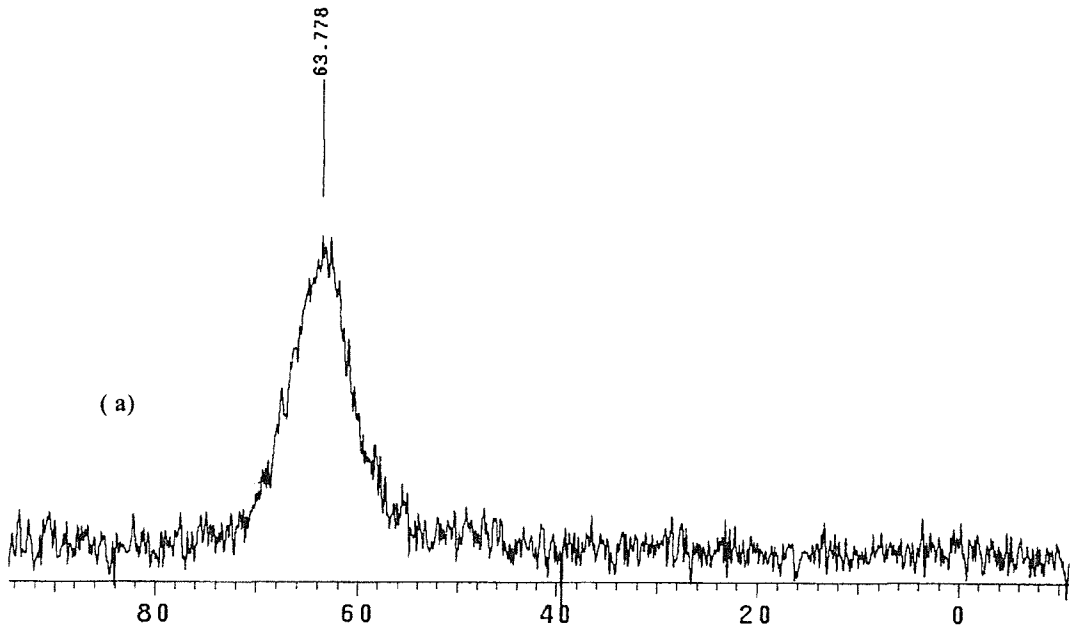

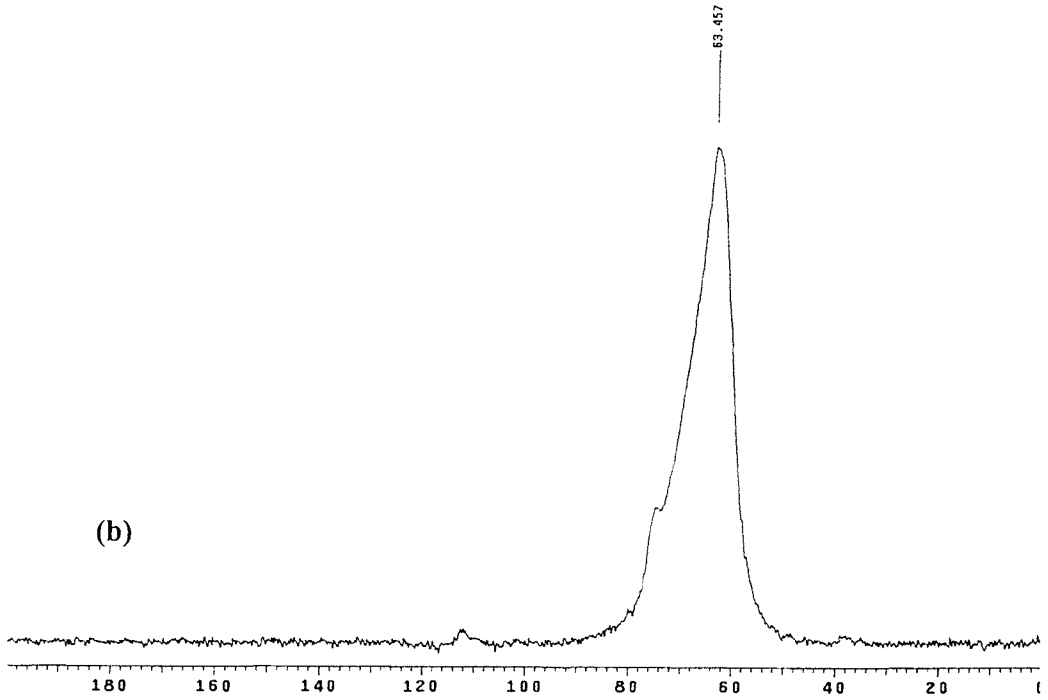

Figure 4.15 :- ^{31}P MAS NMR spectra for a) HPW(18wt%)/Aerosil 200 b) HPW(30wt%)/Aerosil 200, both treated with TEPO.

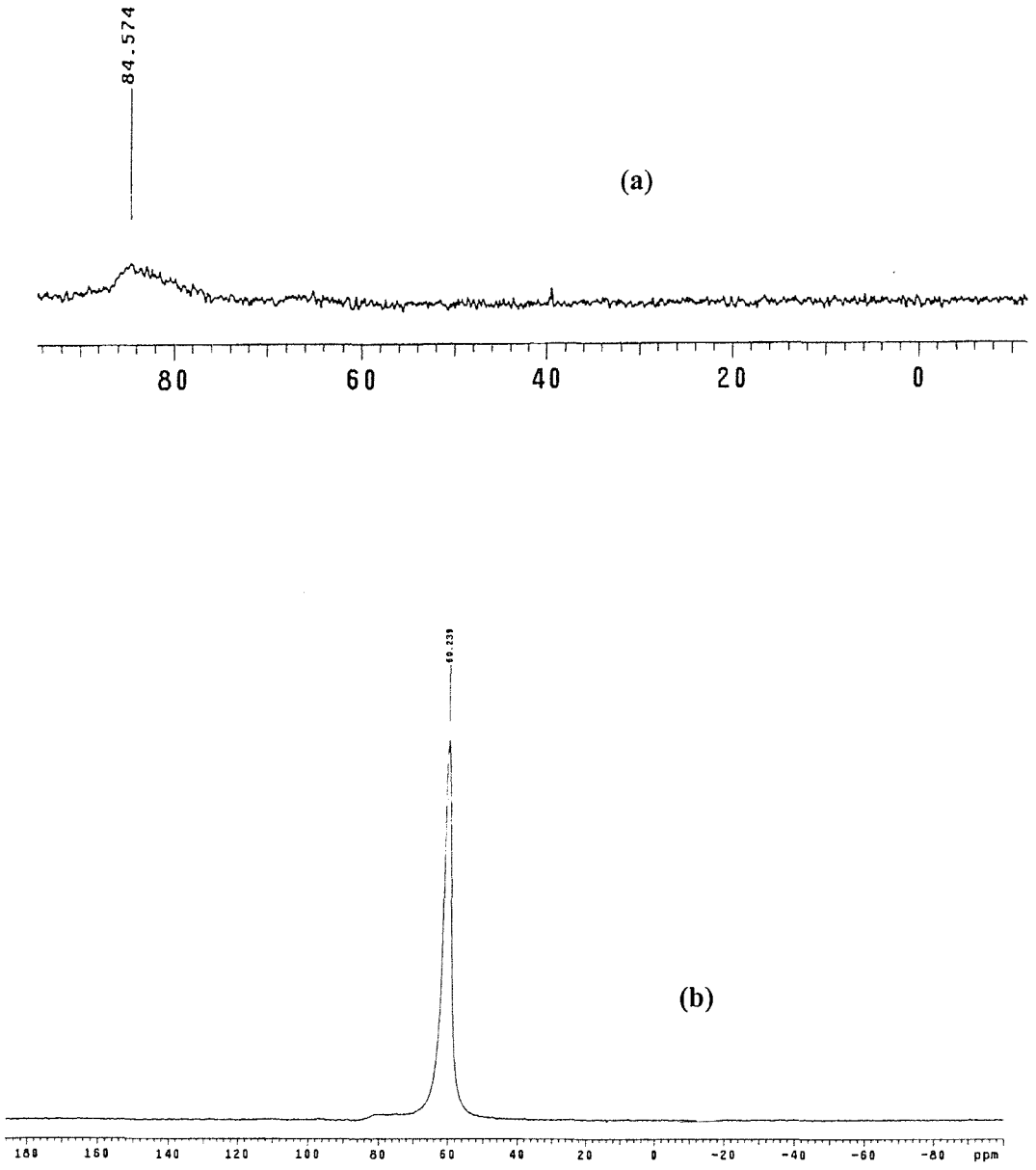

Figure 4.16 :- ^{31}P MAS NMR spectra of a) HPW(15wt%)/H_1SiO_2 b) HPW(40wt%)/H_1SiO_2, both treated with TEPO.

probe, decreasing the electron density about the central phosphorus atom in TEPO. The chemical shift of TEPO will consistently increase with the acid strength until full protonation occurs. If full protonation occurs, no further increase in the chemical shift will occur, as the conjugate acid of TEPO, $HTEPO^+$, can no longer easily donate electron density. According to microcalorimetry results obtained by I.V.Kozhevnikov [29], when loading HPW (20wt%) on SiO_2, the proton sites became weaker and less uniform. Only 20% of the total number of proton sites remain as strong as in bulk HPW.

Figure 4.16 illustrates the ^{31}P MAS NMR spectra for HPW(15wt%)/H_1SiO_2 (b) HPW(40%)/H_1SiO_2, both treated with TEPO. In the high loaded sample, similar spectra with the HPW/Aerosil 200 are observed where a very low intensity peak is obvious around 80 ppm besides a very intense peak at 60 ppm. Only sites with high acidity with corresponding $\Delta\delta$ value of 34 is observed for low loaded sample.

4.3.9 Temperature Programmed Desorption(TPD)

Heteropolyacids have moderately high thermal stability. G.M.Maksimov [30] has presented a table which showed the temperatures of the onset of decomposition of some known heteropolyacids with Keggin structure. Tungsten heteropolyacids have higher thermal stability than molybdenum based heteropolyacids. However, thermally decomposed molybdenum heteropolyacids become reconstructed under exposure to water vapour [31]. In the case of much less labile tungsten heteropolyacids, such reconstruction seems unlikely.

TPD was performed on the modified silicas to study the decomposition of acids after immobilisation. It was found that Keggin acid begins to decompose around 470K as shown in Figure 4.17 for 15wt % HPW on H_1SiO_2. Above 470K, the Keggin structure of HPW collapse and transforms into WO_3 and phosphorus oxides [32]. Masses 47 and 48

were assigned to P=O containing fragments. Lower masses e.g. 15, 28 and 44 could be assigned to some hydrocarbon fragments from the residual silica template. The decomposition causes the loss of their acidity. The results obtained here seems to agree with that reported in the literature [33] where the thermal stability of HPW supported on SiO_2 is lower than that of the parent HPA.

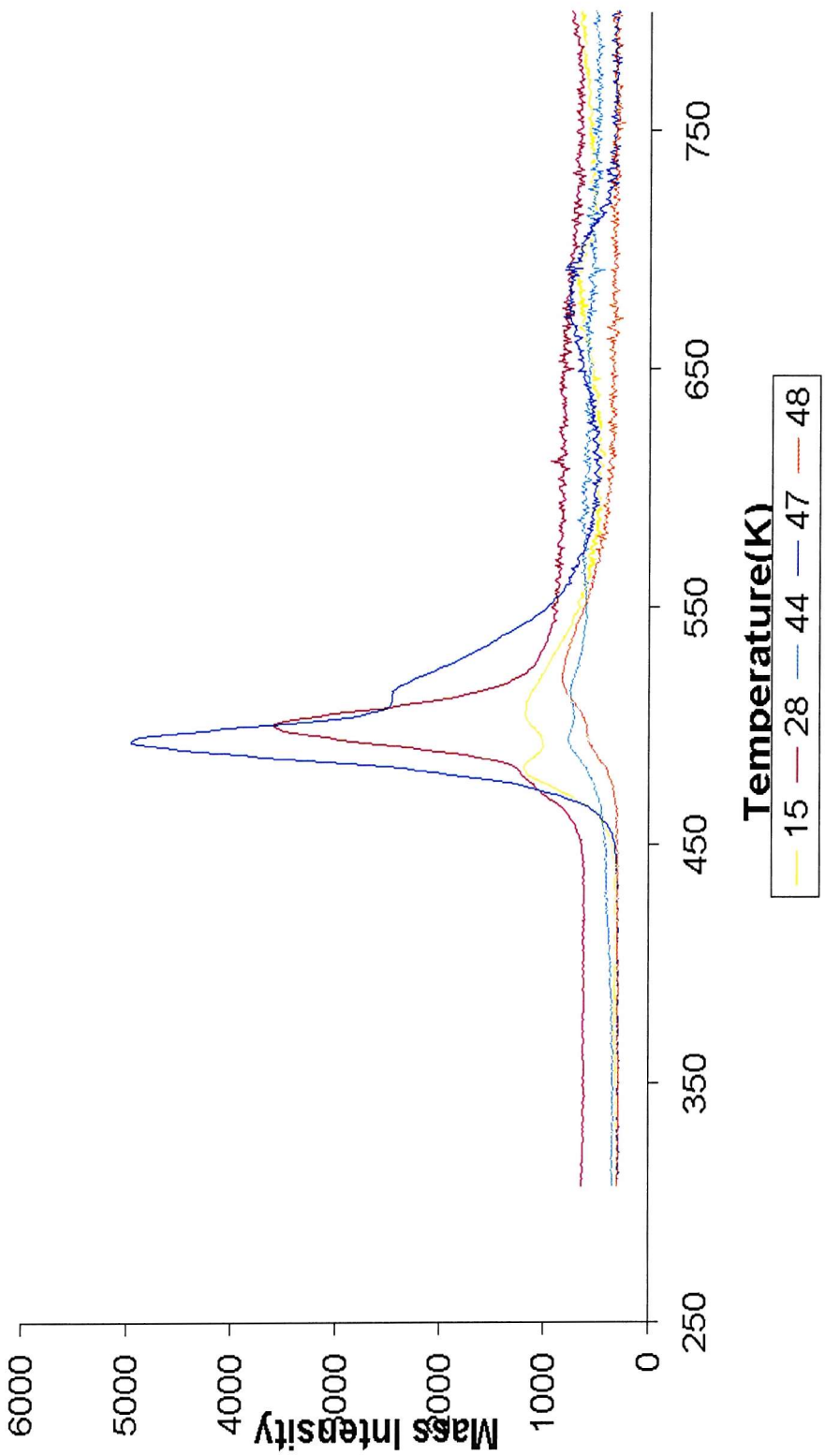

Figure 4.17 :- HPW(15%)/H_1SiO_2 decomposition by temperature programmed desorption(TPD).

4.4 Conclusions

A series of silica based supports modified with 12-phosphotungstic acid(HPW) have been prepared. As a support, amorphous silica(Aerosil 200) and a liquid crystal templated mesoporous silica H_1SiO_2 were used. With the aim of obtaining strongly acidic solid catalysts, the supported HPW were characterised with a wide range of techniques with emphasis on DRIFTS and solid state NMR experiments.

The significant result from this work is the preparation of the catalysts, comprising essentially Keggin-type HPW species on the silica surface over a wide range of HPW loading. This is convenient done by HPW adsorption from organic solvents(dimethylsulfoxide &methanol) in this work. Results from TEPO studies showed that the bulk of the acid sites present were only weakly acidic on both types of silica. However, it is evident from the ^{31}P NMR spectra and basic indicator experiments that a few sites with enhanced acidity were also present. According to microcalorimetric data [29], the proton sites in dehydrated HPW are essentially uniform. They are characterised by the different heat of ammonia adsorption of 140-160 kJ/mol, which is almost the same as that for H-modenite, one of the most acidic zeolites. However, when loaded on silica, the proton sites become weaker and less uniform. This seems to justify the results obtained here.

^{31}P NMR of the supported HPW only showed one main peak around –15 ppm with the absence of other peaks observed in the literature. This can be understood by considering HPW has greater stability towards hydrolysis in organic solvents compared to aqueous solutions.

Acidic properties of the supported HPW have been characterised by a combined study using DRIFTS and TPD. Hydrogen bonded pyridine (~1447 cm^{-1} and ~1599cm^{-1}) were removed at evacuation temperature above 100°C. The amount of pyridine bonded to Brønsted acid sites is far greater for HPW/Aerosil 200 than for HPW/H_1SiO_2. This can be clearly observed by comparing the intensities of the peaks due to Brønsted acidity for both supported HPW. The reason for this observation can be explained by considering the uptake of HPW by both types of silica.

References

[1] G.S.Attard, J.C.Glyde, C.G.Göltner, *Nature*, **366**, 378, 1995.

[2] J.C.Bailar, *Inorg.Syn.*, **1**, 132, 1939.

[3] K.Nowinska, R.Fiedorow, J.Adamiec, *J.Chem.Soc. Faraday Trans.*, **87**, 749, 1991.

[4] I.V.Kozhevnikov, K.R.Kloetstra, A.Sinnema, H.W.Zandbergen, H.van Bekkum, *J.Mol.Catal(A).*, **114**, 287, 1996.

[5] C.Walling, *J.Am.Chem.Soc.*, **72**, 1164, 1950.

[6] L.P.Hammett, A.J.Deyrup, *J.Am.Chem.Soc.*, **54**, 2721, 1932.

[7] K.Tanabe, *'Solid Acids and Bases – Their Catalytic Properties'*, Academic Press, New York, 1970.

[8] A.Corma, *Chem.Rev.*, **95**, 559, 1995.

[9] G.M.Varga, E.Papaconstantinou, M.T.Pope, *Inorg.Chem.*, **9**, 662, 1970.

[10] I.V.Kozhevnikov, *Catal.Lett.*, **30**, 241, 1995.

[11] A.Ghanbari-Siahkali, A.Philippou, J.Dwyer, M.W.Anderson, *Appl.Catal.A.*, **192**, 57, 2000.

[12] Y.Izumi, R.Hasebe, K.Urabe, *J.Catal.*, **84**, 402, 1983.

[13] D.Dollimore, G.R.Heal, *J.Appl.Chem.*, **14**, 109, 1964.

[14] S.Brunauer, L.S.Deming, W.S.Deming, W.Teller, *J.Am.Chem.Soc.*, **62**, 1723, 1940.

[15] T.Blasco, A.Corma, A.Martinez, P.Martinez-Escolano, *J.Catal.*, **177**, 306, 1998.

[16] W.Chu, X.Yang, Y.Shan, X.Ye, Y.Wu, *Catal.Lett.*, **42**, 201, 1996.

[17] A.Jentys, W.Schieber, H.Vinek, *Chem.Comm.*, 335, 1999.

[18] S.Shikata, S.Nakata, T.Okuhara, M.Misono, *J.Catal.*, **166**, 263, 1997.

[19] E.P.Parry, *J.Catal.*, **2**, 371, 1963.

[20] B.K.Hodnett, J.B.Moffat, *J.Catal.*, **88**, 253, 1984.

[21] Y.Kanda, K.Y.Lee, S.Nakata, S.Asaoka, M.Misono, *Chem.Lett.*, 139, 1988.

[22] V.M.Mastikhin, S.M.Kulikov, A.V.Nosov, I.V.Kozhevnikov, I.L.Mudrakovsky, M.N.Timofeeva, *J.Mol.Catal.*, **60**, 65, 1990.

[23] F.Lefebvre, *Chem.Comm.*, 756, 1992.

[24] E.F.Vansant, P.V.D.Voort, K.C.Vrancken, *Stud.Surf.Sci.Catal.*, **93**, 59, 1995.

[25] G.E.Maciel, J.F.Haw, I.Ssuer Chuang, B.L.Hawkins, T.A.Early, D.R.Mckay, L.Petrakis, *J.Am.Chem.Soc.*, **105**, 5529, 1983.

[26] D.Michel, A.Germanus, H.Pfeifer, *J.Chem.Soc. Faraday Trans I*, **78**, 237, 1982.

[27] J.P.Osegovic, R.S.Drago, *J.Catal.*, **182**, 1, 1999.

[28] J.P.Osegovic, R.S.Drago, *J.Phys.Chem.B.*, **104**, 147, 2000.

[29] I.V.Kozhevnikov, *Catal.Rev-Sci.Eng.*, **37**, 311, 1995.

[30] G.M.Maksimov, *Russ.Chem.Rev.*, **64**, 445, 1995.

[31] Y.Konishi, K.Sakata, M.Misono, Y.Yoneda, *J.Catal.*, **77**, 169, 1982.

[32] E.López-Salinas, J.G.Hernández-Cortez, I.Schifter, E.Torres-García, J.Navarrette, A.Gutiérrez-Carrillo, T.López, P.P.Lottici, D.Bersani, *Appl.Catal.A.*, **193**, 215, 2000.

[33] I.V.Kozhevnikov, *Chem.Rev.*, **98**, 171, 1998.

Chapter 5

Synthesis and Characterisation of Supported Sulfonic Acids

5.1 Introduction

In this chapter, the preparation and characterisation of a new class of solid acid catalyst will be reported. Methanesulfonic and trifluoromethanesulfonic acid were attached to two types of silica, Aerosil 200 and mesoporous silica. There are only a few published works in the literature which concern the studies on supported triflic acid [1-4]. Work has only been focused on catalytic studies as is evident in a few patents [2-5]. Very few characterization results are known about these supported triflic acid. To cite one example, a thermally stable solid acid catalyst has been prepared by treating amorphous silica gel with trifluoromethanesulfonic acid at 150°C in a closed glass vessel [1]. A solvent such as 1,1,2-trichloro-2,2,1-trifluoro-ethane (Freon 113) can be conveniently used to dissolve the triflic acid. The obtained material is an active catalyst in the alkylation of isobutane with *n*-butenes to yield high-octane gasoline components. However to date, there is no reported work on supported methanesulfonic acid.

Since the first report of the structure in 1992 [6], a number of studies have been performed aiming to modify the MCM-41 synthesis procedure in order to increase the potential applicability of these materials [7]. Progress in acid catalysis is lagging behind, largely because of the low acid strength of Al-MCM-41 [8]. Recently, some studies reported the syntheses of inorganic-organic hybrid mesoporous materials with alkyl [9,10] and alkylsulfonic acid [11-13] groups. These materials can be prepared either by silylation of pure silica or by co-condensation of alkoxysilanes and 3-mercaptopropyltrimethoxysilane [11,12] which is further oxidised to obtain propylsulfonic acid groups onto framework silicon atoms. These $[SO_3H]$-MCM-41 mesoporous catalysts combine a high acidity and a good accessibility to the active centers, owing to the presence of channels with large diameter, greater than 1.4 nm.

5.2 Experimental

5.2.1 Preparation of methanesulfonic acid supported on silica

About 2.0 gram of silica was used for this preparation. The amount of acid used was in excess and as a general rule, the approximate amount used was according to the ratio of acid to silanol group of 4:1 for Aerosil 200 and 2:1 for H_1SiO_2. Firstly, methanesulfonic acid (Aldrich Chemical Co.) was mixed with a sufficient amount of THF, as a solvent and then added to the silica in a round bottom flask equipped with a magnetic stirrer and a continuous nitrogen gas flow. The mixture was left to stir for 2 days for Aerosil 200 before the mixture was filtered through a glass sinter, washed several times with the solvent and dried under vacuum. For mesoporous silica, the resultant mixture was normally left to stir overnight before vacuum evaporation to remove the solvent. Subsequently, the solid obtained was washed several times with sufficient amount of solvent.

5.2.2 Preparation of trifluoromethanesulfonic acid supported on silica

CF_3SO_3H (Aldrich Chemical Co.) is a clear, extraordinary hygroscopic liquid, which easily develops brownish colour. Consequently, CF_3SO_3H was handled in a glove box. The procedure employed in preparation of the supported triflic acid is similar to the above. The amount of triflic acid used was according to the same ratio, 4:1 for acid to silanol group for Aerosil 200 and 2:1 for H_1SiO_2. The required amount of triflic acid was weighed into a round bottom flask equipped with a stopper, a subaseal and a Young's tap in a glove box. Next, acetonitrile was mixed with the triflic acid and then transferred into another round bottom flask containing the silica with a syringe. The mixture/suspension was left to stir for a period of time and the solvent was filtered off for Aerosil 200. Vacuum evaporation was employed for the modified mesoporous silica.

5.2.3 Acidity Determination by Basic Indicators

Basic indicators of varying strength were used. These included neutral red (pKa= +6.8), methyl yellow (pKa= +3.3), crystal violet (pKa= +0.8), dicinnamalacetone (pKa= -3.0), benzalacetonephenone (pKa= -5.6) and anthraquinone (pKa= -8.2). The preparation of the indicator solutions and the experimental procedures were similar to that described in chapter 4 for supported HPW. All the four modified silica samples with sulphonic acids were tested with these basic indicators.

5.2.4 Base titration of acid supported on silica

About 0.1 gram of modified silica were weighed in a conical flask. This was followed by addition of 10 ml of distilled water. The solution was then titrated with a known concentration of base, e.g. NaOH. Bromothymol blue was used as indicator in this acid base titration. The titration was performed several times until an average titration results were obtained.

5.3 Results and Discussion

5.3.1 Acidity Determination by Basic Indicators

As explained in chapter 4, the acid strength of a solid catalyst can be estimated by noting which members of a series of Hammett indicators (Table 5.1) are adsorbed in the acid form [14]. If the colour is that of the acid form of the indicator, then the value of the Hammett acidity function H_0 of the surface is the same or lower than the pK_a of the conjugate acid of the indicator. Then, the lower the pK_a of the colour changing indicator is, the greater the acid strength of the solid. The results for the indicators test were shown in table 5.2. All the silica samples supported with sulphonic acids changed the colour of indicators with pK_a values up to –3.3. There were some difficulties to discern the colour change involved for the other two indicators, benzalacetophenone and anthraquinone. Therefore, from this

experiment, it can be concluded that there is a presence of acid sites of at least as strong as 50% concentrated sulphuric acid.

Table 5.1 :- Basic indicators used for the measurement of acid strength.

	colour			
Indicators	base form	acid form	pKa	equivalent (H_2SO_4)%
neutral red	yellow	red	+6.8	8×10^{-8}
methyl yellow	yellow	red	+3.3	3×10^{-4}
crystal violet	blue	yellow	+0.8	0.1
dicinnamalacetone	yellow	red	-3.0	48
benzalacetophenone	colourless	yellow	-5.6	71
anthraquinone	colourless	yellow	-8.2	90

Table 5.2 :- Acidity determination by basic indicators (+ = colour change observed).

sample	pK_a			
	+6.8	+3.3	+0.8	-3.0
Aerosil 200/CH_3SO_3H	+	+	+	+
Aerosil 200/CF_3SO_3H	+	+	+	+
H_1SiO_2/CH_3SO_3H	+	+	+	+
H_1SiO_2/CF_3SO_3H	+	+	+	+

5.3.2 Base Titration of supported acids

Base titrations have been carried out for all the supported liquid acids. The loading of acids is displayed in Table 5.3.

Table 5.3 :- Acid loading on both types of silica

Support	Acid	Acid concentration(mmole/g)	No. of acid / nm^2
Aerosil 200	CH_3SO_3H	1.4 ± 0.2	4 ± 0.5
Aerosil 200	CF_3SO_3H	0.9 ± 0.2	3 ± 0.5
H_1SiO_2	CH_3SO_3H	3.0 ± 0.2	2 ± 0.5
H_1SiO_2	CF_3SO_3H	2.8 ± 0.2	2 ± 0.5

From the above table, the number of acid molecules per nm^2 are comparable to the number of OH group on the silica supports. From Grignard titration, it has been found that there are about 4 OH/nm^2 and 2 OH/nm^2 for Aerosil 200 and H_1SiO_2 respectively. Therefore, this confirmed that there is almost a monolayer coverage of the acid molecules when supported on the silica supports.

These titration results showed that the preparative route of these supported acids by adsorption from organic solvents proved to be a recommended method to obtain at least a monolayer coverage of the acids on the silica supports.

5.3.3 Transmission Electron Microscopy

Transmission electron microscopy has been applied to study the morphology of the silica modified with acids. Figure 5.1 and 5.2 showed the presence of the hexagonal array of uniform pores and the equidistant parallel lines arising from the mesoporous material, modified with CF_3SO_3H and CH_3SO_3H respectively. These TEM images showed that the mesostructure of the mesoporous silica is unaffected by the immobilisation process with the liquid acids. The dominant presence of the hexagonal array of pores and the parallel lines characteristic of the mesoporous supports can be clearly observed with this technique, as shown in the TEM micrographs.

Figure 5.1 :- TEM micrograph showing the equidistant parallel lines arising from the mesoporous structure of H_1SiO_2 modified with CH_3SO_3H.

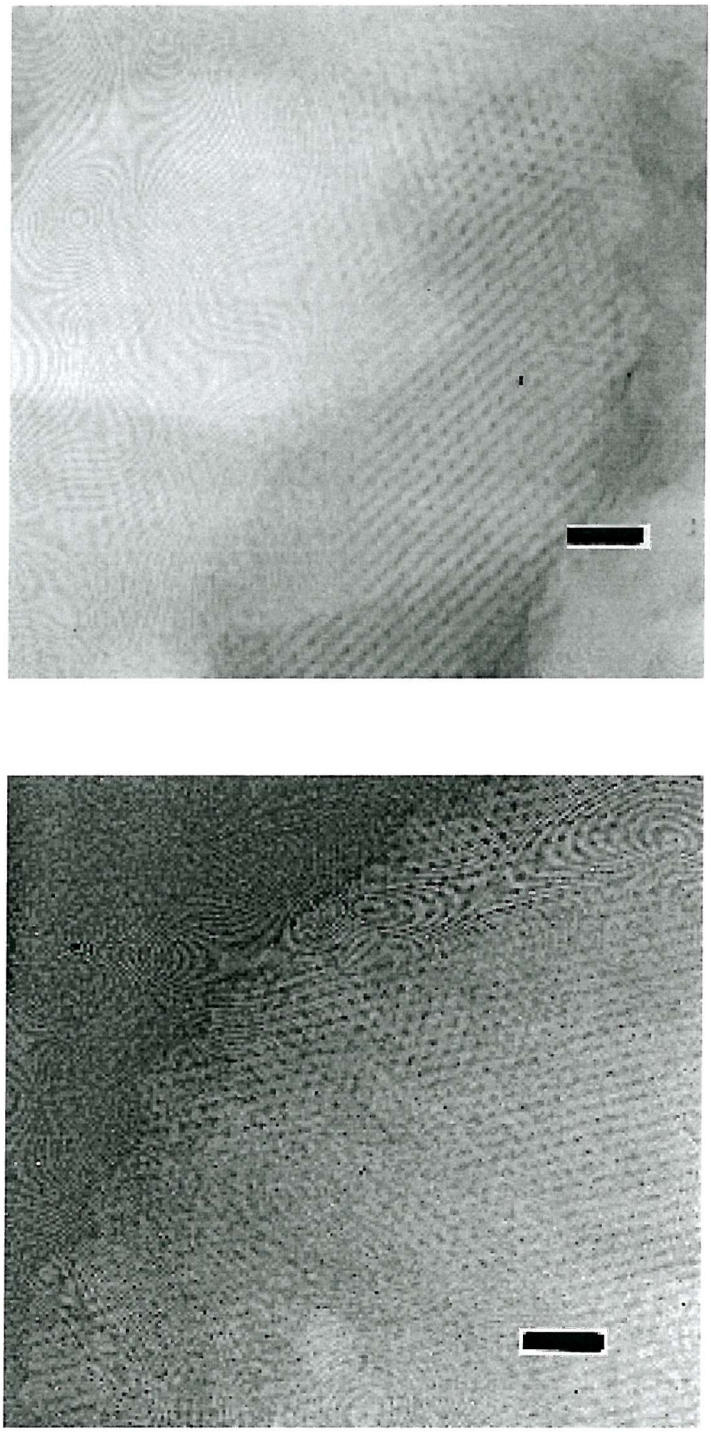

Figure 5.2 :- TEM micrographs showing the hexagonal pore arrangement and the equidistant parallel lines arising from the mesoporous structure of H_1SiO_2 modified with CF_3SO_3H. Scale bar = 20 nm.

5.3.4 Powder X-Ray Diffraction

Shown in Figure 5.3 and 5.4 are PXRD patterns of CF_3SO_3H and CH_3SO_3H supported on H_1SiO_2. The XRD pattern of unmodified H_1SiO_2 shows typically 3 reflections at 42.4Å, 25.3Å and 22.2Å. These reflections are due to ordered hexagonal array of parallel silica tubes and can be indexed assuming a hexagonal unit cell as [100], [110] and [200] (cf. chapter 3). Compared to unmodified H_1SiO_2, two reflection peaks can still be observed in the PXRD patterns of the supported acids. This indicates the mesoporous order is still preserved upon treatment of the mesoporous support with the strong acids. The unit cell parameter given by the formulae $a = 2d_{100}/\sqrt{3}$ (where d_{100} is the X-ray diffraction (100) interplanar spacing) of the unmodified H_1SiO_2 is about 42.4Å. Upon treatment with the strong acids, the gradual shift of the [100] XRD peak to lower angles suggests unit cell enlargement. The main reflection peak has moved to 45.2Å and 47.5Å for supported CH_3SO_3H and CF_3SO_3H respectively. The unit cell expansion was accompanied with loss of structural ordering which manifested itself with broadening and weakening of the [100] peak. Another reason which give rise to the reduced intensity of the main peak observed could be attributed to contrast matching between the silica framework and the liquid superacids moieties that are distributed inside the channels of H_1SiO_2 [15].

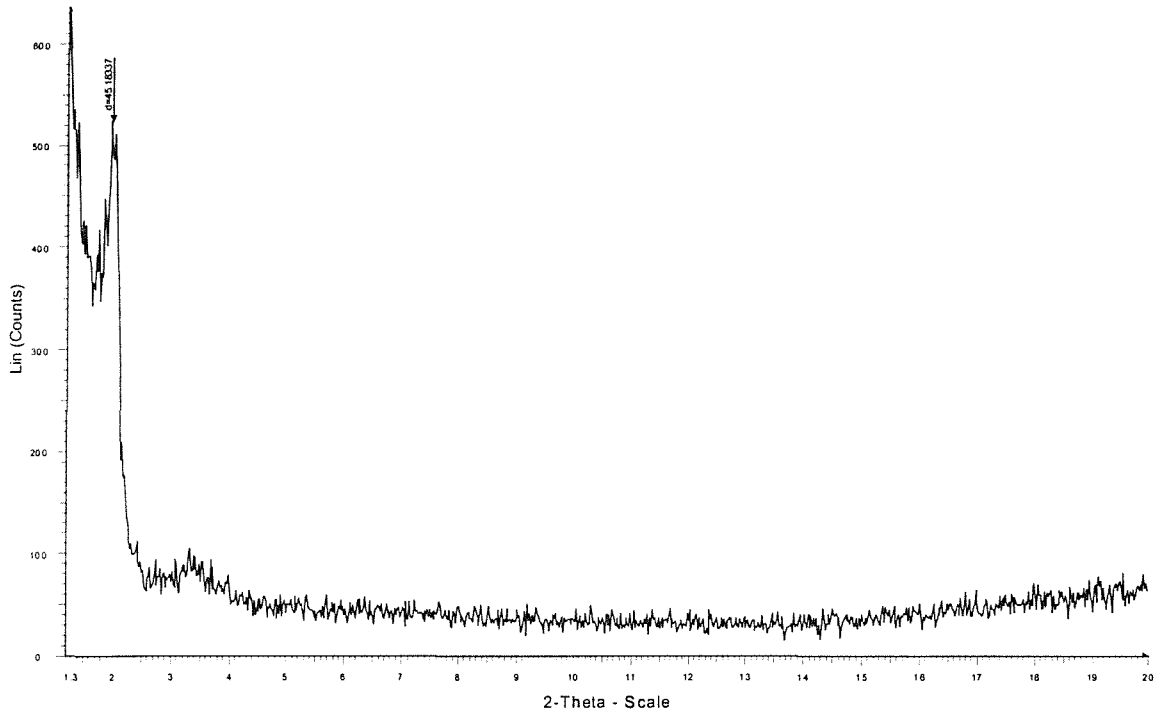

Figure 5.3 :- PXRD pattern of CH_3SO_3H supported on H_1SiO_2 showing reduction in intensity of the main peak with d-spacing at 45.2Å.

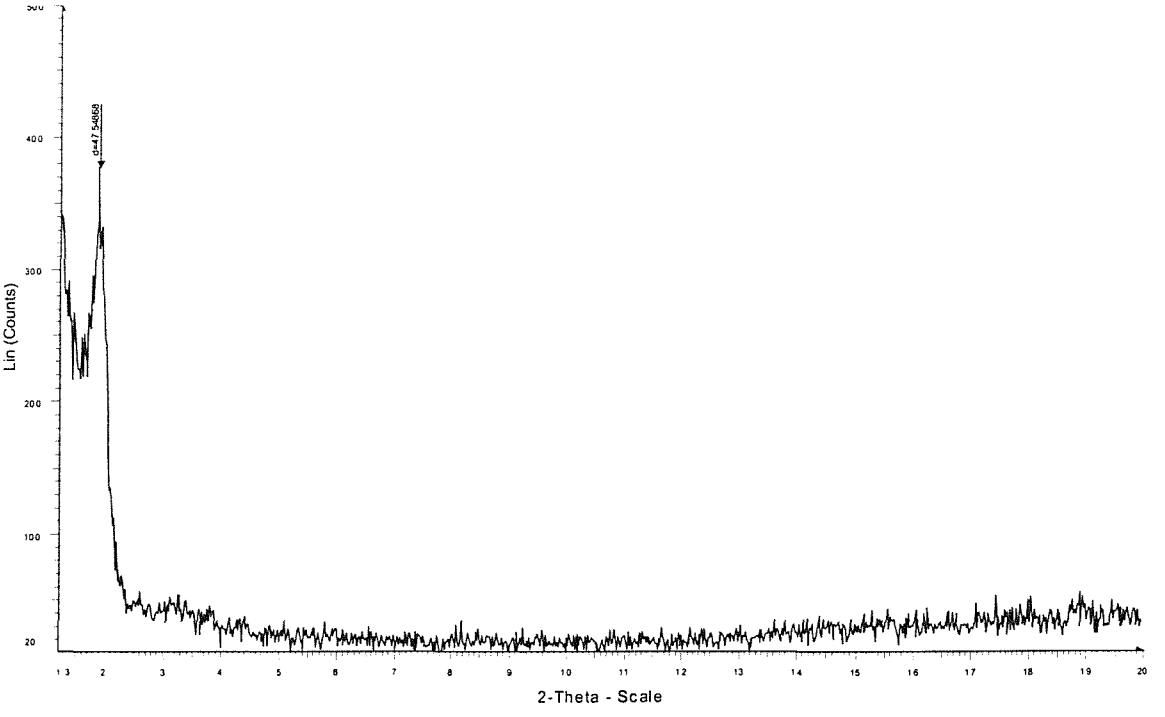

Figure 5.4 :- PXRD pattern of CF_3SO_3H supported on H_1SiO_2 which depicts the reduced intensity of the main reflection peak at 47.5Å.

5.3.5 BET surface area measurements

BET surface areas and pore distributions were calculated using N_2 adsorption at 77K. Table 5.4 displayed the various parameters measured for the liquid acids supported on silica.

Table 5.4 :- Physical parameters for liquid acids supported on silica.

Support	Acid	A_{BET}/m^2g^{-1}	d/Å	V_P/cm^3g^{-1}
Aerosil 200	CH_3SO_3H	120		
Aerosil 200	CF_3SO_3H	100		
H_1SiO_2	CH_3SO_3H	220	30	0.13
H_1SiO_2	CF_3SO_3H	140	28	0.08

Upon loading with the acids, the surface area, pore size and pore volume all decreased as expected. The reduction in surface area for the mesoporous support is much more significant compared to Aerosil samples. The reduction in pore volume from 0.59 cm^3g^{-1} for the unsupported H_1SiO_2 to 0.08-0.13 cm^3g^{-1} for the supported acids suggests the filling of the pores with acids. Figure 5.5 illustrates the pore size distribution curve for CF_3SO_3H supported on H_1SiO_2. With immobilization of the acids, the pore diameter has reduced from 36 Å to about 28-30 Å.

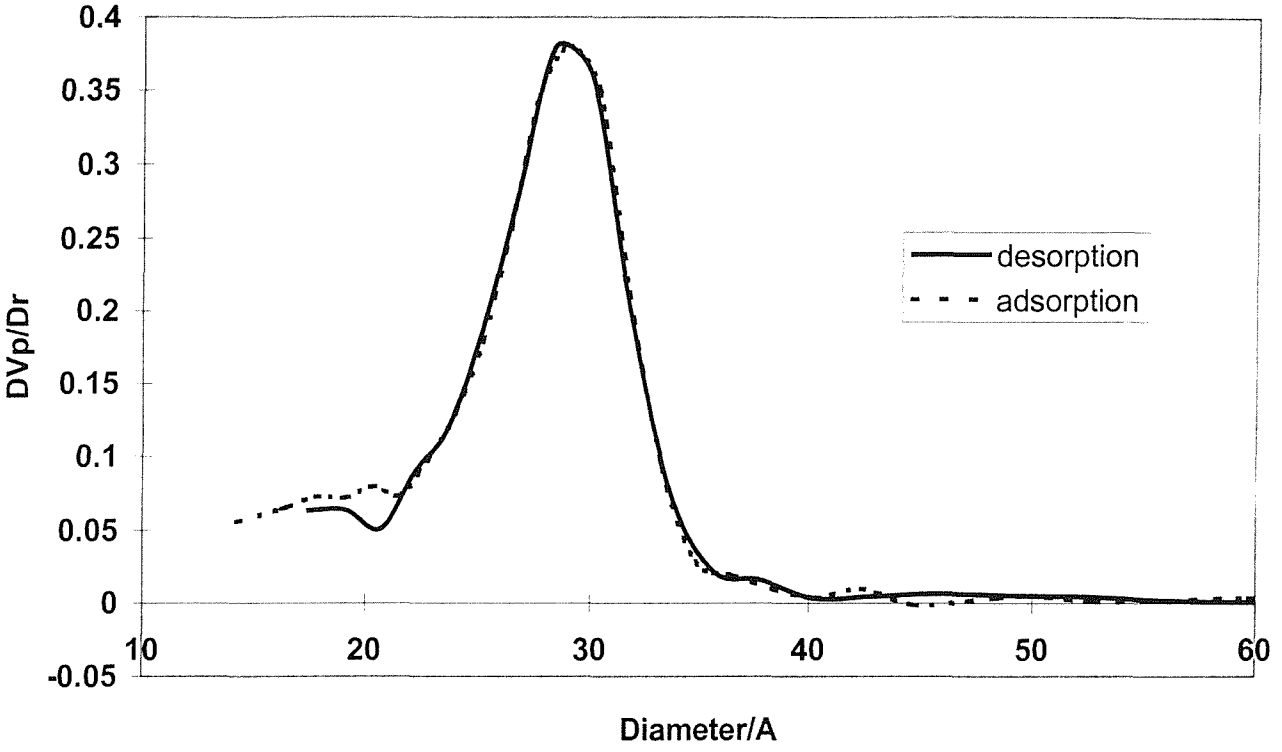

Figure 5.5 :- Pore size distribution of CF_3SO_3H supported on H_1SiO_2

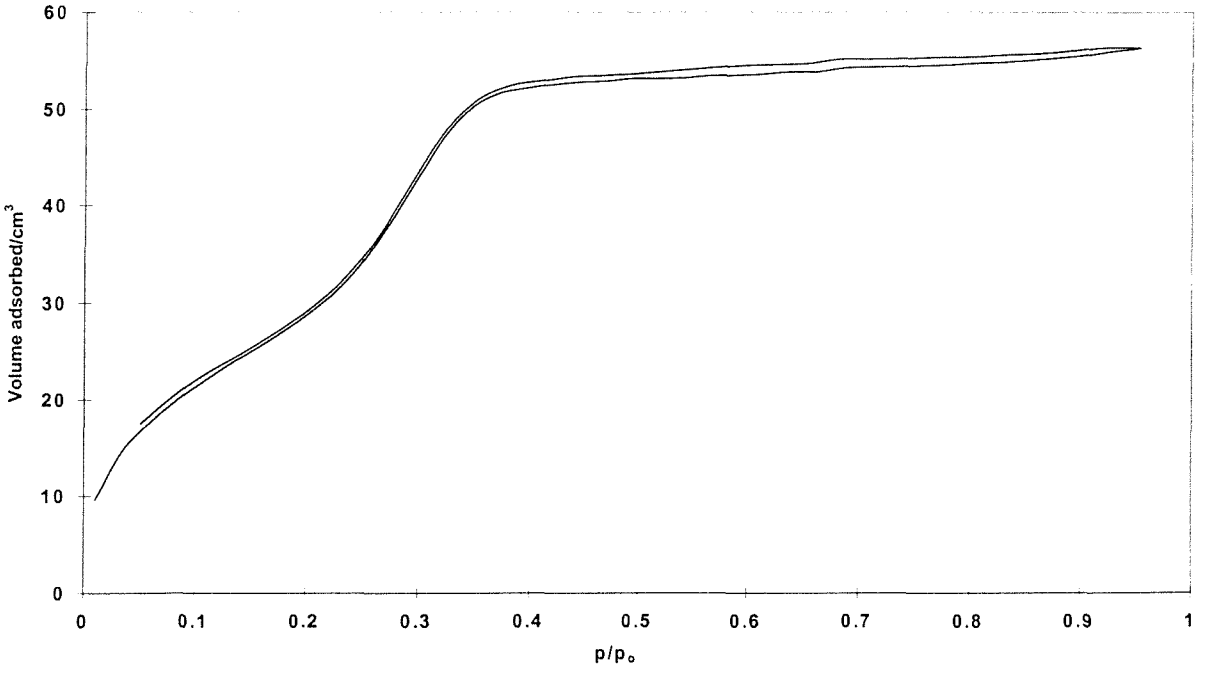

Figure 5.6 :- Adsorption-desorption isotherm of CF_3SO_3H supported on H_1SiO_2

Reversible type IV isotherm (refer chapter 2) of the CF_3SO_3H supported on H_1SiO_2 is shown in figure 5.6. The N_2 adsorption isotherm of the supported CF_3SO_3H is different from that of unmodified H_1SiO_2 in that it displayed a considerable lower N_2 uptake. For example, the total volumes of adsorbed N_2 at 77K and $p/p_o = 0.95$ is 0.09 cm^3g^{-1} compared to 0.54 cm^3g^{-1} for unmodified H_1SiO_2. Again, this strong decrease in the total volume of adsorbed N_2 can be attributed to filling of the mesopores with acids. However, the isotherm was still of type IV. This indicates the textural properties of the silica support were preserved during the immobilisation experiment and that the channels remained accessible. In summary, PXRD and N_2 sorption studies are consistent with homogeneous lining of the pore walls by the acid species reducing the accessible diameter of the pores.

5.3.6 Diffuse Reflectance Infrared Fourier Transform Spectroscopy (DRIFTS)

Chemisorption of pyridine on supported sulfonic acids has been performed for the purpose of characterising the acidic sites present. Parry [16] has reported the utility of pyridine in the infrared study of catalyst acidity. He utilised the fact that pyridine interacting as a Lewis base has a distinctly different spectrum from that of pyridine interacting as a Brønsted base. The difference spectra for CH_3SO_3H supported on both types of silica treated with pyridine are illustrated in figure 5.7. Modified silica before treatment with pyridine was used as the background in the recording of all the difference spectra. CH_3SO_3H supported on mesoporous silica, H_1SiO_2 also produced identical difference spectrum. The observed peak positions at room temperature were ~1631, ~1549 and ~1489 cm^{-1}. In this spectrum, peaks around ~3061 and ~3090 cm^{-1} could also be observed. These positions are in good agreement with the data reported by Parry [16]. These peak positions indicate essentially only the presence of Brønsted acidity on the supported CH_3SO_3H. The bands observed at ~3061 and ~3090 cm^{-1} were assigned to CH vibration of the pyridine ring and bands positions at ~1638 and ~1545 cm^{-1} were attributed to the combined C-C stretching and in-plane CH and NH bending mode [16]. Peaks indicative of isolated silanol groups around ~3700 cm^{-1} were not observed from these spectra. Unmodified silica surface (cf. chapter 4) only shows two bands at ~1447 cm^{-1} and 1599 cm^{-1} which indicate the presence of only hydrogen bonded pyridine.

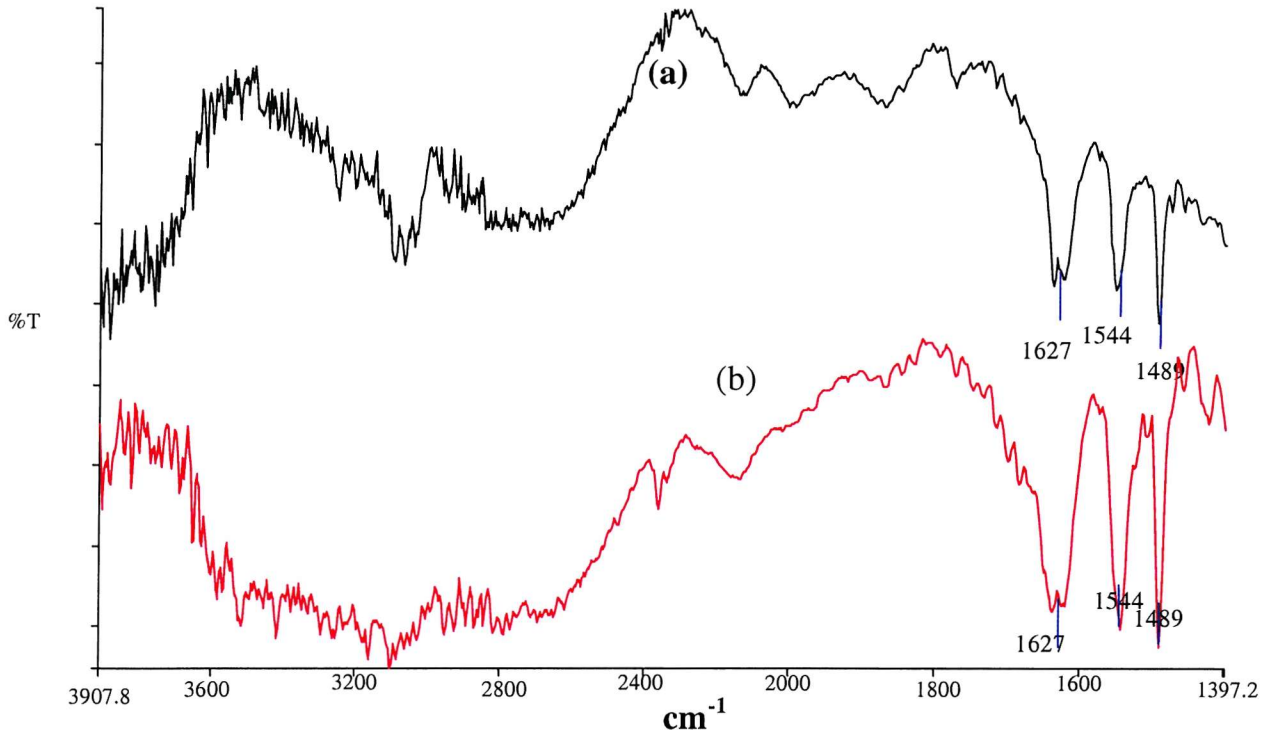

Figure 5.7 :- DRIFTS difference spectra of supported CH_3SO_3H on a) Aerosil 200 and b) H_1SiO_2, both treated with pyridine showing the presence of only Brønsted acidity.

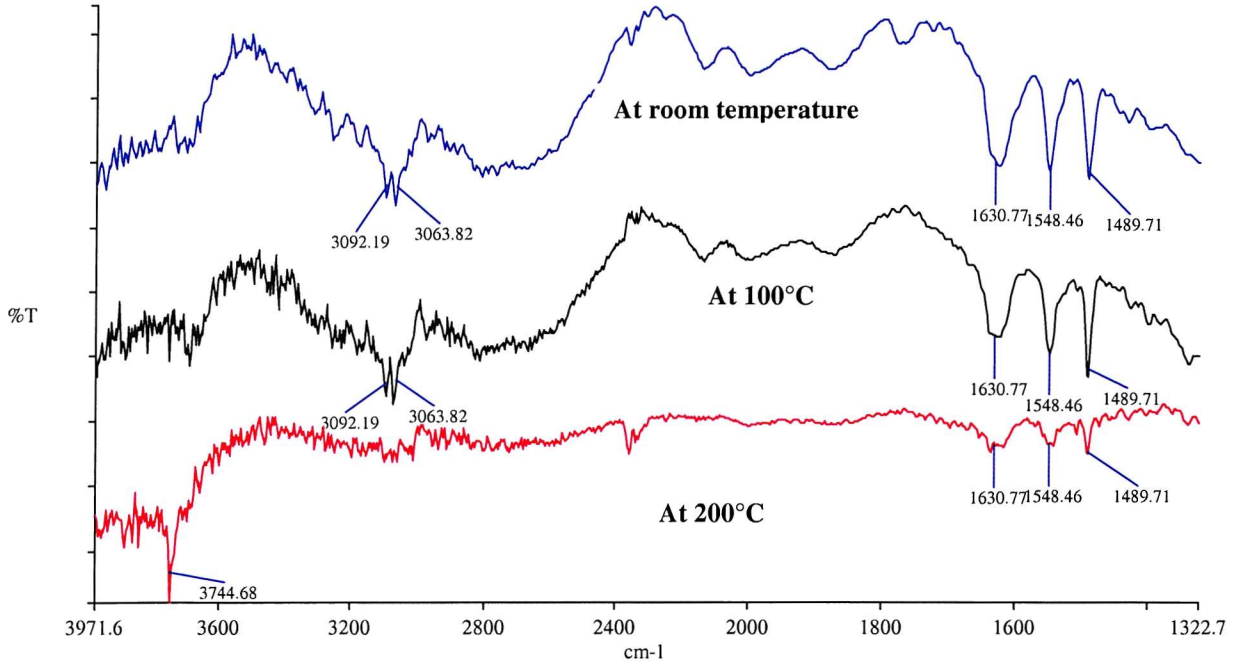

Figure 5.8 :- DRIFTS difference spectra of the effect of elevated temperature on supported CH_3SO_3H on Aerosil 200 treated with pyridine.

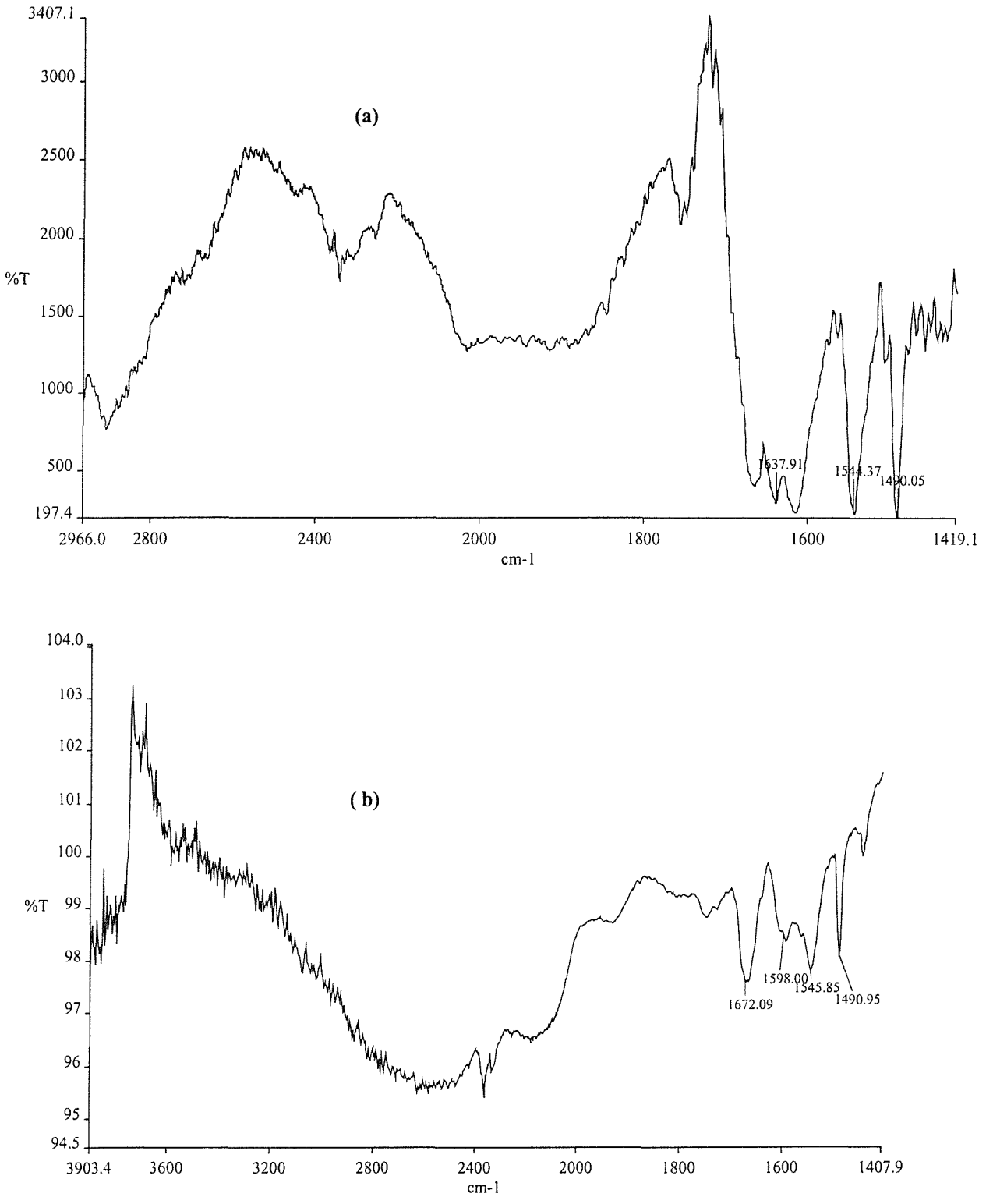

Figure 5.9 :- DRIFTS difference spectra of CF_3SO_3H supported on a) Aerosil 200 and b) H_1SiO_2, both treated with pyridine. Modified silicas before treatment with pyridine were used as the background in all cases to obtain the difference spectra.

The effect of elevated temperature on the pyridine chemisorption on supported CH_3SO_3H on Aerosil 200 is illustrated in figure 5.8. At 100°C, there was no change in the difference spectrum of the supported CH_3SO_3H, only peaks due to Brønsted acidity were observed. However, as the temperature was raised to 200°C, the intensities of the Brønsted acid bands decreased readily. At this temperature, the appearance of the hydroxyl band around ~3700 cm^{-1} can be seen.

Figure 5.9 displayed the difference DRIFTS spectrum for pyridine adsorbed on supported CF_3SO_3H on Aerosil 200 and H_1SiO_2 respectively. The peaks observed in both spectra are very similar. In figure 5.9a, the bands positioned at ~1637, ~1543 and ~1489 cm^{-1} were assigned to Brønsted acidity. CF_3SO_3H supported on H_1SiO_2 also showed the presence of only Brønsted sites at ~ 1491, ~1546, ~1598 and 1672 cm^{-1}. Wavenumbers in figure 5.8 – 5.9 should be taken to the nearest whole integer values.

5.3.7 Solution and Solid State NMR

To investigate how the liquid acids react and bind with the silica supports, the solid acid materials were studied by solution and solid state NMR of nuclides such as ^{31}C, ^{31}P, ^{19}F and ^{1}H.

In order to elucidate the ionization state of the liquid acids when supported on silicas, ^{31}C and ^{19}F NMR have been performed on the supported and unsupported acids. In water, the ^{13}C chemical shift of ionized $CH_3SO_3^-$ is 39.0 ppm and the δ value moved very slightly downfield to 39.5 for neat CH_3SO_3H. The supported CH_3SO_3H on both types of silica give a chemical shift for ^{13}C at 39.9 ppm and 40.7 ppm for CH_3SO_3H supported on H_1SiO_2 and Aerosil 200 respectively (cf. figure 5.10). Clearly, the variations of δ are too small to obtain any useful information on the ionization state of the supported CH_3SO_3H.

The difference in chemical shift for ^{19}F nuclei obtained for supported and unsupported CF_3SO_3H also produced similar results. The ^{19}F chemical shift for neat CF_3SO_3H is –76.8 ppm with reference to $CFCl_3$. The supported CF_3SO_3H on Aerosil 200 and H_1SiO_2 give

chemical shift at –79.0 ppm and –78.4 ppm respectively (c.f. figure 5.11). The total variation for δ is only about 1-2 ppm and consequently, the determination of the state of the supported acids could not be performed by comparing the difference in chemical shift values. The results obtained here are in agreement with published data [18]. One reason which may explain why the chemical shifts are not much influenced by the acid strength is the carbon and fluorine atoms are both located on the methyl group which are not directly involved in acid-base equilibrium.

For ^{1}H NMR spectra, the chemical shift values depend on the electronic depletion of the acid hydrogen nucleus; consequently a higher value of chemical shift may be considered as a measure of increased acid strength. The large chemical shifts at 7.7 and 8.2 ppm downfield for supported CF_3SO_3H and CH_3SO_3H respectively (c.f. figure 5.14 and 5.15) on Aerosil 200 are attributable to the acidic proton of the liquid acids. The hydrogen bonded silanol groups on amorphous silica can also be observed at 2.4 and 2.9 ppm. The signal due to the CH_3 group of CH_3SO_3H might be overlapping with the hydrogen bonded silanol groups signal since the expected chemical shift for the CH_3 is around 2.7 ppm. The large chemical shifts at 7.9 ppm and 7.8 ppm downfield for supported CF_3SO_3H and CH_3SO_3H respectively on H_ISiO_2 are shown in figure 5.12 and 5.13. Compare to the ^{1}H chemical shift for the neat acids, upon immobilisation of the acids on the silicas, the acid strength has decreased as shown by the upfield shift of the acidic proton for the supported acids.

The change in chemical shift of TEPO has been measured for all the supported acids. ^{31}P solid state NMR for supported CH_3SO_3H are showed in Figure 5.16 and 5.17 respectively. The large chemical shift values at 89.3 ppm and 87.6 ppm for CH_3SO_3H supported on Aerosil 200 and H_ISiO_2 respectively indicate the presence of strong acidic sites. The corresponding Δδ values are ~39 and ~37 for the supported CH_3SO_3H. Compare to the scale of acidity for various solid acids obtained by Drago and Osegovic, the acid strength of the supported CH_3SO_3H is comparable to supported sulfated tungsten oxide and 12-phosphotungstic acid [19].

^{31}P solid state NMR spectra of adsorbed TEPO on supported CF_3SO_3H are depicted in figure 5.18 and 5.19. CF_3SO_3H supported on Aerosil 200 has lower ^{31}P chemical shift for adsorbed TEPO compared to CF_3SO_3H supported on H_1SiO_2. The ^{31}P chemical shift for adsorbed TEPO on supported CF_3SO_3H is 76.8 ppm and 85.0 ppm for Aerosil 200 and H_1SiO_2 silica support respectively.

Table 5.4 – 5.7 provide a summary for all the chemical shift values obtained for the supported acids.

Table 5.4 :- Comparison of ^{13}C chemical shifts of neat CH_3SO_3H and supported CH_3SO_3H.

	^{13}C chemical shifts/ppm
neat CH_3SO_3H	39.0
ionised $CH_3SO_3^-$	39.5
supported CH_3SO_3H on Aerosil 200	40.7
supported CH_3SO_3H on H_1SiO_2	39.9

Table 5.5 :- Comparison of ^{19}F chemical shifts of neat CF_3SO_3H and supported CF_3SO_3H.

	^{19}F chemical shifts/ppm
neat CF_3SO_3H	-76.8
supported CF_3SO_3H on Aerosil 200	-79.0
supported CF_3SO_3H on H_1SiO_2	-78.4

Table 5.6 :- ^{1}H chemical shifts of acidic proton for the neat acids and supported acids.

	^{1}H chemical shifts/ppm	
	CH_3SO_3H	CF_3SO_3H
neat acid	10.4	12.0 [1]
supported on Aerosil 200	8.2	7.7
supported on H_1SiO_2	8.0	7.8

Table 5.7 :- ^{31}P chemical shifts of TEPO adsorbed on supported acids.

silica support	acid	^{31}P chemical shifts/ppm
Aerosil 200	CH_3SO_3H	89.3
Aerosil 200	CF_3SO_3H	76.8
H_1SiO_2	CH_3SO_3H	87.6
H_1SiO_2	CF_3SO_3H	85.0

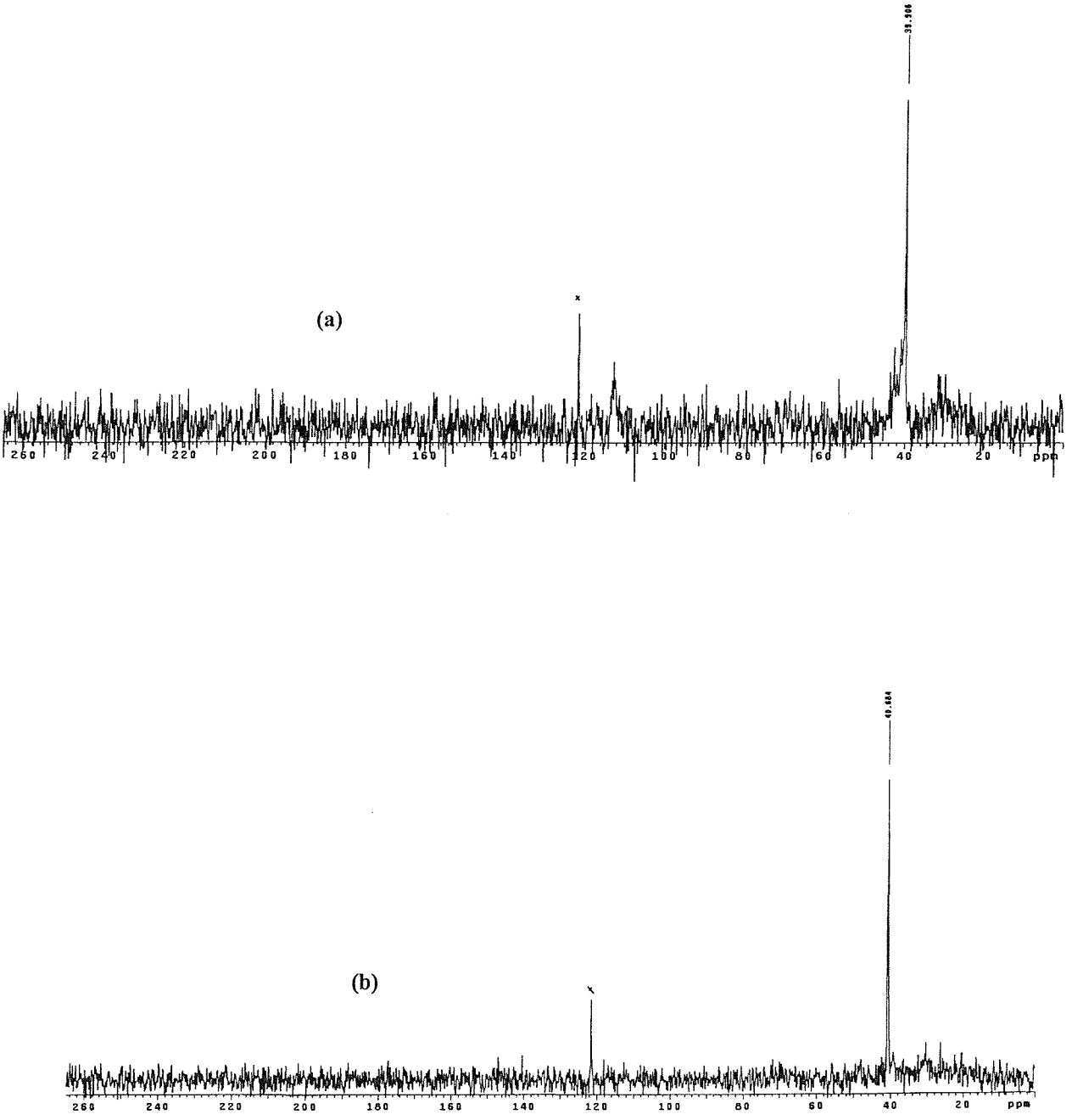

Figure 5.10 :- ^{13}C chemical shifts for supported CH_3SO_3H on a) H_1SiO_2 and b) Aerosil 200 (peaks marked X are artefact peaks).

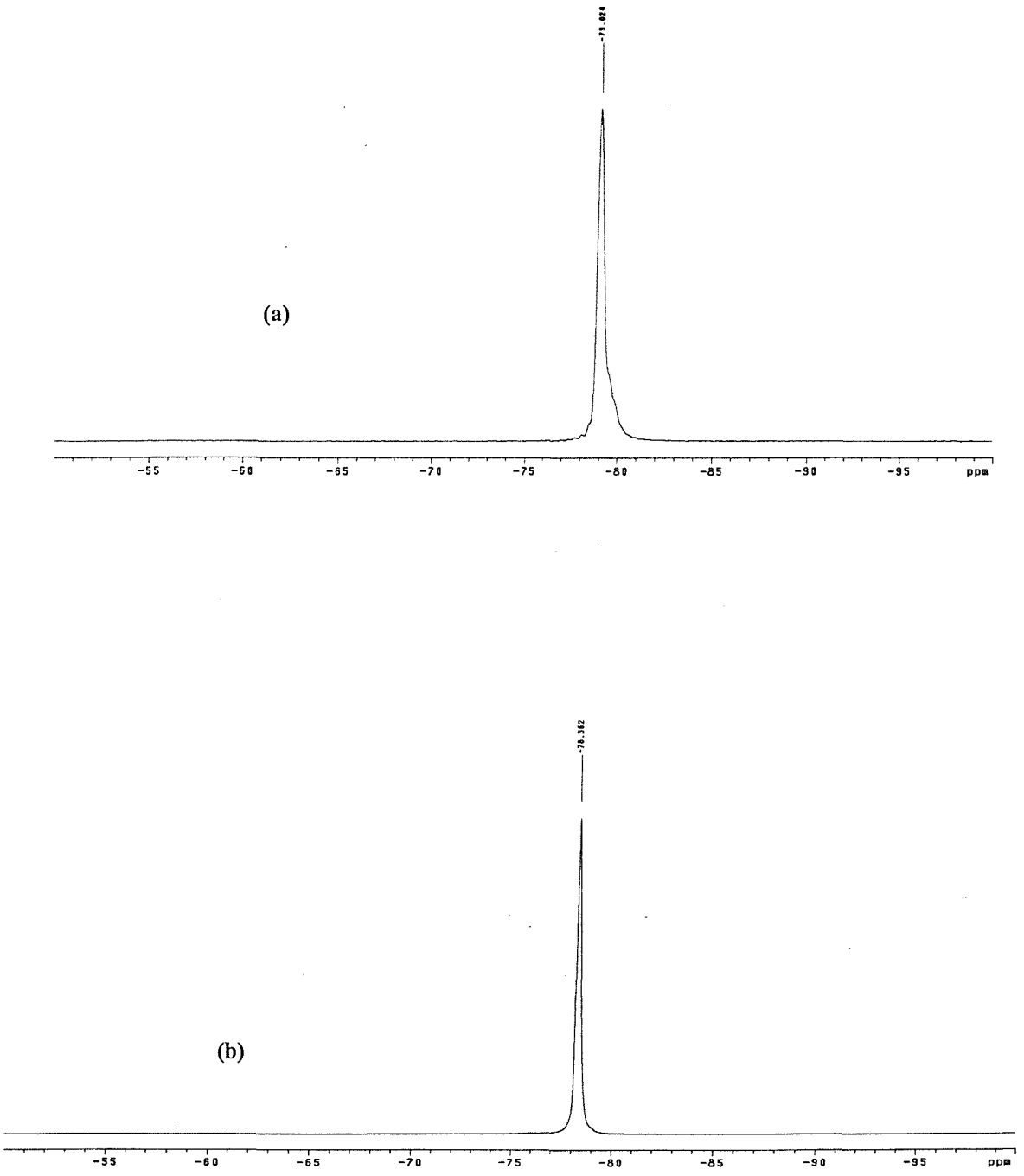

Figure 5.11 :- ^{19}F chemical shifts for supported CF_3SO_3H on a) Aerosil 200 and b) H_1SiO_2 respectively.

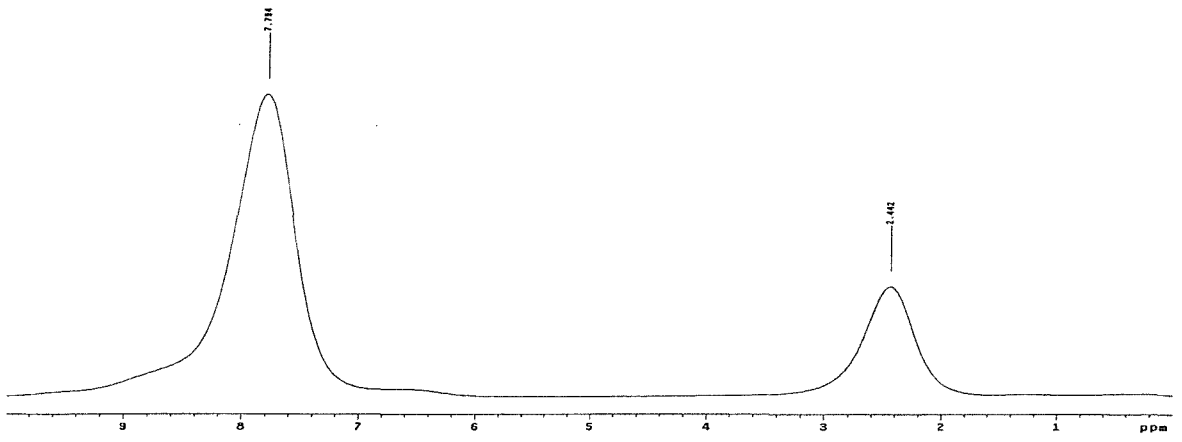

Figure 5.12 :- ^{1}H NMR of CF_3SO_3H supported on H_1SiO_2.

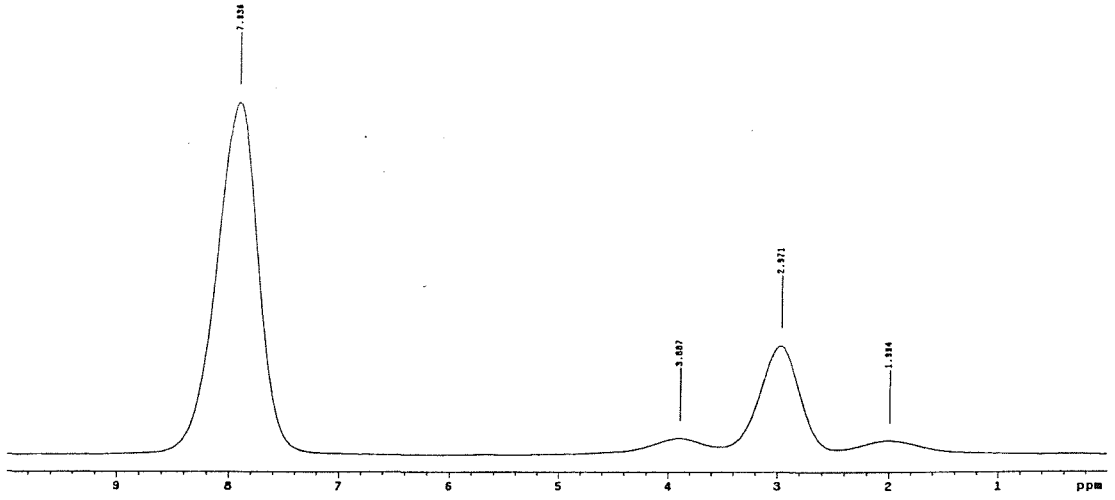

Figure 5.13 :- ^{1}H NMR of CH_3SO_3H supported on H_1SiO_2.

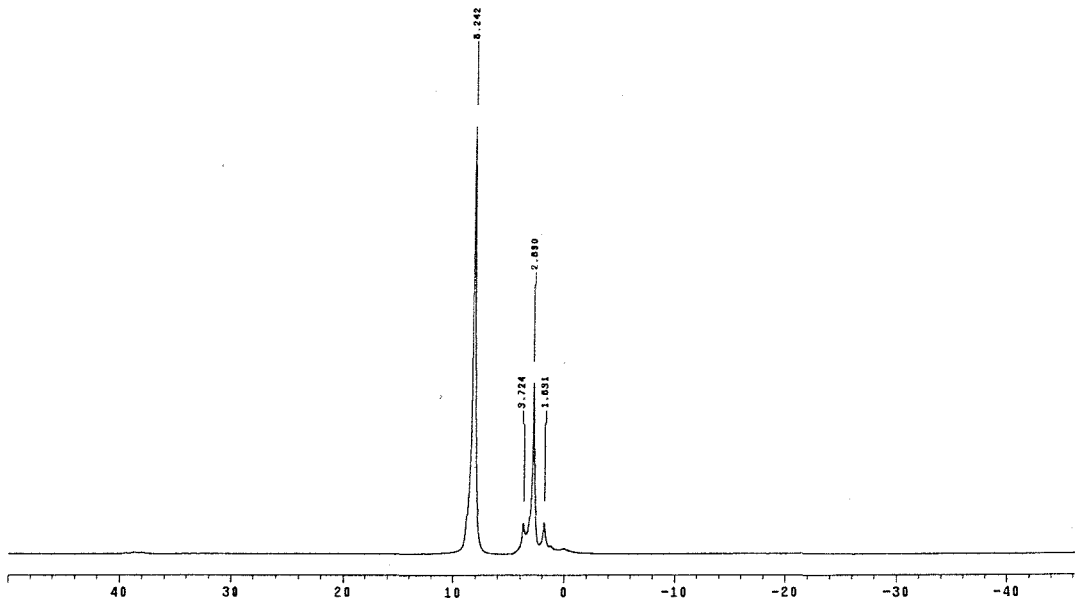

Figure 5.14 :- ^{1}H NMR of CH_3SO_3H supported on Aerosil 200.

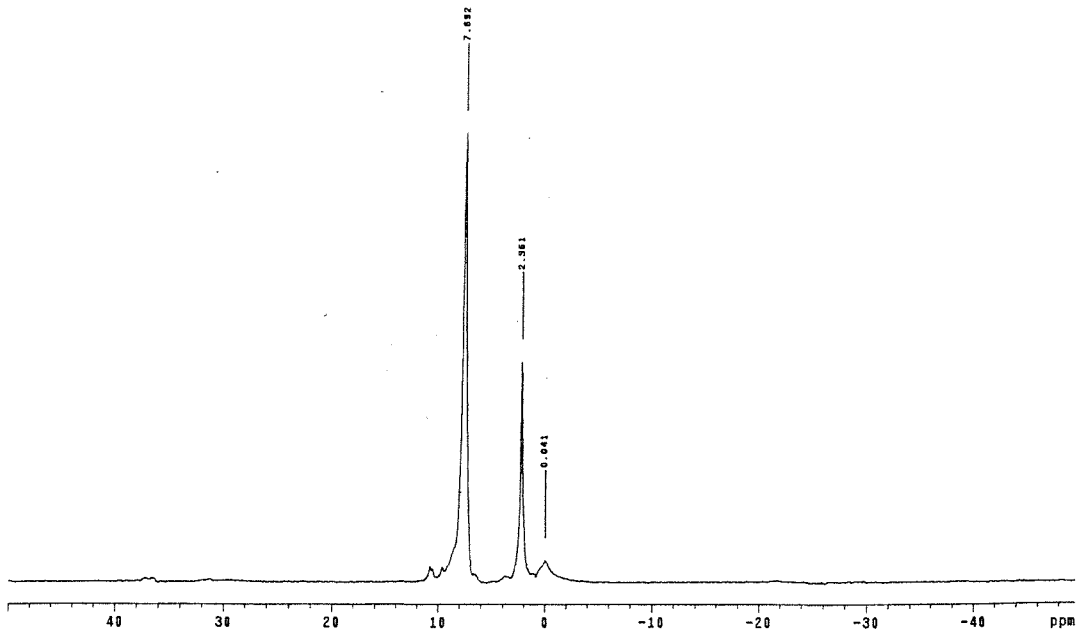

Figure 5.15 :- ^{1}H NMR of supported CF_3SO_3H on Aerosil 200

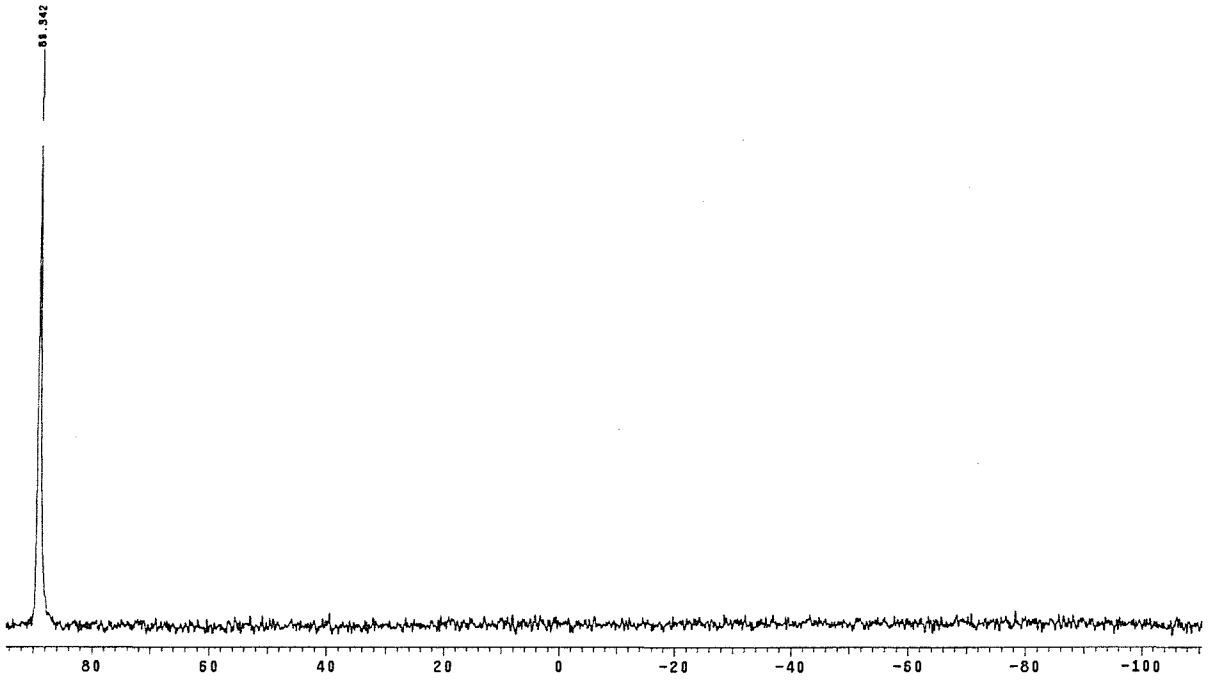

Figure 5.16 :- ^{31}P solid state NMR of adsorbed TEPO on CH_3SO_3H supported on Aerosil 200

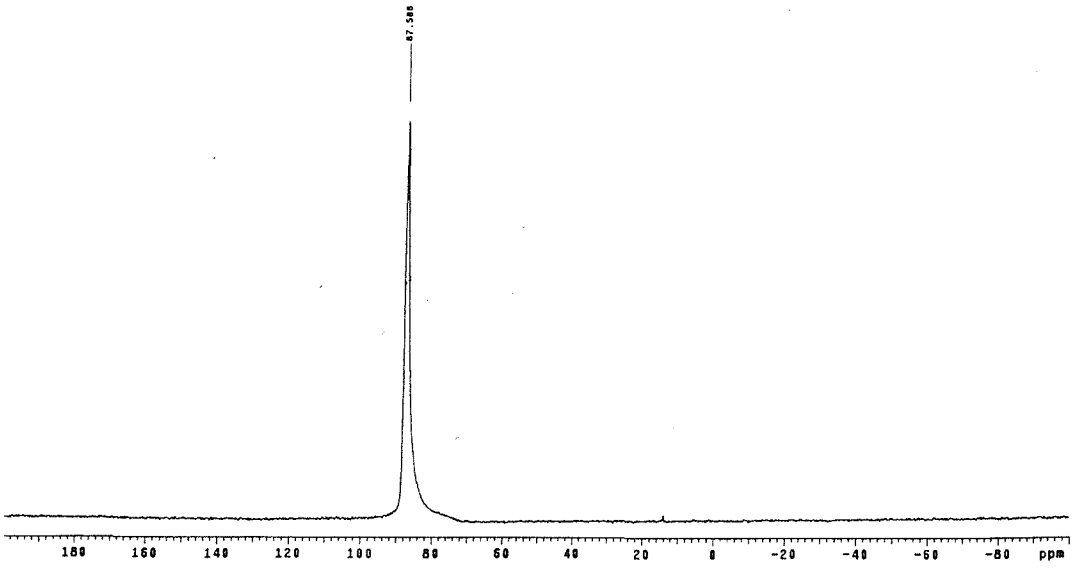

Figure 5.17 :- ^{31}P solid state NMR of adsorbed TEPO on CH_3SO_3H supported on H_1SiO_2.

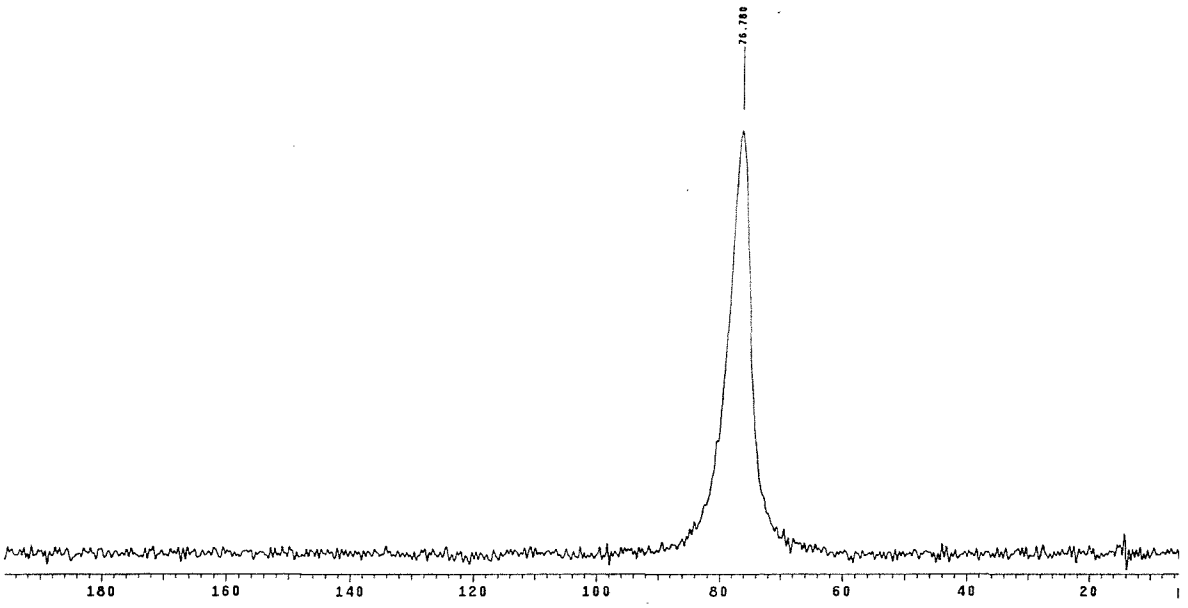

Figure 5.18 :- ^{31}P solid state NMR of adsorbed TEPO on CF_3SO_3H supported on Aerosil 200.

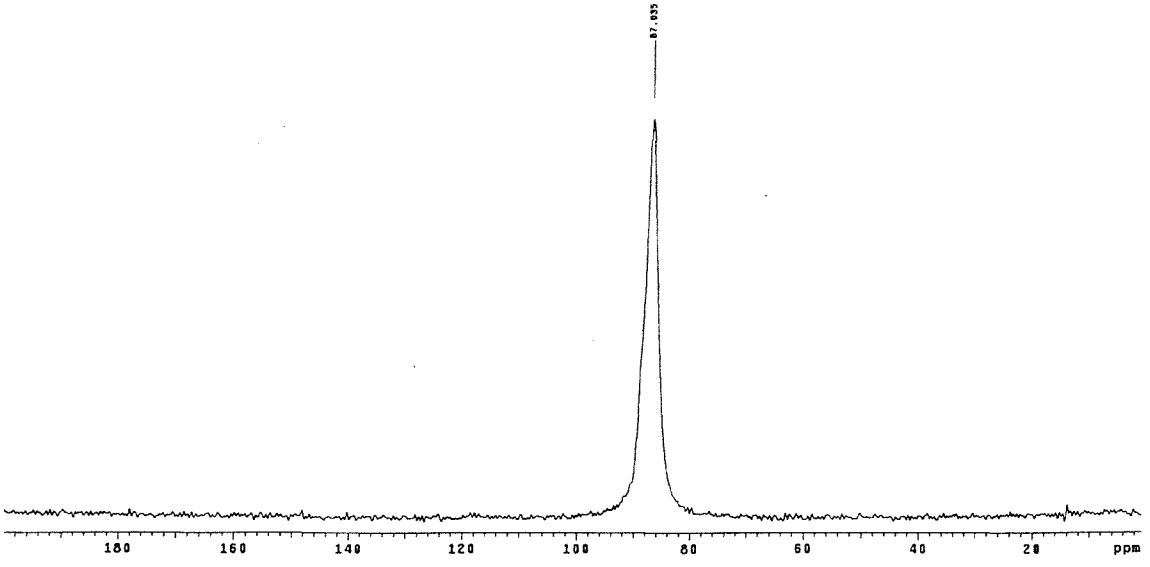

Figure 5.19 :- ^{31}P solid state NMR of adsorbed TEPO on CF_3SO_3H supported on H_1SiO_2.

5.3.8 Temperature Programmed Desorption of supported acids

Temperature programmed desorption study has been undertaken to examine the stability of the supported liquid acids. Figure 5.20 and 5.21 show the TPD spectra of CH_3SO_3H supported on Aerosil 200 and H_1SiO_2 respectively. Decomposition was only evident at 600 K with evolution of sulphur containing gas species. This observation is confirmed by appearance of masses 32, 48 and 64 which can be assigned to S, SO and SO_2 species. Figure 5.22 showed the TPD spectra of supported CF_3SO_3H on H_1SiO_2. The decomposition of the acid only starts occuring around 600K by producing mass fragments of 32, 48 and 64 which can be attributed to sulphur containing species. As a summary, the supported acids are thermally stable up to 600 K and this is an attractive feature for application of the supported liquid acids as solid acid catalysts.

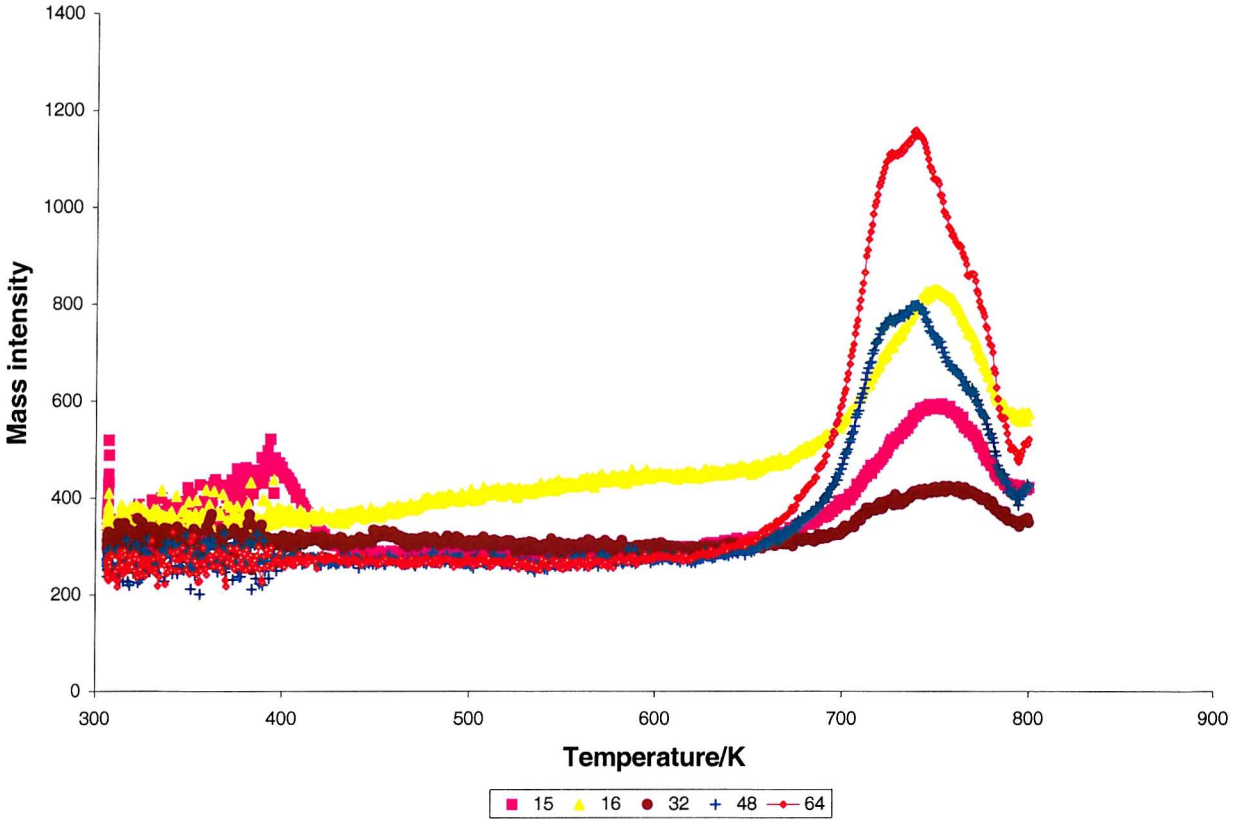

Figure 5.20 :- TPD of supported CH_3SO_3H on H_1SiO_2.

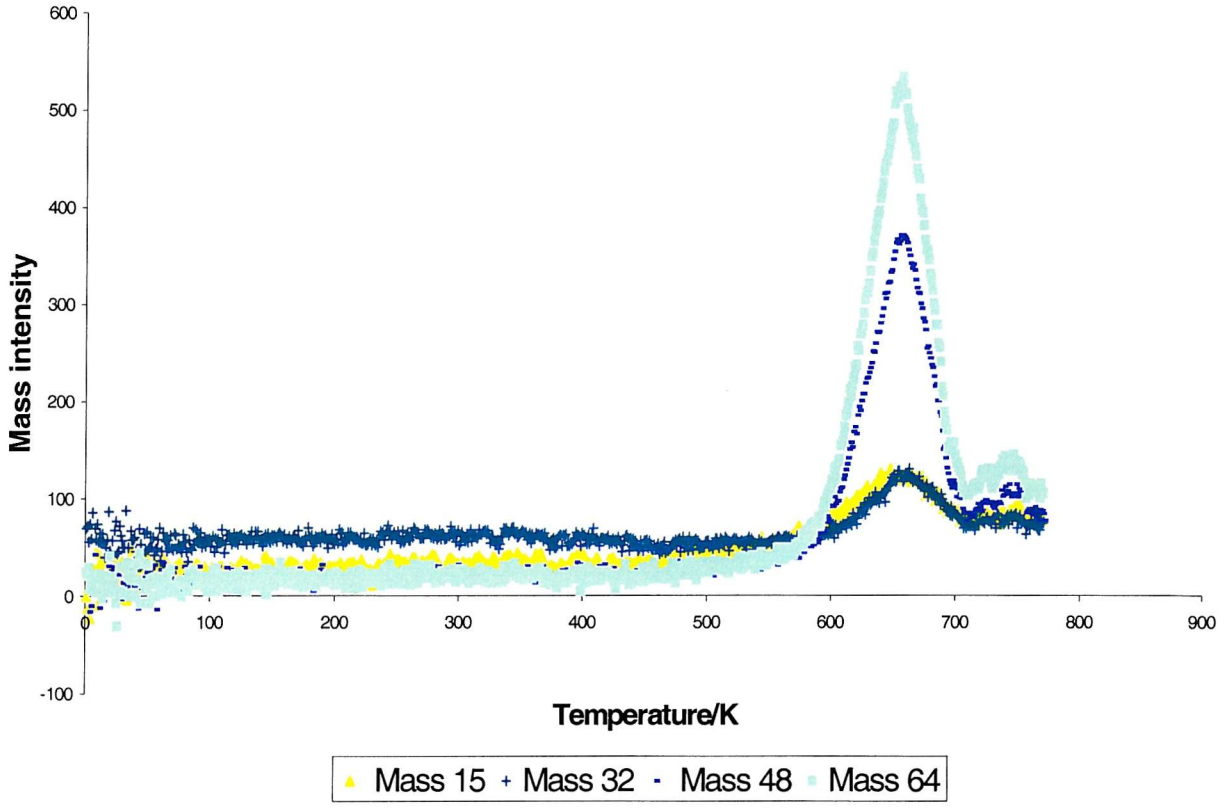

Figure 5.21 :- TPD of supported CH_3SO_3H on Aerosil 200.

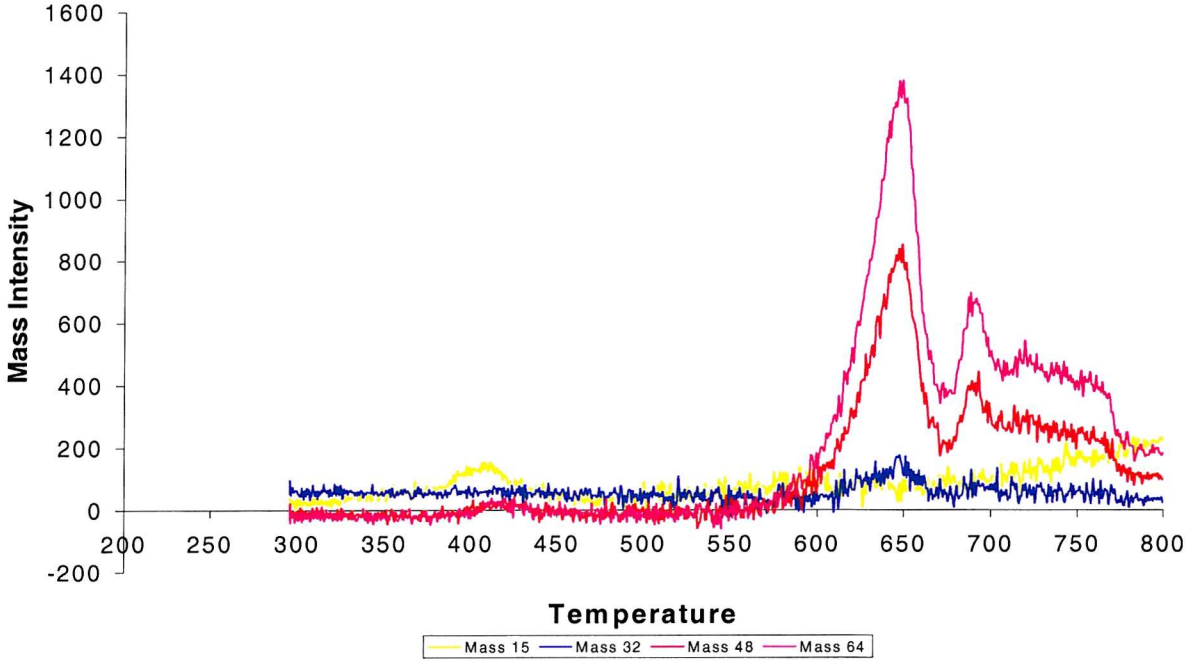

Figure 5.22 :- TPD of supported CF_3SO_3H on H_1SiO_2 monitored for the temperature range of between 300°C and 800°C.

5.4 Conclusions

With the aim of developing new solid acid catalysts with advanced characteristics as to acid strength, surface area, thermal stability and porosity, a series of silica based supports modified with two strong liquid acids have been prepared. The liquid acids used were sulphonic acids, CH_3SO_3H and CF_3SO_3H. The effect of the acids on the structure and surface properties of the silica supports have been investigated with a range of characterisation techniques.

The amount of CH_3SO_3H and CF_3SO_3H loaded on the support was found to be ~3-4 molecule of acids/nm^2 and 2 molecule of acids/nm^2 for amorphous and H_ISiO_2 silica respectively. Compared to the silanol groups on the silica, these results indicate there is at least a monolayer coverage of the acid molecules on the supports. Acidity determination was performed by basic indicators, ^{31}P solid state NMR of adsorbed triethylphosphine oxide (TEPO) and pyridine adsorption monitored by DRIFTS. Results from basic indicator experiments indicates there is a presence of acid sites of at least equivalent to 50% concentrated sulphuric acid for both types of silica supported with sulphonic acids. Pyridine adsorption on both types of silica modified with CH_3SO_3H and CF_3SO_3H showed protonation to pyridinium ion, indicating essentially saturation of the surface with acid sites. Solid state NMR analysis of the adsorbed TEPO showed a ^{31}P chemical shift of 85-90 ppm suggesting the presence of highly acidic sites.

Silica modified with both acids also possesses higher thermal stability by TPD studies, supported CH_3SO_3H decomposed at temperature about 680 K and supported CF_3SO_3H at slightly lower temperature, around 650 K. After immobilization of the acids on H_ISiO_2, the position of the main reflection peak which corresponds to the [100] reflection has shifted to higher angle. The shift in d-spacing observed can be explained by the expansion of the unit cell dimension of the material after treatment with the acids. The intensity of the main refelction peak also decreased sharply after modified with the acids. BET surface area also displayed a decrease in surface area, pore volume and pore diameter. However, the supported acids still have fairly high surface area of at least 100 m^2/g. TEM images of

H_1SiO_2 modified with acids showed dominantly the presence of both hexagonal pore arrangement and equidistant parallel lines arising from the mesoporous structure of H_1SiO_2. This observation indicates the mesoporous architecture of the mesoporous support is structurally unchanged and the acids may well dispersed inside the channel pores. This is confirmed by the reduction in pore volume from 0.59 cm^3g^{-1} for the unsupported H_1SiO_2 to 0.08-0.13 cm^3g^{-1} for the supported acids. If the location of the acids were at the pore openings, a larger reduction in pore volume will be expected from calculation.

References

[1] A.De Angelis, C.Flego, P.Ingallina, L.Montanari, M.G.Clerici, C.Carati, C.Perego, *Catal. Today*, **65**, 363, 2001.

[2] S.I.Hommeloft, H.F.A.Tøpsoe, *US Pat.*, 5 245 100, 1993.

[3] E.Benazzi, J-F Joly, *US Pat.*, 5 906 957, 1999.

[4] L.R.Kallenbach, M.M.Johnson, *US Pat.*, 5 349 116, 1994.

[5] M.G.Clerici, C.Perego, A De Angelis, L.Montanari, *Eur.Pat.*, 0 638 363 A1, 1994.

[6] J.S.Beck, J.C.Vartuli, W.J.Roth, M.E.Leonowicz, C.T.Kresge, K.D. Schmitt, C.T.W.Chu, D.H.Olson, E.W.Sheppard, S.B.Mullen, J.B.Higgins, J.L.Schlenker, *J.Am.Chem.Soc.*, **114**, 10834, 1992.

[7] A.Corma, *Chem.Rev.*, **97**, 2373, 1997.

[8] E.Armengol, M.L.Cano, A.Corma, H.García, M.T.Navarro, *Chem.Comm.* , 519, 1995.

[9] S.L.Burkett, S.D.Sims, S.Mann, *Chem.Comm.* , 1467, 1996.

[10] M.L.Lim, C.F.Blanford, A.Stein, *J.Am.Chem.Soc.*, **119**, 4090, 1997.

[11] M.H.Lim, C.F.Blanford, A.Stein, *Chem.Mater.*, **10**, 467, 1998.

[12] W.M.Van Rhijn, D.E.De Vos, W.Bossaert, J.Bullen, B.Wouters, P.J.Grobet, P.A.Jacobs, *Stud.Surf.Sci.Catal.*, **117**, 183, 1998.

[13] W.M.Van Rhijn, D.E.De Vos, W.Bossaert, P.A.Jacobs, *Chem.Comm.*, 317, 1998.

[14] A.Corma, *Chem.Rev.*, **95**, 559, 1995.

[15] M.Pillinger, I.S.Gorçalves, A.D.Lopes, J.Madureira, P.Ferreira, A.A.Valente, T.M.Santos, J.Rocha, J.F.S.Menezes, L.D.Carlos, *J.Chem.Soc., Dalton Trans.*, 1628, 2001.

[16] E.P.Parry, *J.Catal.*, **2**, 371, 1963.

[17] M.R.Basila, T.R.Kantner, K.H.Rhee, *J.Phys.Chem.*, **68**, 3197, 1964.

[18] R.L.Benoit, M.Fréchette, D.Boulet, *Can.J.Chem.*, **67**, 2148, 1989.

[19] J.P.Osegovic, R.S.Drago, *J.Phys.Chem.B.*, **104**, 147, 2000.

Chapter 6

Characterisation of Supported Zirconocene on Silica Modified with Acids

6.1 Introduction

Many key transformations in heterogeneous catalysis involve the creation or modification of surface metal-hydrocarbyl (alkyl, aryl, etc.) functionalities. One attractive approach to characterising such highly reactive species is to create them by adsorption of well-defined molecular precursors onto carefully prepared inorganic surfaces [1,2]. For several classes of early transition metal hydrocarbyls, it has been known since the 1960s that adsorption on high surface area metal oxides is accompanied by dramatic enhancements in activity for olefin transformations such as polymerisation and metathesis [3,4]. Despite such motivations and much empirical data, it is fair to say that our understanding of the overall surface coordination chemistry as well as the precise nature of the catalytically active sites has been at a primitive level.

Determination of active site structure could be crucial in the understanding of the catalysts behaviour. Initial subjects were organoactinide molecules, since the chemistry, spectroscopy and thermochemistry of such species are reaching an instructive level of sophistication [5]. In the 1980s, Marks proposed a detailed description of surface organometallic adsorbates for a series of organoactinides but little work has been done for group IV metallocenes [6,7].

A supported metallocene catalyst should have several basic structural characteristics : a strong chemical bond to the support (to avoid leaching), one or two cyclopentadienyl ligands, an alkyl group (the propagation center) and finally, a cationic charge. It may be that the anionic coountercharge must well be separated from this ideal structure site in order to achieve maximum catalyst activity. One should note that supported metallocene complexes would be less mobile than the analogous molecules in solution. In classical organometallic chemistry, molecular motion prevents ion pair separation ; this effect is overcome by the use of noncoordinating anions (e.g., PF_6^- [8], $B(C_6F_5)_4^-$ [9]). A surface may, as a factor of rigidity, favour the separation of the cation from the anion.

This chapter concerns the study of a metallocene complex, $[ZrCp_2Me_2]$ supported on the silica modified or supported with the sulfonic acids. The silica supported with acids present

essentially Brønsted acid sites with strong acidity as shown in chapter 5. Marks et al have reported that sulphated zirconia prepared by thermal decomposition of $Zr(SO)_4.4H_2O$, have strongly Brønsted acidic hydroxyl groups on the surface which are active as catalysts when metallocenes were immobilised on the sulfonated zirconia [7]. Therefore, in an attempt to examine the possible active species present on the silica surface with immobilised dimethyl zirconocene [$ZrCp_2Me_2$], two main spectroscopy techniques, infra red and solid state NMR were utilised in this work. A carbonyl complex, [$Fe(CO)_3(COT)$] where COT = cyclooctatetraene, was also supported on the silica modified with sulphonic acids which served as a model to determine if the cationic species, $[Fe(CO)_3(COTH)]^+$ were generated upon immobilisation on the modified silica.

6.2 Experimental

6.2.1 [$Fe(CO)_3(COT)$] supported on Silica

The [$Fe(CO)_3(COT)$] complex was used as received from Sigma Aldrich and deposited on both types of silica. [$Fe(CO)_3(COT)$] (0.122 g, 0.5 mmole/g of Aerosil 200, 0.28 g, 1.15 mmole/g of H_1SiO_2) was suspended in dried pentane (10 ml) and added to the calcined silica (1.0 g). The amount of the iron complex deposited was approximately ~1.0 molecule/nm^2. The mixture was allowed to stir under nitrogen atmosphere for 1 day and the solvent removed by filtration through fritted disc.

6.2.2 Preparation of Dimethyl Zirconocene, [$ZrCp_2Me_2$]

The preparation of [$ZrCp_2Me_2$] was according to the literature[10]. [Cp_2ZrCl_2] (0.7 mmol, 0.2 g) was suspended in dried diethyl ether (20 ml) in nitrogen. An excess of methyl lithium was added (2 ml, 2.8 mmol) to the suspension, at –20 °C. The formation of the dimethyl zirconocene was monitored by the colour of the suspension turning white. The reaction was complete after 30 minutes. The solution was then filtered and the filtrate was finally placed under vacuum to evaporate the solvent. A creamy product was obtained.

6.2.3 [$ZrCp_2Me_2$] supported on Silica

[$ZrCp_2Me_2$] (0.063 g, 0.25 mmole/g of Aerosil 200, 0.188 g, 0.75 mmole/g of H_1SiO_2) was suspended in dried toluene (20 ml) and injected to a round bottom flask containing pre-weighed silica. The amount of zirconocene deposited was calculated to be about ~1.0 molecule/nm^2 on both modified silica supports. The mixture under nitrogen was left to stir for a day before the product was dried under vacuum and kept under nitrogen atmosphere.

6.3 Results and Discussion

6.3.1 Reaction of [$Fe(CO)_3(COT)$] with silica modified with Sulfonic Acids

Since the discovery of cyclooctatetraene iron carbonyl complexes by at least 3 independent research groups in 1958 to 1959 [11-13], these compounds have received much attention. The mononuclear [$(C_8H_8)Fe(CO)_3$] (figure 6.1) is particularly interesting as the complex was first converted, via protonation in etheral solution of fluoroboric acid, into tetrafluoroborate salt by Schrauzer and thought to be cyclooctatrienyl iron tricarbonyl cation 2 [14]. A year later, Davidson, McFarlane, Pratt and Wilkinson refuted structure 2 and unequivocally presented structure 3 to be the actual cation formed [15]. At even lower temperature (-120°C), Brookhart *et al* were able to obtain the monocyclic cyclooctatrienyl iron tricarbonyl cation 4 initially formed from 1 by protonation in FSO_3H-SO_2F_2 solution [16]. Structure 4 was confirmed by their proton NMR spectroscopic study. Furthermore, upon warming the solution of 4 to -60°C, cation 3 was quantitatively formed via a first order electrocyclic ring-closure reaction.

In this study, [$(C_8H_8)Fe(CO)_3$] has been reacted with the silica premodified with both sulfonic acids. The purpose of this study is to determine the possibilities of protonation of this iron complex, [$(C_8H_8)Fe(CO)_3$] upon reaction with the acidic silica supports.

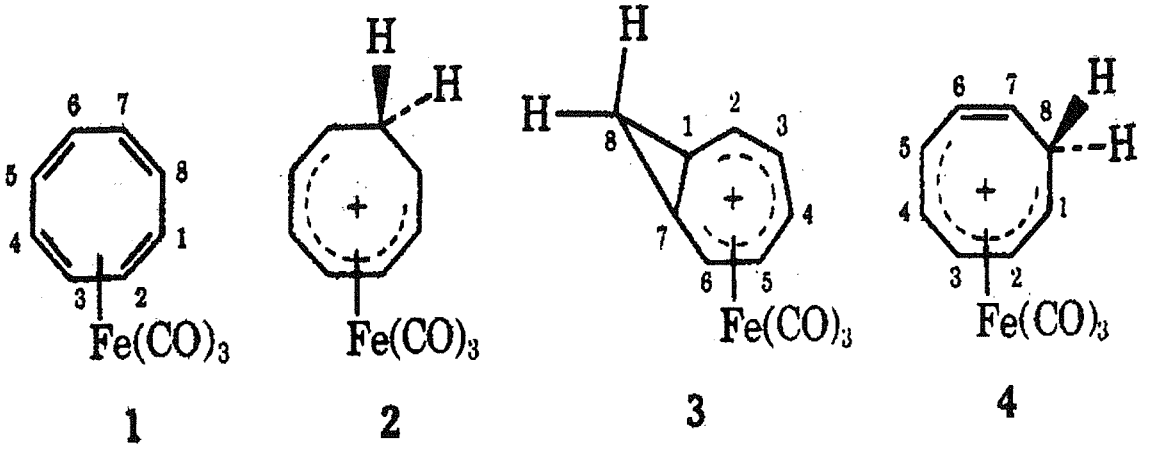

Figure 6.1 :- $[Fe(CO)_3(COT)]$ and its protonated forms 2,3,4.(COT = cyclooctatetraene)

The nujol mull infrared spectra of the supported $[Fe(CO)_3(COT)]$ on modified mesoporous silica are shown in figure 6.2 and 6.3. Both spectra exhibit 2 main peaks at ~2107, ~2061 cm^{-1} and ~2112, ~2068 cm^{-1} for H_ISiO_2 modified with CF_3SO_3H and CH_3SO_3H respectively when treated with the $[Fe(CO)_3(COT)]$ complex. These peaks are assigned to the terminal carbonyl groups stretching. The shift of the peaks to higher wavenumber compare to the neutral cyclooctatetraene iron tricarbonyl complex indicates protonation has taken place to form the protonated species, $[Fe(CO)_3(COTH)]^+$.

The nujol mull infrared spectra of the supported $[Fe(CO)_3(COT)]$ on modified Aerosil 200 are displayed in figure 6.4 and 6.5. Besides the 2 characteristic carbonyl stretching peaks observed, other peaks at ~1994 and ~1976 cm^{-1} are also present. These two peaks can be assigned to the unreacted or excess $[Fe(CO)_3(COT)]$ complex on the silica. $[Fe(CO)_3(COT)]$ in pentane shows 3 sharp peaks at ~2054, ~1997 and ~1979 cm^{-1} which are assigned to the stretching of the terminal carbonyl groups. As explained previously, the 2 main peaks observed in both spectra were due to carbonyl groups stretching in the protonated complex,

$[Fe(CO)_3(COTH)]^+$. A smaller peak which appeared as a shoulder in the infrared spectra of figure 6.3 and 6.4 at ~2021 cm^{-1} may indicate the presence of another form of the protonated species, $[Fe(CO)_3(COTH)]^+$. As reported in the literature [15,16], the protonated complex $[Fe(CO)_3(COTH)]^+$ can exist in 2 forms, as illustrated in figure 6.1. All the wavenumbers reported in figure 6.2- 6.5 should be taken to the nearest whole integer.

^1H and ^{13}C solid state NMR have also been performed on the supported $[Fe(CO)_3(COT)]$ on the modified silica surfaces. However, only one ^1H NMR spectrum for the supported $[Fe(CO)_3(COT)]$ on H_ISiO_2 modified with CF_3SO_3H has been obtained as presented in figure 6.6. The remoteness of the CO carbon from hydrogen, inefficiency of the cross polarisation process and insufficient carbon in the silica samples can be among the reasons for the failure to obtain good ^1H and ^{13}C solid state NMR spectra.

Not many well resolved peaks can be obtained from the ^1H NMR spectrum of supported $[Fe(CO)_3(COT)]$. The broad band at ~12.32 ppm was attributed to the acidic proton of CF_3SO_3H and the cyclooctatetraene protons can be observed at ~6.42 ppm. Due to line broadening in solid state spectrum, solid state NMR experiments cannot provide much useful information regarding the state of the supported complex, $[Fe(CO)_3(COT)]$ and hence, cannot confirm the presence of the cationic complex, $[Fe(CO)_3(COTH)]^+$.

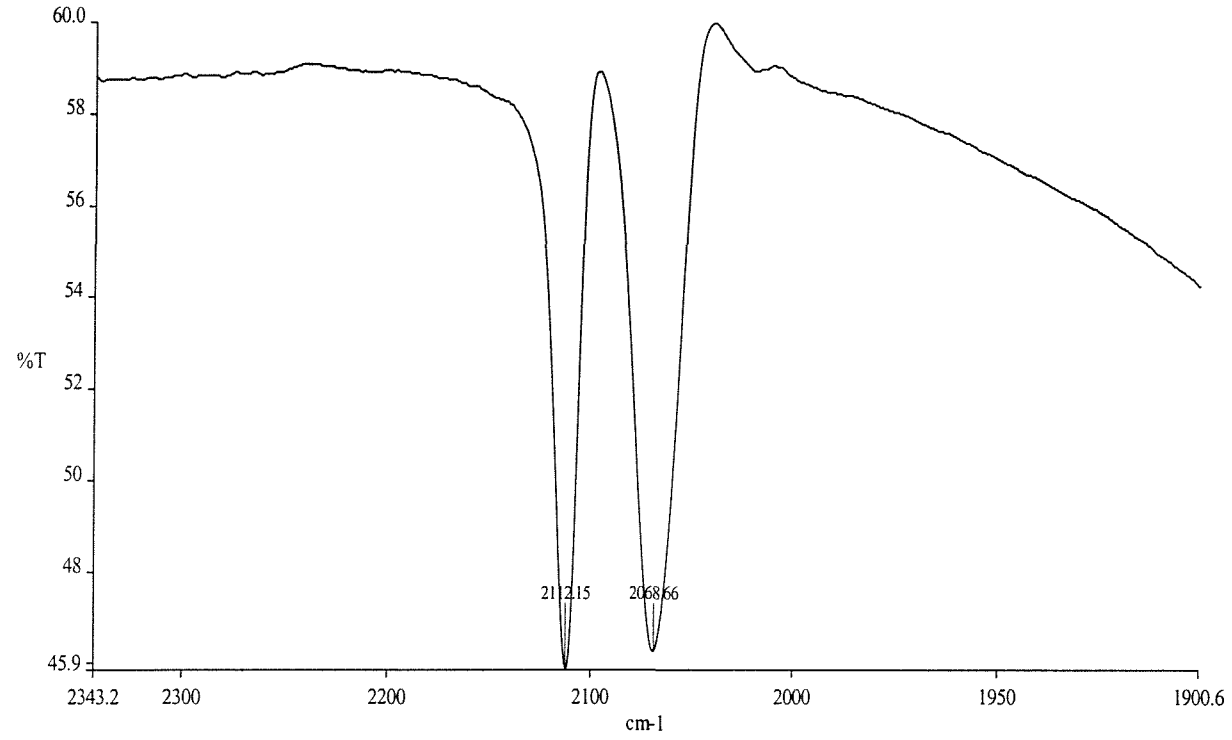

Figure 6.2 :- IR spectrum of supported $Fe(CO)_3COT$ on H_1SiO_2 modified with CF_3SO_3H.

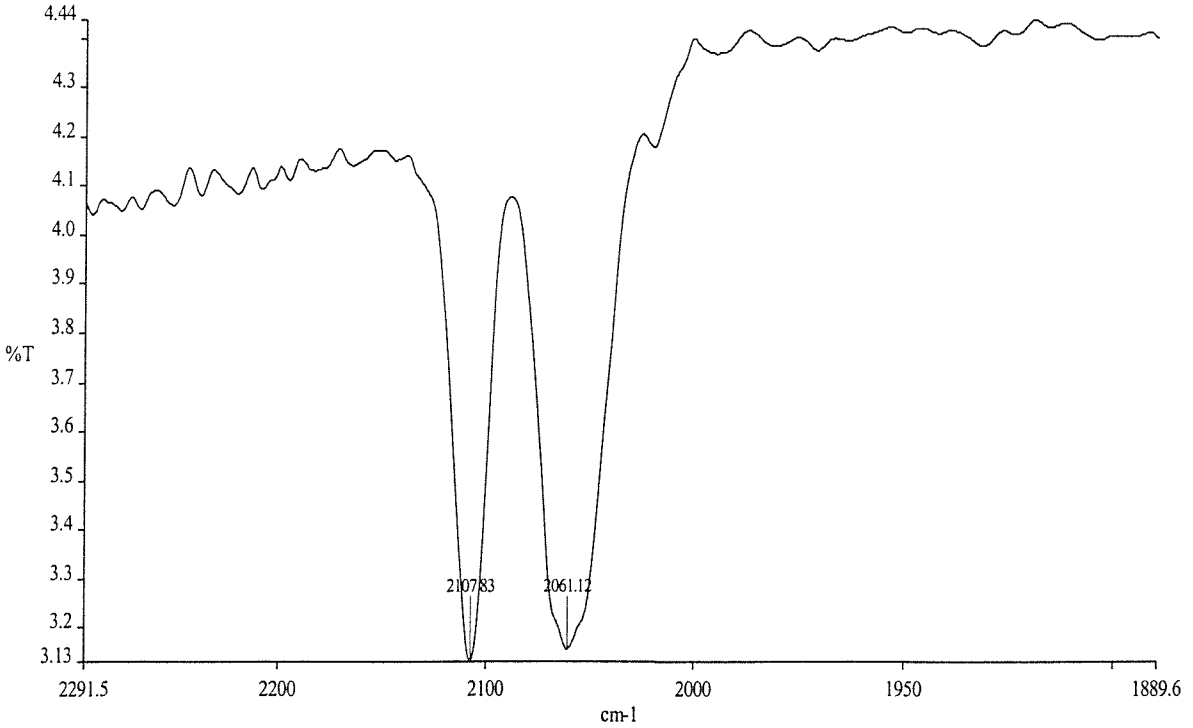

Figure 6.3 :- IR spectrum of supported $Fe(CO)_3COT$ on H_1SiO_2 modified with CH_3SO_3H.

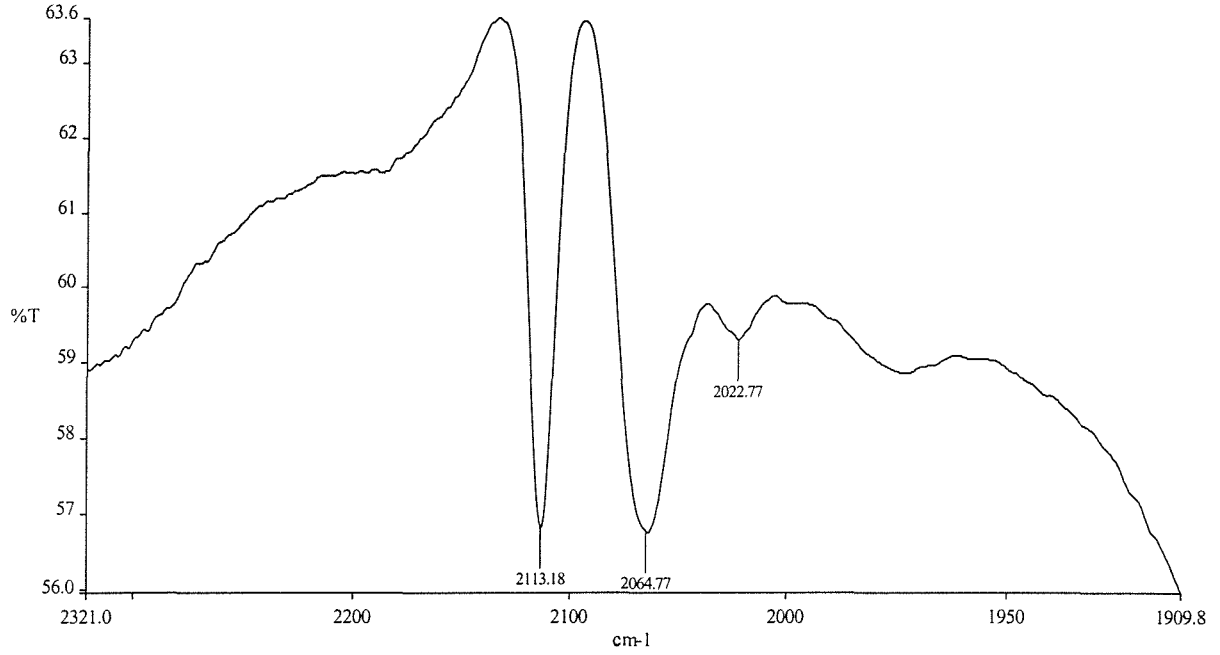

Figure 6.4 :- IR spectrum of supported $Fe(CO)_3COT$ on Aerosil 200 modified with CH_3SO_3H.

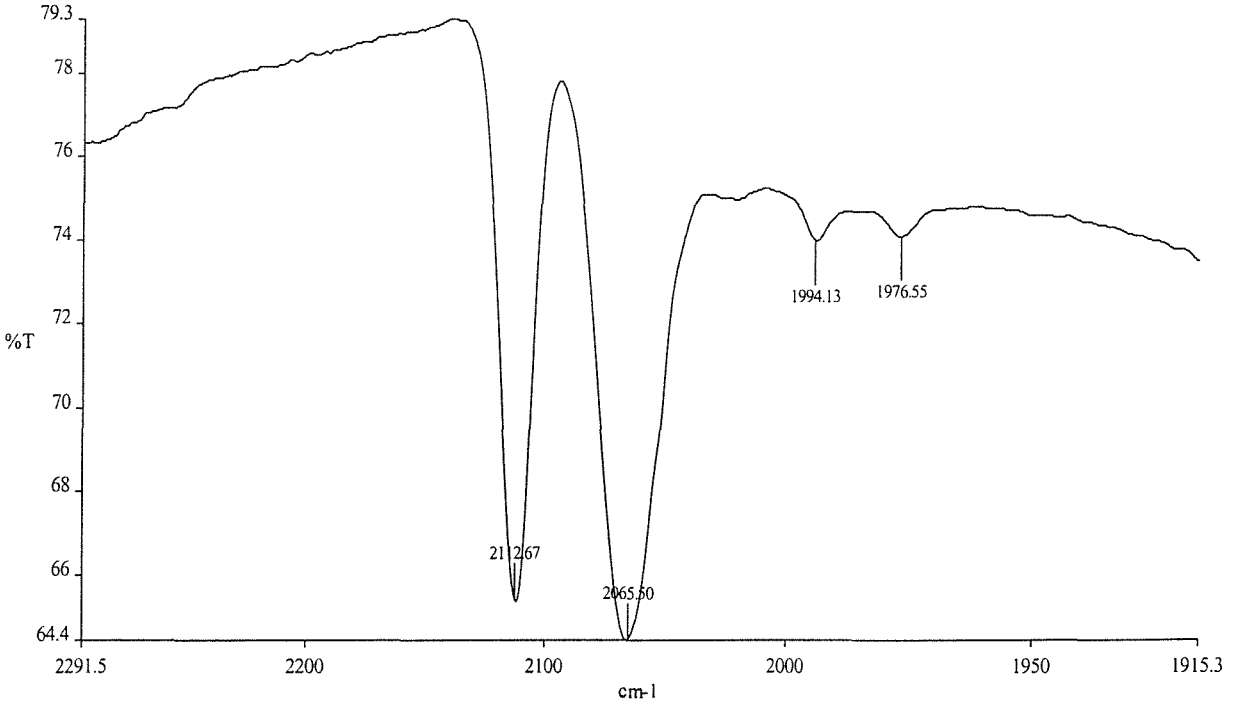

Figure 6.5 :- IR spectrum of supported $Fe(CO)_3COT$ on Aerosil 200 modified with CF_3SO_3H.

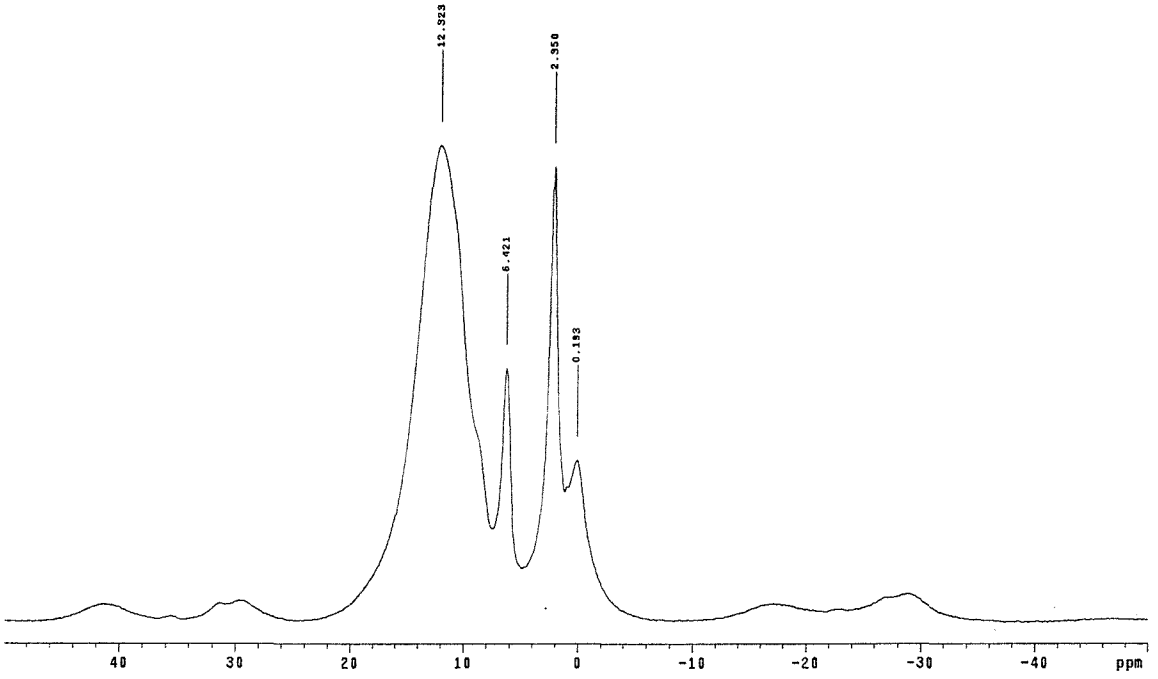

Figure 6.6 :- ^{1}H solid state NMR spectrum of $Fe(CO)_3COT$ supported on H_1SiO_2 modified with CF_3SO_3H.

6.3.2 Reaction of $[ZrCp_2Me_2]$ with Aerosil 200 supported with methanesulfonic acid

When $[ZrCp_2Me_2]$ was reacted with Aerosil 200 modified with methanesulfonic acid, infrared bands attributed to the C-H stretching of the cyclopentadienyl ring and Zr-CH_3 group could be observed at ~3117 and ~2960 cm^{-1}. Further characterisation of the surface species formed was achieved by solid state NMR spectroscopy. ^{1}H solid state NMR and ^{13}C CP-MAS spectra are shown in figure 6.8 and 6.9.

The ^{1}H solid state NMR spectrum indicated the presence of four signals at 6.34, 2.59, 0.112 and –0.132 ppm. The signal at 6.34 ppm was unambiguously attributed to the protons of the cyclopentadienyl rings and the signal at 2.59 ppm was assigned to the hydrogen bonded silanol groups [17]. The sharp resonance at 0.112 ppm could be due to the presence of direct attachment of methyl group onto the silica surface forming Si-CH_3 bond [18]. The presence of the sharp resonance at –0.132 ppm in ^{1}H NMR spectrum of unmodified silica rule out the

possibilities that this peak could be due to the immobilised $[Zr(Cp)_2Me_2]$. The reason for its existence could be due to the silica support alone or the presence of slight amount of grease.

The ^{13}C CP-MAS spectrum in figure 6.9 displayed 3 signals at 116, 39.7 and –1.7 ppm. The signals at 116 and 39.7 ppm were characteristic of the carbons of the cyclopentadienyl ring and the carbon of the methyl group of the sulfonic acid (chapter 5). The presence of the direct attachment of CH_3 to silicon is further supported by the appearance of a peak around –1.7 ppm in the ^{13}C CP-MAS spectrum. This type of behaviour was reported by Marks and co-workers [18] for a homogeneous zirconocene-alumoxane olefin polymerisation catalyst. The solid state ^{13}C CP-MAS NMR spectrum gave a large broad resonance around –5 ppm corresponding to $^{13}CH_3$-^{27}Al as well as the cyclopentadienyl resonance at 115 ppm. The carbons of the methyl groups bonded directly to the zirconium atom were not detected which would be expected around the region of 30-40 ppm. The carbon of the methyl directly bonded to a metal is very often not detected or seen with a very weak intensity in CP-MAS solid state ^{13}C NMR, probably due to a long T_1 relaxation time (phenomenon often seen for organometallics in close proximity to the surface) [19]. Gas titration experiments showed evolution of a gas, most probably methane when the complex, $[ZrCp_2Me_2]$ was supported on the modified silica. This observation indicates that there were some loss of methyl groups which evolved as methane during this reaction.

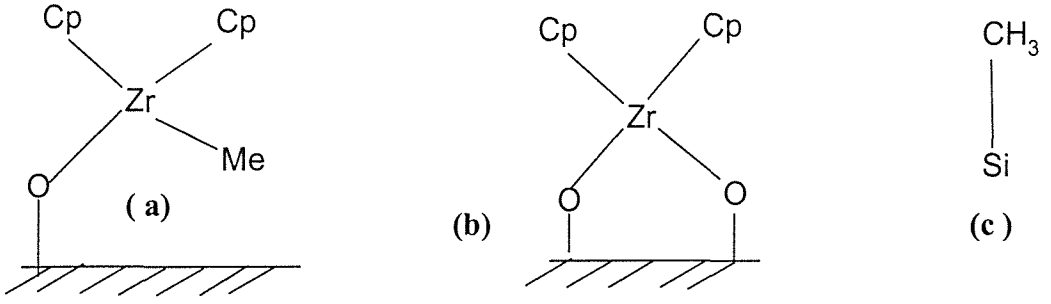

Figure 6.7 :- Possible products from the reaction of $[ZrCp_2Me_2]$ with silica supported with methanesulfonic acid, a) bridged species with the zirconium center attached to one oxygen atom on the surface b) attached to two oxygen atoms on the surface c) methyl group attached to the silica surface.

Several important observations can be made for the grafting reaction of $[ZrCp_2Me_2]$ on the modified Aerosil 200. There appear to be several species present on the silica surface, most notably the bridged species with the zirconium center attached to one or two oxygen atoms on the surface and also a small proportion of methyl groups attached to the silicon on the silica surface (c.f. figure 6.7) . Similar studies have also shown the presence of these species on silica gel [19-21]. Surface elemental analysis and EXAFS would need to be carried out to obtain detail informations regarding the possible surface species present.

Table 6.1 :- Comparison of ^1H and ^{13}C NMR chemical shifts of $[ZrCp_2Me_2]$ and $[ZrCp_2Cl_2]$ supported on silica and $[ZrCp_2Me_2]$ supported on silica modified with methanesulphonic acid respectively.

	^{13}C NMR shifts/ppm	^1H NMR shifts/ppm
$[ZrCp_2Cl_2]$/silica	114.3 [20]	6.3 [21]
$[ZrCp_2Me_2]$/silica	110.4, -1.4 [20]	5.7, -0.12 [19,24]
$[ZrCp_2Me_2]$/modified silica with methanesulphonic acid	116, 39.7, -1.7	6.34, 0.112

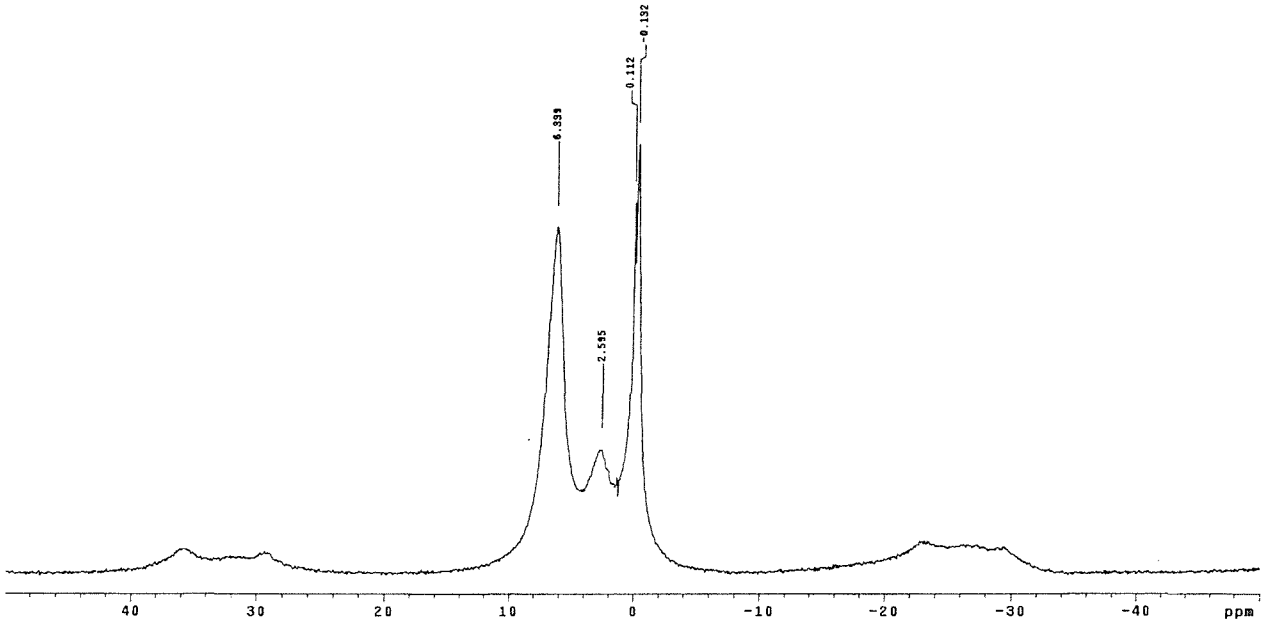

Figure 6.8 :- ^{1}H solid state NMR of $[ZrCp_2Me_2]$ supported on Aerosil 200 modified with methanesulfonic acid.

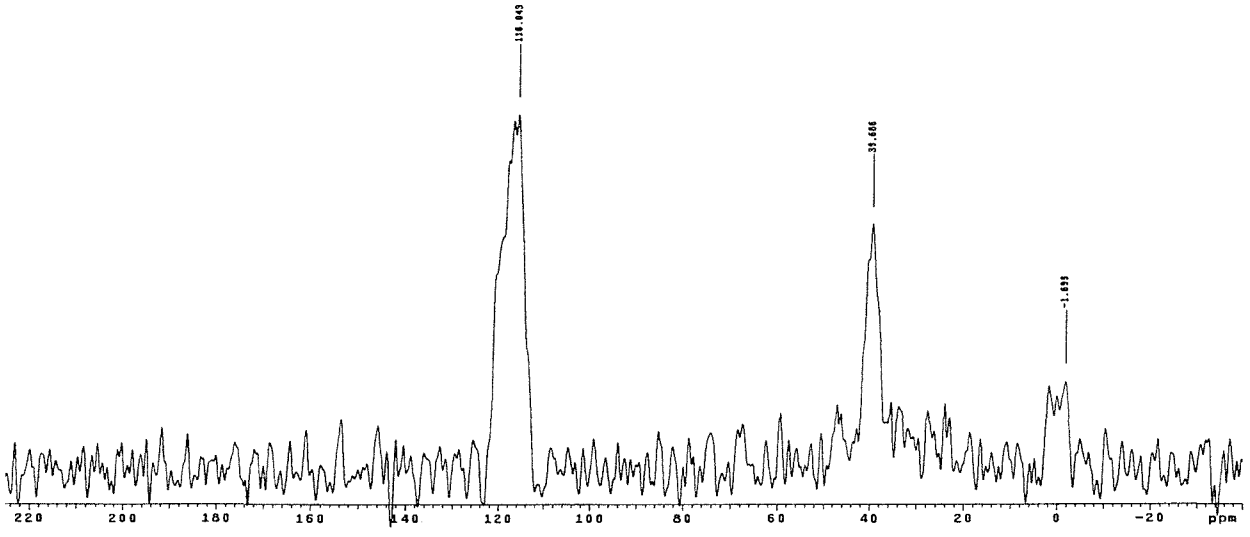

Figure 6.9 :- ^{13}C CP-MAS NMR of $[ZrCp_2Me_2]$ supported on Aerosil 200 modified with methanesulfonic acid.

6.3.3 Reaction of $[ZrCp_2Me_2]$ with H_1SiO_2 supported with methanesulfonic acid

The solid state ^1H and ^{13}C NMR of the supported $[ZrCp_2Me_2]$ on modified H_1SiO_2 with methanesulfonic acid were shown in figure 6.11 and 6.12. In general, two types of signals, corresponding to the cyclopentadienyl protons and hydrogen bonded silanol groups were observed at chemical shifts 6.99 and 2.15 ppm respectively. The remaining signals were due to the presence of the solvent, THF and small amount of grease applied to glassware joints during experiments. During the preparation procedure of supported methanesulfonic acid on H_1SiO_2, some residual of the solvent, THF was expected to remain physisorbed on the surface, since all materials were prepared and dried at room temperature.

From ^{13}C CP-MAS NMR spectrum in figure 6.12, toluene and THF have been found systematically as well as cyclopentadienyl ligands and the carbons of the methyl group of the sulfonic acid. All the signals due to physisorbed solvents were marked as + and * in the spectrum. On careful inspection of the baseline of the ^{13}C spectrum, there appears to be a small broad band in the region of 20-60 ppm which could possibly be traces of $Zr\text{-}CH_3$, however, ^{13}C labelling studies would need to be done to confirm this. Methane that was evolved during the deposition reaction of the $[ZrCp_2Me_2]$ complex can be formed via reaction with the modified silica surface. There are two possible reactions which can take place. $[ZrCp_2Me_2]$ could react with the surface silanol groups with the formation of a partially charged species and loss of a methyl group to form methane which was detected during the deposition reaction. The slight low field shift of the signal due to the carbon of the cyclopentadienyl rings at 117.3 ppm may suggest the presence of the partially charged species, $Zr^+\text{-}CH_3$ on the surface which was formed as a result of the reaction of the complex with the surface silanol groups. The other possibility is the reaction of $ZrCp_2Me_2$ with the supported methanesulphonic acid as represented in equation 6.1.

$$ZrCp_2Me_2 + HOSO_2Me \rightleftharpoons [ZrCp_2Me]^+ + CH_4 + {}^-OSO_2Me \qquad \textbf{6.1}$$

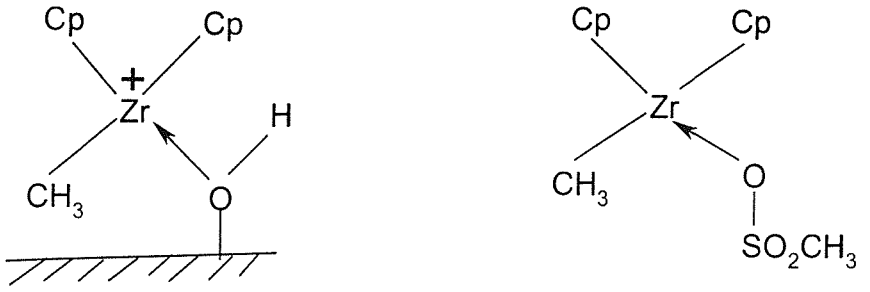

Figure 6.10 :- Possible zirconium species formed on the modified silica surface, a charged or partially charged and a neutral zirconium species.

A neutral species as illustrated in figure 6.10 could be formed. Recently, it has been reported that the methyl group on a cationic or partially cationic zirconium complex also appears around the same region of 30-40 ppm [19,22]. Given the broadness and the weak intensity of this signal, one cannot determine with certainty by NMR alone either the peak is due to one or several species or whether the species in question involve a neutral Zr-CH_3 or a partially charged Zr^{+}-CH_3 group.

Table 6.2 :- ^{1}H and ^{13}C NMR chemical shifts of $[ZrCp_2Me_2]$ supported on H_1SiO_2 modified with methanesulphonic acid.

	^{1}H shifts/ppm	^{13}C shifts/ppm
$[ZrCp_2Me_2]$/modified H_1SiO_2 with methanesulphonic acid	6.99, 2.15	39.5, 40.4, 117.3 20-60 (broad)

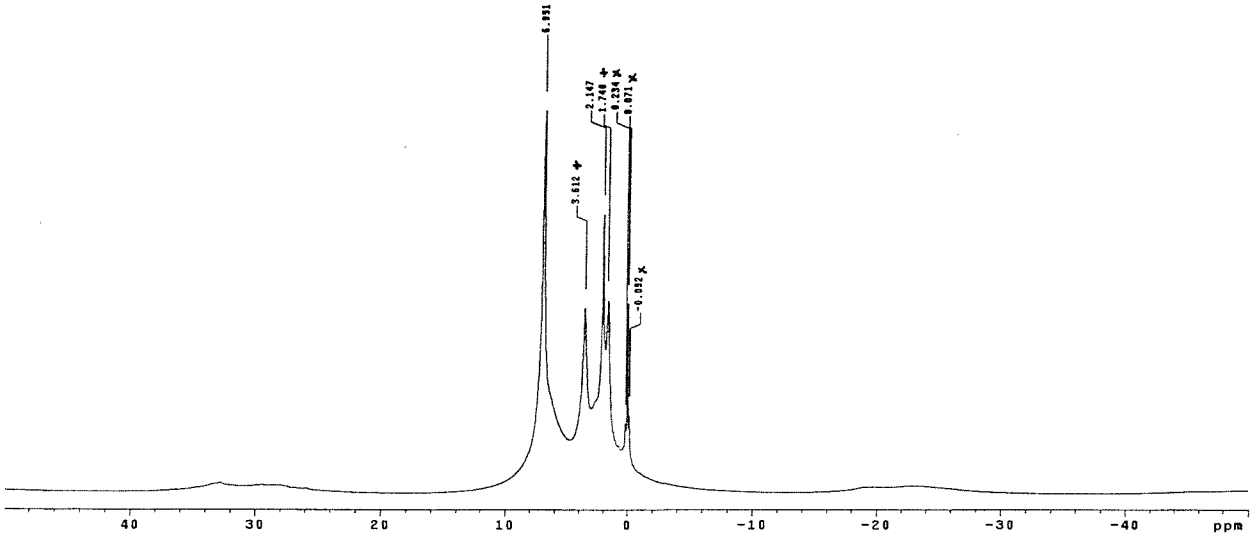

Figure 6.11 :- ^{1}H solid state NMR of $[ZrCp_2Me_2]$ supported on H_1SiO_2 modified with methanesulfonic acid. (Peaks marked as + and × were due to THF solvent and grease respectively)

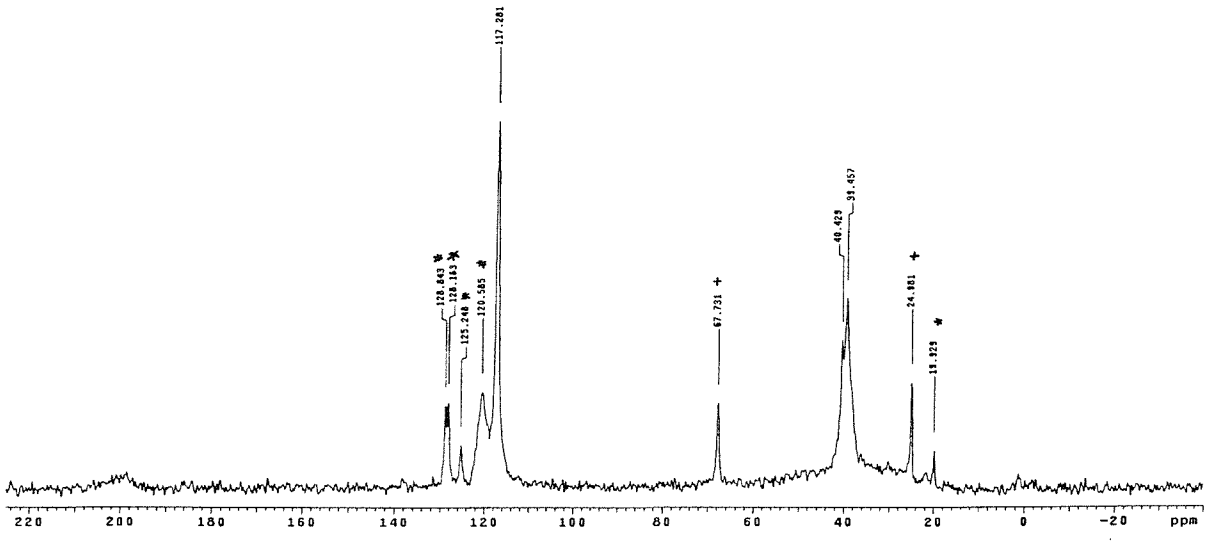

Figure 6.12 :- ^{13}C CP-MAS NMR of $[ZrCp_2Me_2]$ supported on H_1SiO_2 modified with methanesulfonic acid. (Peaks marked as + and * were due to residual THF and toluene)

6.3.4 Reaction of $[ZrCp_2Me_2]$ with Aerosil 200 supported with trifluoromethanesulfonic acid

The infrared spectrum of the supported $[ZrCp_2Me_2]$ on Aerosil 200 modified with CF_3SO_3H exhibits two bands at ~3100 cm^{-1} and 2960 cm^{-1} which were assigned to the C-H stretching of the cyclopentadienyl ring and Zr-CH_3 group respectively.

The ^1H solid state NMR spectrum is presented in figure 6.13. As expected, the two main signals corresponding to the cyclopentadienyl ring protons and the hydrogen bonded groups were observed at 6.38 and 2.11 ppm respectively. As mentioned previously, the sharp signal at –0.132 ppm could not be assigned to any species due to the immobilisation of the $[ZrCp_2Me_2]$ complex. ^1H solid state NMR spectrum of the unmodified silica has shown the presence of a peak around the same chemical shift which could be attributed to the silica support itself or grease.

^{13}C CP-MAS spectrum shows basically 3 signals as presented in figure 6.14. A broad band around the 20-60 ppm region, a slightly low field shift of the carbons of the Cp ring at 118.9 ppm and a sharp signal at –0.24 ppm can be observed from the ^{13}C spectrum. As explained previously, the broad band around the 20-60 ppm region could be due to the presence of Zr-CH_3 or a partially charged Zr-CH_3 species. Aerosil 200 modified with trifluoromethanesulfonic acid possess Brønsted acidity as described in chapter 5 and it may explain the presence of the broad band around the 20-60 ppm region in the ^{13}C NMR spectrum. The higher chemical shift for the carbons of the cyclopentadienyl rings as observed at 118.9 ppm compared to the neutral $[ZrCp_2Me_2]$ complex which has a corresponding shift of the carbon of the Cp rings at ~115 ppm may indicate the Cp rings are on a cationic or partially cationic zirconium complex. A similar behaviour has been observed for both the methyl group and Cp ligand of a zirconium complex where the downfield Zr-CH_3 and Zr-Cp displacements are typical of "cation-like" $Cp_2ZrR^+/Cp_2Zr(L)R^+$ complexes [18,22,23]. Finally, the signal at –0.242 ppm could be assigned to direct attachment of methyl group to the silicon atom forming a Si-CH_3 bond.

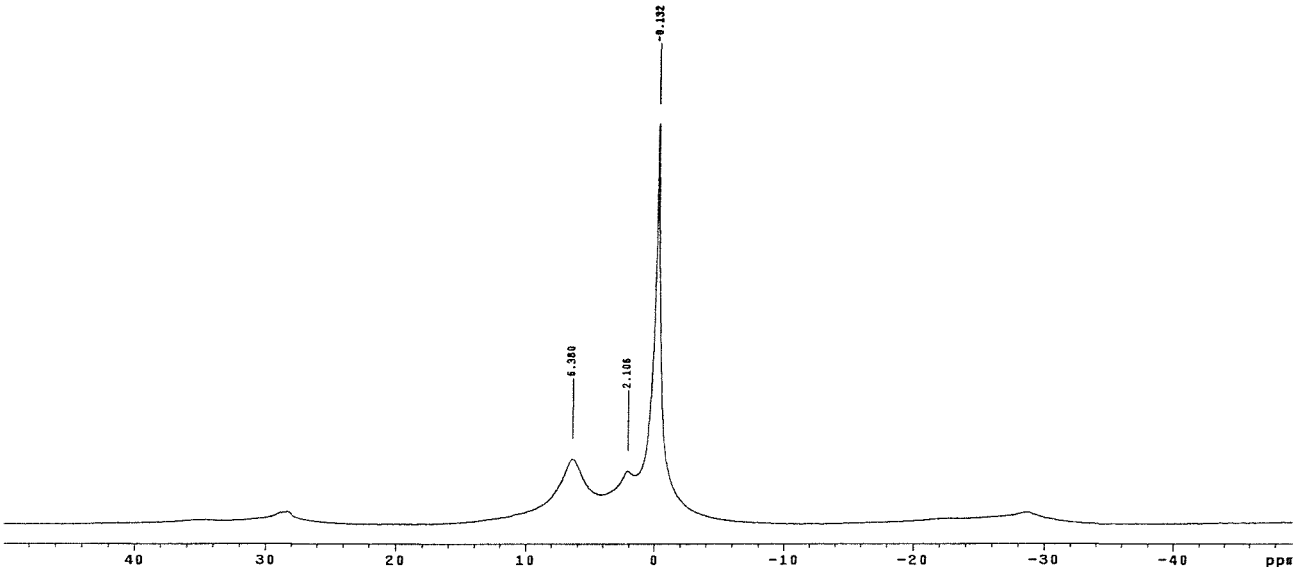

Figure 6.13 :- ^{1}H solid state NMR of $[ZrCp_2Me_2]$ supported on Aerosil 200 modified with trifluoromethanesulfonic acid.

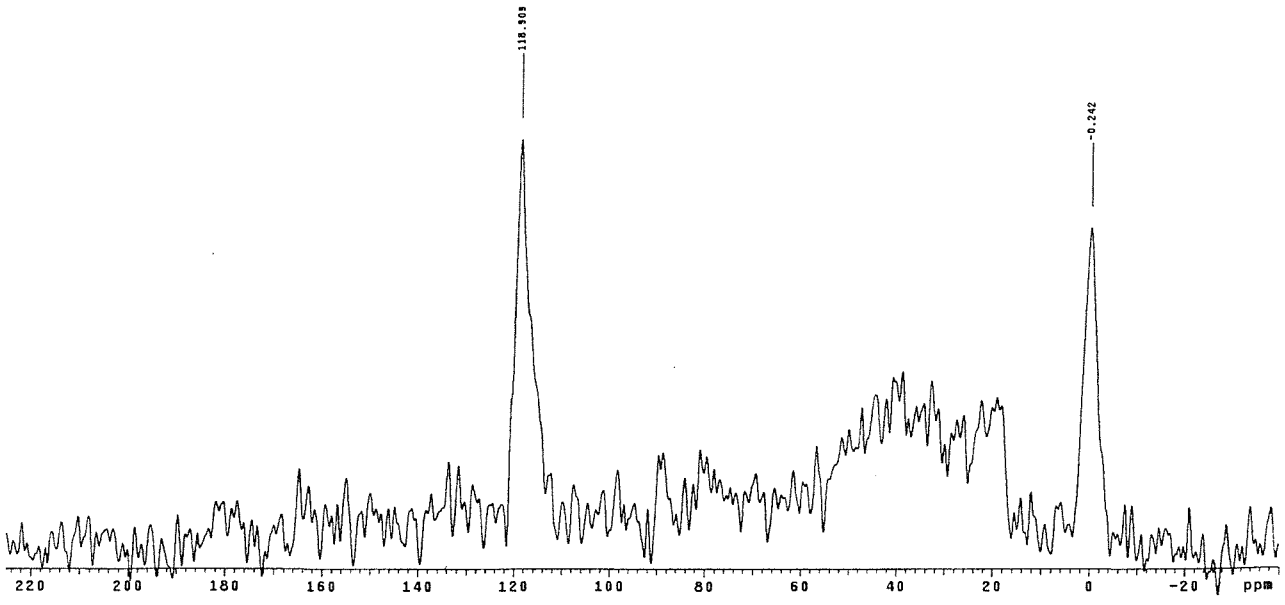

Figure 6.14 :- ^{13}C CP-MAS of $[ZrCp_2Me_2]$ supported on Aerosil 200 modified with trifluoromethanesulfonic acid.

6.3.5 Reaction of $[ZrCp_2Me_2]$ with H_1SiO_2 supported with trifluoromethanesulphonic acid

The ^1H solid state spectrum is presented in figure 6.15. In general, two types of signal, characteristic of the cyclopentadienyl ring protons and hydrogen bonded silanol groups were observed at 6.51 and 2.38 ppm. The weak signal at 0.06 ppm could not be ascertained if it were due to a methyl group attached to a surface silicon or the presence of a very small amount of grease.

^{13}C CP-MAS spectrum is shown in figure 6.16. From the spectrum, three signals could be clearly observed. A intense signal at 117.2 ppm which was assigned to the carbons of the cyclopentadienyl rings where the Cp ring position could be attached to a partially charged zirconium center judging from the higher chemical shift value obtained compared to the corresponding neutral complex. A weak broad band is also observed around the same region, previously seen at 20-60 ppm would could suggest the presence of $Zr\text{-}CH_3$ species. However, due to the broadness of the observed band, one cannot determine with certainty either whether the peak is due to one or several species. The weak signal at –0.77 ppm can be assigned to the methyl carbons attached to the surface silicons. Another very weak peak positioned at 179.4 ppm was due to the supported trifluoromethanesulfonic acid as this peak was also present in the solution ^{13}C NMR spectrum of CF_3SO_3H. The peak at 21.2 ppm is due to physisorbed THF residual solvent.

Table 6.3 :- ^1H and ^{13}C NMR chemical shifts of $[ZrCp_2Me_2]$ supported on both types of silica modified with trifluoromethanesulphonic acid.

	^1H shifts/ppm	^{13}C shifts/ppm
$[ZrCp_2Me_2]$/Aerosil 200 modified with trifluoromethanesulphonic acid	6.38, 2.11	-0.24, 20-60 (broad), 118.9
$[ZrCp_2Me_2]/H_1SiO_2$ modified with trifluoromethanesulphonic acid	6.51, 2.38	-0.77, 20-60 (broad), 117.2

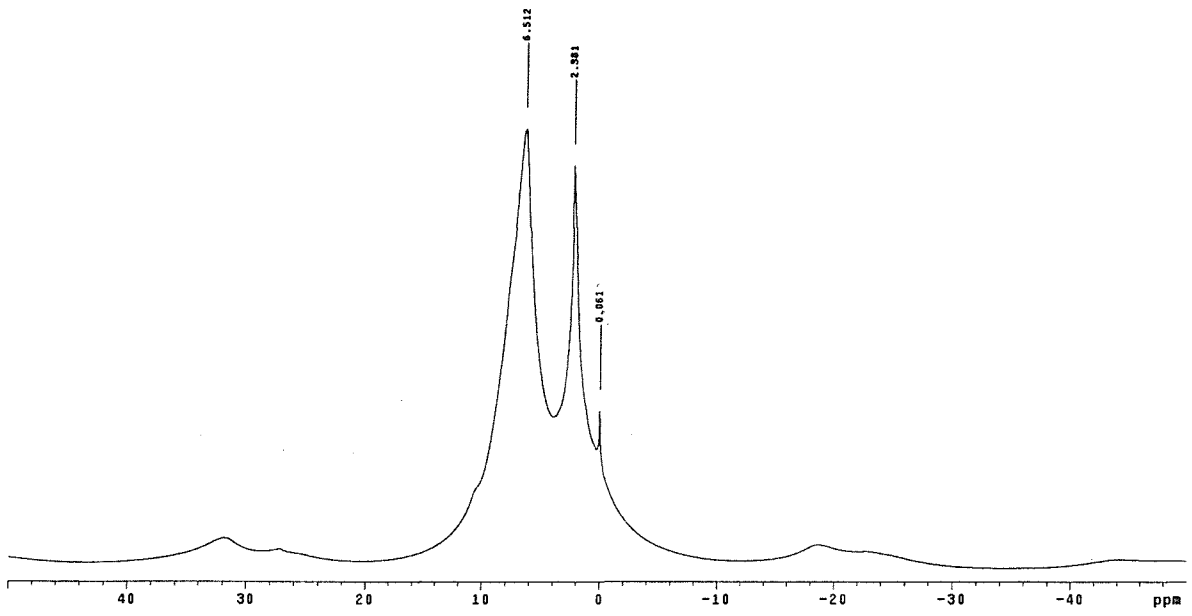

Figure 6.15 :- ^{1}H solid state NMR of $[ZrCp_2Me_2]$ supported on H_1SiO_2 modified with trifluoromethanesulfonic acid.

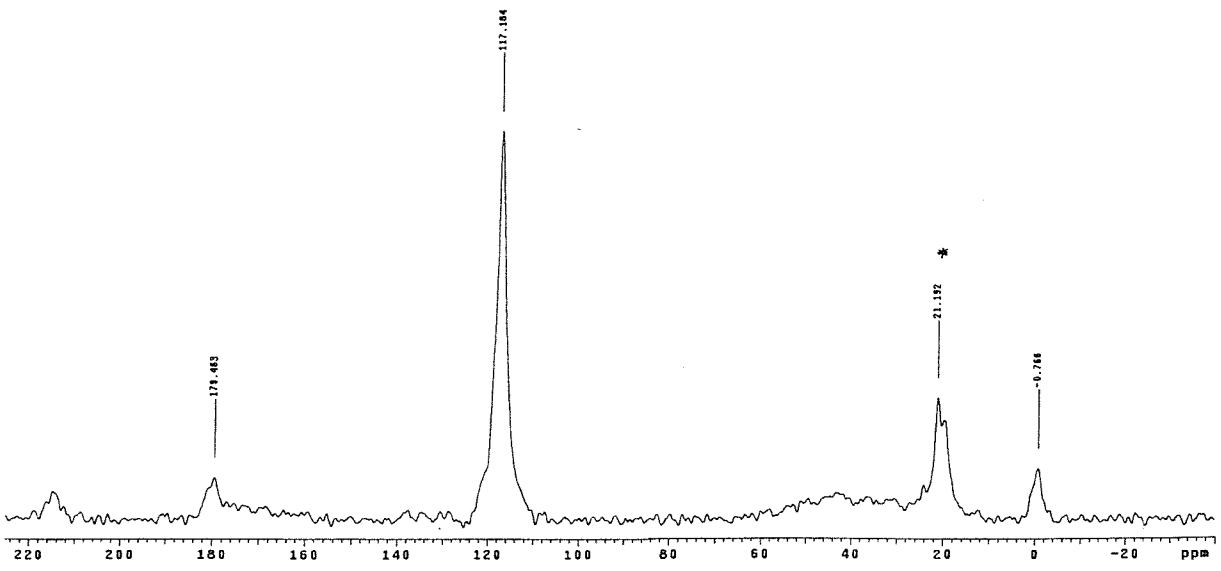

Figure 6.16 :- ^{13}C CP-MAS NMR of $[ZrCp_2Me_2]$ supported on H_1SiO_2 modified with trifluoromethanesulfonic acid.

6.4 Conclusions

All the synthesised modified silica with sulfonic acids have been shown to possess the ability to generate the protonated species of tricarbonyl cyclooctatetraeneiron, $[Fe(CO)_3(COTH)]^+$. The results obtained here resemble the protonation of tricarbonyl cyclooctatetraeneiron in strong acid e.g. sulfuric acid as reported in the literature [16]. The presence of Brønsted acidity on the modified silica surface must have played a role in the formation of the observed protonated tricarbonyl cyclooctatetraeneiron species.

Several important observations can be drawn from the reaction of $[ZrCp_2Me_2]$ with the silica supported with sulfonic acids. In all the cases, the main reaction which takes place on the surface is the formation of the μ-oxo species via $Zr\text{-}CH_3$ protonolysis. The resulting zirconium species are at least linked to the surface via one covalent Si-O-Zr bond. A general structure of the type, $[Si\text{-}O\text{-}]Zr(Cp)_2CH_3$ or $[Si\text{-}O\text{-}]_2Zr(Cp)_2$ where the zirconium atom is surrounded by two Cp ligands and one or none methyl group could be ascribed to the supported zirconium species. Previous work [6,19] has consistently shown that reaction of $[ZrCp_2Me_2]$ with partially dehydroxylated oxides e.g. silica, silica-alumina and γ-alumina would led to the formation of grafted species having an identical chemical formula : two cyclopentadienyl ligands and one methyl group per zirconium atom and one covalent link via an M-O bond (M=Si,Al). However, surface microanalysis, qualitative and quantitative analysis of evolved gases during the surface reactions and solid state NMR using ^{13}C-enriched compounds would provide a more accurate picture of the supported zirconium species present.

Nevertheless, for the silica modified with sulfonic acids prepared in this work, one cannot rule out the possibility that Brønsted acid sites could generate a neutral species from the interaction of the $^-OSO_2Me$ group with the zirconium centre. Besides this possibility, there is also the probable presence of a partially charged zirconium species if the zirconium complex was interacting with the silanol groups on the silica. These two possibilities may explained the consistent presence of a broad band around the region of 20-60 ppm. However, the presence of these type of species are only of very low percentage as ^{13}C CP-MAS spectra

only showed the presence of a very weak broad signal. In addition, some methyl groups appeared to be directly linked to the silica surface could also be observed.

References

[1] J.M.Basset , Eds., *Surface Organometallic Chemistry : Molecular Approaches to Surface Catalysis*, Kluwer, Dordrecht, 1988.

[2] T.R.Lee, G.M.Whitesides, *J.Am.Chem.Soc.*, **113**, 2576, 1991.

[3] W.Kaminsky, H.Sinn, Eds.,*Transition Metals and Organometallics as Catalysts for Olefin Polymerisation*, Springer, New York, 1988.

[4] T.Keii, K.Soga, Eds., *Catalytic Polymerisation of Olefins*, Elsevier, Armsterdam, 1986.

[5] T.J.Marks, A.Streitwieser Jr., *The Chemistry of the Actinide Elements*, 2nd edition, Chapman and Hall, London, 1986.

[6] T.J.Marks, *Acc.Chem.Res.*, **25**, 57, 1992.

[7] H.Ahn, T.J.Marks, *J.Am.Chem.Soc.*, **120**, 13533, 1998.

[8] R.F.Jordan, W.E.Dasher, S.F.Echols, *J.Am.Chem.Soc.*, **108**, 1718, 1986.

[9] M.Bochmann, A.J.Jaggar, *J.Organomet.Chem.*, 424, C5-C7, 1992.

[10] E.Samuel, M.D.Rausch, *J.Am.Chem.Soc.*, 6263, 1973.

[11] T.A.Samuel, F.G.A.Stone, *J.Am.Chem.Soc.*, **82**, 366, 1960.

[12] M.D.Rausch, G.N.Schrauzer, *Chem.Ind.*, 957, 1959.

[13] A.Nakamura, N.Hagihara, *Bull.Chem.Soc.Jpn.*, **32**, 880, 1959.

[14] G.N.Schrauzer, *J.Am.Chem.Soc.*, **83**, 2966, 1961.

[15] A.Davidson, W.McFarlane, L.Pratt, G.Wilkinson, *J.Chem.Soc.*, 482, 1962.

[16] M.Brookhart, E.RDavis, *J.Am.Chem.Soc.*, **92**, 7622, 1970.

[17] S.Haukka, E.L.Lakomaa, A.Root, *J.Phys.Chem.*, **97**, 5085, 1993.

[18] C.Sishta, R.M.Hathorn, T.J.Marks, *J.Am.Chem.Soc.*, **114**, 1112, 1993.

[19] M.Jezequel, V.Dufaud, M.J.Ruiz-Garcia, F.Carrillo-Hermosilla, U.Neugebauer, G.P.Niccolai, F.Lefebvre, F.Bayard, J.Corker, S.Fiddy, J.Evans, J-P Broyer, J.Malinge, J.M Bassett, *J.Am.Chem.Soc.*, **123**, 2520, 2001.

[20] J.C.Grimshaw, PhD thesis, University of Southampton, 1999.

[21] Sandra Turin, PhD thesis, University of Southampton, 2001.

[22] D.J.Gillis, R.Quyuom, M.J.Tudoret, Q.Wang, D.Jeremic, A.W.Roszak, M.C.Baird, *Organometallics*, **15**, 3600, 1996.

[23] D.J.Gillis, M.J.Tudoret, M.C.Baird, *J.Am.Chem.Soc.*, **115**, 2543, 1993.

[24] B.L.Moroz, N.V.Semikolenova, A.V.Nosov, V.A.Zakarov, S.Nagy, N.J.O'Reilly, *J.Mol.Catal.A.*, **130**, 121, 1998.

Summary and Conclusions

In this thesis, three main aspects have been studied. They are the synthesis of the supported acids and their characterisations and finally, the reaction of transition metal complexes, $[Fe(CO)_3(COT)]$ and $[ZrCp_2Me_2]$ with the modified silica.

Before modifying and utilising the silica materials, it is important to have a clear understanding of their structure and dimensions, since once the materials have been modified, they become even more complex in nature. Various characterisation techniques are utilised including methane gas titration, PXRD, BET surface area measurements, TEM, SEM, ^{29}Si MAS NMR and IR spectroscopy. The total concentration determined by methane gas titration was ~4 molecules and ~2 molecules per nm^2 for Aerosil 200 which was vacuum dehydroxylated at 480°C and H_1SiO_2 calcined at 470°C respectively .

A solid acid, 12-phosphotungstic acid (HPW), the strongest heteropolyacid in the Keggin series, was chosen to be supported on both types of silica. The supported heteropolyacid was prepared by adsorption from organic solvents which is different from the method commonly used in the literature to prepare the supported heteropolyacids. The significant results from this work is the preparation of the catalysts, comprising essentially Keggin type HPW species on the silica surface over a wide range of HPW loading. Characterisation of the supported HPW was carried out by uv-visible and solid state NMR spectroscopy, PXRD, sorption of N_2 and electron microscopy. Results from TEPO studies showed that the bulk of the acid sites present were only weakly acidic on both types of silica. However, it is evident from ^{31}P NMR spectra that a few sites with enhanced acidity were also present. ^{31}P NMR of the supported HPW only showed one main peak around –15 ppm with the absence of other peaks observed in the literature. This can be understood by considering HPW has greater stability towards hydrolysis in organic solvents compared to aqueous solutions.

There are only a few published works in the literature which concern the studies of supported triflic acid and the work reported has only been focused on catalytic studies. However, to date, there is no reported work on supported methanesulphonic acid. Therefore, in this study, methane and trifluoromethane sulphonic acid have been supported on both

types of silica. Compared to the silanol groups on the silica, base titration results indicate there is at least a monolayer coverage of the acid molecules on the supports. Acidity determination was performed by basic indicators, ^{31}P solid state NMR of adsorbed triethylphosphine oxide (TEPO) and pyridine adsorption monitored by DRIFTS. Results from basic indicator experiment indicates there is a presence of acid sites of at least equivalent to 50% concentrated sulphuric acid for both types of silica supported with sulphonic acids. TEM images of H_1SiO_2 modified with acids showed dominantly the presence of both hexagonal pore arrangement and equidistant parallel lines arising from the mesoporous structure of H_1SiO_2. This observation indicate the mesoporous architecture of the mesoporous support is structurally unchanged and the acids may well dispersed inside the channel pores. This is confirmed by the reduction in pore volume from 0.59 cm^3g^{-1} for the unsupported H_1SiO_2 to 0.08-0.13 cm^3g^{-1} for the supported acids. If the location of the acids were at the pore openings, a larger reduction in pore volume will be expected from calculation.

All the synthesised modified silica with sulfonic acids have been shown to possess the ability to generate the protonated species of tricarbonyl cyclooctatetraeneiron, $[Fe(CO)_3(COTH)]^+$. Several important observations can be drawn from the reaction of $[ZrCp_2Me_2]$ with the silica supported with sulfonic acids. In all the cases, the main reaction which takes place on the surface is the formation of the μ-oxo species via Zr-CH_3 protonolysis. Nevertheless, for the silica modified with sulfonic acids prepared in this work, the presence of Brønsted acid sites could generate a neutral species from the interaction of the $^-OSO_2Me$ group with the zirconium center. Besides this possibility, there is also the probable presence of a partially charged zirconium species if the zirconium complex was interacting with the silanol groups on the silica. These two possibilities may explained the consistent presence of a broad band around the region of 20-60 ppm. However, the presence of these type of species are only of very low percentage as ^{13}C CP-MAS spectra only showed the presence of a very weak broad signal. In addition, some methyl groups appeared to be directly linked to the silica surface could also be observed.